ABSTRACT

BATIO$_3$-EPOXY-ZNO BASED MULTIFUNCTIONAL COMPOSITES: VARIATION IN ELECTRON TRANSPORT PROPERTIES DUE TO THE INTERACTION OF ZNO NANOPARTICLES WITH THE COMPOSITE MICROSTRUCTURE

Piezoelectric and electro-active composites are being investigated as a generation of self-powered energy harvesting devices for a wide range of applications. More specifically, three-phase piezoelectric composites are capable of maintaining high reliability, durability, and sensitivity, all while being economically feasible and non-toxic. In addition, three-phase composites can be tailored towards multifunctional applications depending on which material is incorporated as the third-phase. The criteria that governs the applicability of these composites depend upon their electromechanical properties such as their impedance, resistivity, conductivity, and dielectric constant. Therefore, the present work involves the fabrication of barium titanate-epoxy-zinc oxide (BT-Ep-ZnO) multifunctional composites, and the study of the variation of their electron transport properties. The volume fraction of BT was held constant at 0.40, while the volume fraction of ZnO was varied from 0.01 to 0.10. The dipoles of the electro-active phases were aligned using a contactless corona plasma discharge poling technique. The impedance, resistance, conductance, and capacitance were measured over a frequency range of 20 Hz to 10 MHz. The geometry of the composites was measured and used to normalize the data by calculating the resistivity, conductivity, and dielectric constant. The piezoelectric strain coefficients, d_{33} and d_{31}, were measured using a piezometer at a frequency of 110 Hz. The fractured surface morphology and distribution of the particles were observed with a scanning electron microscope.

Walker Tuff
May 2019

$BATIO_3$-EPOXY-ZNO BASED MULTIFUNCTIONAL COMPOSITES: VARIATION IN ELECTRON TRANSPORT PROPERTIES DUE TO THE INTERACTION OF ZNO NANOPARTICLES WITH THE COMPOSITE MICROSTRUCTURE

by

Walker James Tuff

A thesis

submitted in partial

fulfillment of the requirements for the degree of

Master of Science in Engineering

in the Lyles College of Engineering

California State University, Fresno

May 2019

APPROVED

For the Department of: Mechanical Engineering

We, the undersigned, certify that the thesis of the following student meets the required standards of scholarship, format, and style of the university and the student's graduate degree program for the awarding of the master's degree.

Walker James Tuff
Thesis Author

Sankha Banerjee (Chair) Mechanical Engineering

Ajith Weerasinghe Mechanical Engineering

Yuanyuan Xie Mechanical Engineering

For the University Graduate Committee:

Dean, Division of Graduate Studies

AUTHORIZATION FOR REPRODUCTION

OF MASTER'S THESIS

_____ I grant permission for the reproduction of this thesis in part or in its entirety without further authorization from me, on the condition that the person or agency requesting reproduction absorbs the cost and provides proper acknowledgment of authorship.

__X__ Permission to reproduce this thesis in part or in its entirety must be obtained from me.

Signature of thesis author:_____

ACKNOWLEDGMENTS

First and foremost, I would like to thank my advisor, Dr. Sankha Banerjee, for his constant support over the last three years. I would not have been able to finish my research without his guidance, and I will always treasure our many “arguments” in his office about various research topics. In addition, I would like to acknowledge that he was also there for me when the times got tough and mentored me through some very difficult times. I can definitively say that I would not be the researcher or person I am today without his guidance.

I would also like to thank my committee members, Dr. Ajith Weerasinghe and Dr. Yuanyuan Xie, for their encouragement, time, and insight towards my research.

I would like to acknowledge the Department of Defense, Southern California Edison, and the Lyles College of Engineering Graduate Sponsorship Program for their support and funding of my research.

I would also like to thank the researchers who have helped me with my thesis work: Yerli Cervantes, Diego Ruggiero, Emma Van Fossen, Patrick Mangera, Joseph Tilghman, and Eric Mah.

I would like to thank my original engineering family: Majerle Reeves, Abbie Sandquist, Ridge Bertuccio, Jessica Gartrell, Christian Ramirez, David Martinez, and Christopher Bush; I would not have made it to grad school without them, and our engineering dinners will always be treasured memories. Similarly, I would like to thank my current engineering family: Majerle Reeves, Emma Van Fossen, Christopher Doda, Fahad Alzuwaid, Diego Ruggiero, and Austin Moore, as well as all the regular members of ASME; grad school would not have been anywhere near as much fun as it was without them.

Last, but not least, I would like to thank my family, especially my mom, who have always been supporting and motivating me to continue and further my education.

Walker Tuff

California State University, Fresno

April 2019

TABLE OF CONTENTS

Page

LIST OF TABLES viii

LIST OF FIGURES ix

INTRODUCTION 1

Piezoelectricity 1

Ferroelectricity 5

LITERATURE REVIEW 12

Energy Harvesting Composites 12

Material Selection 14

METHODOLOGY 17

Fabrication Procedure 17

Measurementation and Post Processing 19

RESULTS AND DISCUSSION 20

Electrical Properties (20 Hz to 10 MHz) 21

Electrical Properties (1 MHz) 24

Piezoelectric Strain Coefficients (d_{33} and d_{31}) 29

Scanning Electron Microscope Micrographs 30

Post Processing Results (Agglomerations) 57

CONCLUSION 58

Future Work 58

REFERENCES 60

APPENDICES 65

APPENDIX A: SUPPLEMENTAL SEM MICROGRAPHS 66

APPENDIX B: MATLAB PROGRAM 90

Page

APPENDIX C: AGGLOMERATION MATLAB PROGRAM 119

LIST OF TABLES

Page

Table 1. The quantities of zinc oxide, barium titanate, epoxy resin, epoxy hardener, and ethanol used to fabricate each composite based on the volume fraction of zinc oxide (VF of ZnO)..... 18

LIST OF FIGURES

Page

Figure 1. A depiction of the microstructure of a quartz crystal that has (a) no polarity when symmetric and (b) a polarity when elongated due to an external force. 2

Figure 2. A demonstration of the direct piezoelectric effect with a piezoelectric material that is (a) not exposed to a mechanical input, (b) exposed to a tensile force, and (c) exposed to a compressive force. 3

Figure 3. A demonstration of the indirect piezoelectric effect with a piezoelectric material that is (a) not exposed to an electrical input, (b) exposed to an electric field with the opposite polarity, and (c) exposed to an electric field with the same polarity. 4

Figure 4. The polarization curve for piezoelectric materials where the electric dipoles are unaligned at state A, are being polarized at state B and C. The x-axis is the applied electric field (E), and the y-axis is the polarization of the electric dipoles (P). 4

Figure 5. The ferroelectric hysteresis curve where the dipoles are unaligned at state A, are being polarized at state B, have a remnant polarization at state C, are reversing their alignment at state D, and have a reversed remnant polarization at state E. The x-axis is the applied electric field (E), and the y-axis is the polarization of the electric dipoles (P). 6

Figure 6. An example of a ferroelectric microstructure (perovskite with an ABX_3 composition) showing (a) the symmetry at temperatures higher than the Curie temperature, and (b) the lack of symmetry and displacement of the ions at temperatures below than the Curie temperature. 7

Figure 7. The different alignments of the microstructures of the grains of polycrystalline materials. 8

Figure 8. Depictions of (a) the unaligned electric dipoles, (b) the poling process aligning the electric dipoles, and (c) the remnant polarization after poling in ferroelectric materials. 8

Figure 9. The corona plasma poling setup. 11

Figure 10. The microstructure of barium titanate showing (a) the symmetry at temperatures greater than the Curie temperature, and (b) the lack of symmetry and displacement of the titanium ion at temperature lower than the Curie temperature. 15

Page

Figure 11. (a) A depiction of the Wurtzite microstructure of zinc oxide, and (b) a front view of the microstructure showing the alternating planes of differently charged ions. 16

Figure 12. A schematic of the fabrication procedure: (1) addition of ethanol and ZnO to a beaker, (2) sonication for 1 h, (3) addition of BT to the beaker, (4) sonication for 30 min, (5) addition of epoxy resin to beaker, (6) sonication for 1 h, (7) addition of epoxy hardener to the beaker, (8) sonication for 10 min, (9) spin-coating of 1 ml of solution onto stainless steel substrates for 2 min, and (10) curing of composites on a hot plate for 8 h. 18

Figure 13. Some of the final fabricated and poled samples ready for testing. 20

Figure 14. The relative size of the composites as compared to a nickel. 20

Figure 15. A demonstration of the flexibility of the composites (shows a 90° bend). 21

Figure 16. The average impedance of the composites for each volume fraction of zinc oxide with respect to frequency. 22

Figure 17. The average resistivity of the composites for each volume fraction of zinc oxide with respect to frequency. 22

Figure 18. The average conductivity of the composites for each volume fraction of zinc oxide with respect to frequency. 23

Figure 19. The average dielectric constant of the composites for each volume fraction of zinc oxide with respect to frequency. 23

Figure 20. The average impedance (magnitude) of the composites for each volume fraction of zinc oxide at a frequency of 1 MHz. 25

Figure 21. The average resistivity of the composites for each volume fraction of zinc oxide at a frequency of 1 MHz. 25

Figure 22. The average conductivity of the composites for each volume fraction of zinc oxide at a frequency of 1 MHz. 26

Figure 23. The average dielectric constant of the composites for each volume fraction of zinc oxide at a frequency of 1 MHz. 26

Figure 24. A depiction of how the number of contact points decreases within the composites with (a) a small volume fraction of zinc oxide and a small number of contact points (i.e. volume fraction of 0.01), (b) a small volume fraction of zinc oxide and a large number of contact points (i.e. a volume fraction of 0.03), and (c) a large volume fraction of zinc oxide and a small number of contact points (i.e. volume fraction of 0.10). 27

Page

Figure 25. The average piezoelectric strain coefficient, d_{33}, for each volume fraction of zinc oxide. 30

Figure 26. The average piezoelectric strain coefficient, d_{31}, for each volume fraction of zinc oxide. 30

Figure 27. SEM micrograph of the surface of a composite with a volume fraction of zinc oxide of 0.01 at a magnification of 40.0 kx, a working distance of 7.50 mm, and voltage of 30.0 kV. 32

Figure 28. SEM micrograph of the surface of a composite with a volume fraction of zinc oxide of 0.02 at a magnification of 40.0 kx, a working distance of 7.50 mm, and voltage of 30.0 kV. 33

Figure 29. SEM micrograph of the surface of a composite with a volume fraction of zinc oxide of 0.03 at a magnification of 40.0 kx, a working distance of 7.50 mm, and voltage of 30.0 kV. 34

Figure 30. SEM micrograph of the surface of a composite with a volume fraction of zinc oxide of 0.04 at a magnification of 40.0 kx, a working distance of 7.50 mm, and voltage of 30.0 kV. 35

Figure 31. SEM micrograph of the surface of a composite with a volume fraction of zinc oxide of 0.05 at a magnification of 40.0 kx, a working distance of 7.50 mm, and voltage of 30.0 kV. 36

Figure 32. SEM micrograph of the surface of a composite with a volume fraction of zinc oxide of 0.06 at a magnification of 40.0 kx, a working distance of 7.50 mm, and voltage of 30.0 kV. 37

Figure 33. SEM micrograph of the surface of a composite with a volume fraction of zinc oxide of 0.07 at a magnification of 40.0 kx, a working distance of 7.50 mm, and voltage of 30.0 kV. 38

Figure 34. SEM micrograph of the surface of a composite with a volume fraction of zinc oxide of 0.08 at a magnification of 40.0 kx, a working distance of 7.50 mm, and voltage of 30.0 kV. 39

Figure 35. SEM micrograph of the surface of a composite with a volume fraction of zinc oxide of 0.09 at a magnification of 40.0 kx, a working distance of 7.50 mm, and voltage of 30.0 kV. 40

Figure 36. SEM micrograph of the surface of a composite with a volume fraction of zinc oxide of 0.10 at a magnification of 40.0 kx, a working distance of 7.50 mm, and voltage of 30.0 kV. 41

Figure 37. SEM micrograph of the fractured surface of a composite with a volume fraction of zinc oxide of 0.01 at a magnification of 53.3 kx, a working distance of 7.50 mm, and voltage of 30.0 kV. 42

Page

Figure 38. SEM micrograph of the fractured surface of a composite with a volume fraction of zinc oxide of 0.02 at a magnification of 53.3 kx, a working distance of 7.50 mm, and voltage of 30.0 kV. 43

Figure 39. SEM micrograph of the fractured surface of a composite with a volume fraction of zinc oxide of 0.03 at a magnification of 80.0 kx, a working distance of 7.50 mm, and voltage of 30.0 kV. 44

Figure 40. SEM micrograph of the fractured surface of a composite with a volume fraction of zinc oxide of 0.04 at a magnification of 53.3 kx, a working distance of 7.50 mm, and voltage of 30.0 kV. 45

Figure 41. SEM micrograph of the fractured surface of a composite with a volume fraction of zinc oxide of 0.05 at a magnification of 53.3 kx, a working distance of 7.50 mm, and voltage of 30.0 kV. 46

Figure 42. SEM micrograph of the fractured surface of a composite with a volume fraction of zinc oxide of 0.06 at a magnification of 53.3 kx, a working distance of 7.50 mm, and voltage of 30.0 kV. 47

Figure 43. SEM micrograph of the fractured surface of a composite with a volume fraction of zinc oxide of 0.07 at a magnification of 53.3 kx, a working distance of 7.50 mm, and voltage of 30.0 kV. 48

Figure 44. SEM micrograph of the fractured surface of a composite with a volume fraction of zinc oxide of 0.08 at a magnification of 53.3 kx, a working distance of 7.50 mm, and voltage of 30.0 kV. 49

Figure 45. SEM micrograph of the fractured surface of a composite with a volume fraction of zinc oxide of 0.09 at a magnification of 53.3 kx, a working distance of 7.50 mm, and voltage of 30.0 kV. 50

Figure 46. SEM micrograph of the fractured surface of a composite with a volume fraction of zinc oxide of 0.10 at a magnification of 53.3 kx, a working distance of 7.50 mm, and voltage of 30.0 kV. 51

Figure 47. SEM micrographs with indications showing how the zinc oxide agglomerations and barium titanate particles appear in composites with a volume fraction of (a) 0.03 and (b) 0.05. 52

Figure 48. SEM micrograph of the cross-section of a composite with a volume fraction of zinc oxide of 0.01 at a magnification of 9.33 kx, a working distance of 7.50 mm, and voltage of 30.0 kV. The thickness of the composites is 24.25 µm. 53

Figure 49. SEM micrograph of the cross-section of a composite with a volume fraction of zinc oxide of 0.03 at a magnification of 9.33 kx, a working distance of 7.50 mm, and voltage of 30.0 kV. The thickness of the composites is 35.98 µm. 54

Page

Figure 50. SEM micrograph of the cross-section of a composite with a volume fraction of zinc oxide of 0.04 at a magnification of 9.33 kx, a working distance of 7.50 mm, and voltage of 30.0 kV. The thickness of the composites is 23.89 µm. 55

Figure 51. SEM micrograph of the cross-section of a composite with a volume fraction of zinc oxide of 0.10 at a magnification of 9.33 kx, a working distance of 7.50 mm, and voltage of 30.0 kV. The thickness of the composites is 46.08 µm. 56

Figure 52. The percent of zinc oxide agglomerations for each volume fraction of zinc oxide from the post processing of the SEM micrographs with ImageJ. 57

Figure 53. SEM micrograph of the surface of a composite with a volume fraction of zinc oxide of 0.01 at a magnification of 2.67 kx, a working distance of 7.50 mm, and voltage of 30.0 kV. 68

Figure 54. SEM micrograph of the surface of a composite with a volume fraction of zinc oxide of 0.02 at a magnification of 2.67 kx, a working distance of 7.50 mm, and voltage of 30.0 kV. 69

Figure 55. SEM micrograph of the surface of a composite with a volume fraction of zinc oxide of 0.03 at a magnification of 2.67 kx, a working distance of 7.50 mm, and voltage of 30.0 kV. 70

Figure 56. SEM micrograph of the surface of a composite with a volume fraction of zinc oxide of 0.04 at a magnification of 2.67 kx, a working distance of 7.50 mm, and voltage of 30.0 kV. 71

Figure 57. SEM micrograph of the surface of a composite with a volume fraction of zinc oxide of 0.05 at a magnification of 2.67 kx, a working distance of 7.50 mm, and voltage of 30.0 kV. 72

Figure 58. SEM micrograph of the surface of a composite with a volume fraction of zinc oxide of 0.06 at a magnification of 2.67 kx, a working distance of 7.50 mm, and voltage of 30.0 kV. 73

Figure 59. SEM micrograph of the surface of a composite with a volume fraction of zinc oxide of 0.07 at a magnification of 2.67 kx, a working distance of 7.50 mm, and voltage of 30.0 kV. 74

Figure 60. SEM micrograph of the surface of a composite with a volume fraction of zinc oxide of 0.08 at a magnification of 2.67 kx, a working distance of 7.50 mm, and voltage of 30.0 kV. 75

Figure 61. SEM micrograph of the surface of a composite with a volume fraction of zinc oxide of 0.09 at a magnification of 2.67 kx, a working distance of 7.50 mm, and voltage of 30.0 kV. 76

Page

Figure 62. SEM micrograph of the surface of a composite with a volume fraction of zinc oxide of 0.10 at a magnification of 26.7 kx, a working distance of 7.50 mm, and voltage of 30.0 kV. 77

Figure 63. SEM micrograph of the surface of a composite with a volume fraction of zinc oxide of 0.01 at a magnification of 26.7 kx, a working distance of 7.50 mm, and voltage of 30.0 kV. 79

Figure 64. SEM micrograph of the surface of a composite with a volume fraction of zinc oxide of 0.10 at a magnification of 26.7 kx, a working distance of 7.50 mm, and voltage of 30.0 kV. 80

Figure 65. SEM micrograph of the surface of a composite with a volume fraction of zinc oxide of 0.02 at a magnification of 26.7 kx, a working distance of 7.50 mm, and voltage of 30.0 kV. 81

Figure 66. SEM micrograph of the surface of a composite with a volume fraction of zinc oxide of 0.03 at a magnification of 26.7 kx, a working distance of 7.50 mm, and voltage of 30.0 kV. 82

Figure 67. SEM micrograph of the surface of a composite with a volume fraction of zinc oxide of 0.04 at a magnification of 26.7 kx, a working distance of 7.50 mm, and voltage of 30.0 kV. 83

Figure 68. SEM micrograph of the surface of a composite with a volume fraction of zinc oxide of 0.05 at a magnification of 26.7 kx, a working distance of 7.50 mm, and voltage of 30.0 kV. 84

Figure 69. SEM micrograph of the surface of a composite with a volume fraction of zinc oxide of 0.06 at a magnification of 26.7 kx, a working distance of 7.50 mm, and voltage of 30.0 kV. 85

Figure 70. SEM micrograph of the surface of a composite with a volume fraction of zinc oxide of 0.07 at a magnification of 26.7 kx, a working distance of 7.50 mm, and voltage of 30.0 kV. 86

Figure 71. SEM micrograph of the surface of a composite with a volume fraction of zinc oxide of 0.08 at a magnification of 26.7 kx, a working distance of 7.50 mm, and voltage of 30.0 kV. 87

Figure 72. SEM micrograph of the surface of a composite with a volume fraction of zinc oxide of 0.09 at a magnification of 26.7 kx, a working distance of 7.50 mm, and voltage of 30.0 kV. 88

Figure 73. SEM micrograph of the surface of a composite with a volume fraction of zinc oxide of 0.10 at a magnification of 26.7 kx, a working distance of 7.50 mm, and voltage of 30.0 kV. 89

INTRODUCTION

Recently, there has been a growing demand for more efficient small-scale and self-powered devices [1-2] such as phones, tablets, smartwatches, and laptops. This demand has, in turn, increased researchers' interest in developing innovative methods for powering such devices at a reduced cost [2]. One such method is to fabricate energy harvesters that can collect the energy (i.e. heat, light, and vibrations) that is a byproduct of existing processes that already consume energy [3]. These sources of waste energy are abundant and include everything from the light produced by the fusion reactions in the sun, to the vibrations through a floor that people are walking on. In addition, since the waste energy is a byproduct of already existing processes, it is often an economically feasible method to generate clean electrical energy [4]. An analysis of the different type of waste energy, however, reveals that vibrations are arguably the most consistent and abundant [1-3,5-7]; therefore, vibrational energy harvesters are well suited for powering small-scale devices [5,7].

Vibrational energy harvesters should be simple, easy to manufacture, and easily incorporated into existing mechanical and electrical systems; consequently, this eliminates electromagnetic, electrostatic, bimetal, and thermo-air pressure energy harvesters [7,8]. On the other hand, piezoelectric energy harvesters that use electric dipoles to convert vibrations into electrical charges, meet all the requirements of an ideal energy harvester, since they are simple, easily scalable, and have high conversion efficiencies [2-3,8-9].

Piezoelectricity

Piezoelectric materials are a class of smart materials that researchers can use to convert mechanical inputs into electrical outputs, or vice versa [10]. They are used in a variety of applications such as actuating, sensing, charging batteries, powering

nanodevices, vibrational damping, structural health monitoring, and energy harvesting [5,7,8,11-14], and they can also be used as capacitors, inductors, and resonators [13]. Researchers can achieve this by taking advantage of these materials' microstructures which can produce an electric dipole [15]. One of the most common and simplest examples is a quartz crystal [16]. The microstructure of a quartz crystal is a hexagon with alternating silicon and oxygen ions (see Figure 1). When the quartz crystal is undisturbed, the hexagonal microstructure is symmetrical, and the polarity of the ions balance each other resulting in no electric dipole. If the microstructure is distorted, however, an electric dipole is created within the microstructure that has its own polarity (i.e. a positive and negative electrical orientation) [15]. The distortion of the crystal is often caused by a compressive or tensile force (i.e. the mechanical input), and the electric dipole is often represented by a voltage or charge (i.e. the electrical output). Once the distortion is removed, the crystal regains its symmetry and loses its dipole. This conversion process is called the piezoelectric effect [15].

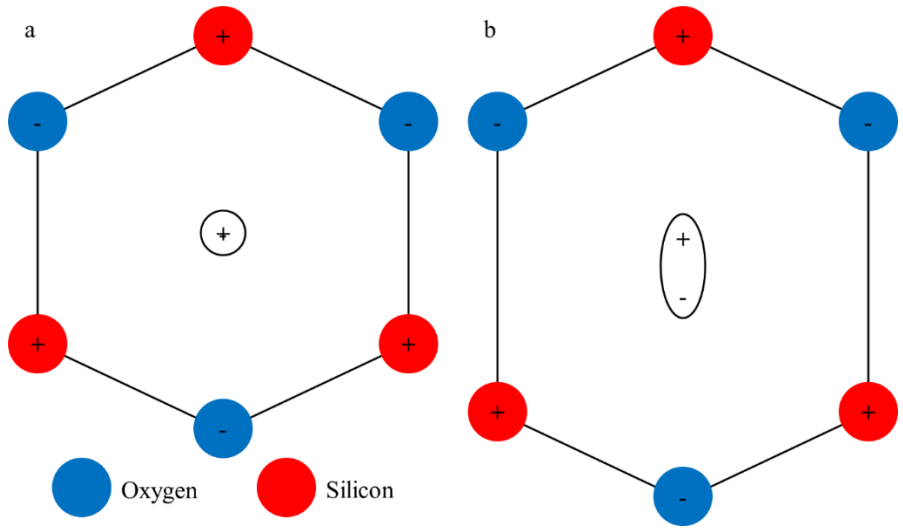

Figure 1. A depiction of the microstructure of a quartz crystal that has (a) no polarity when symmetric and (b) a polarity when elongated due to an external force.

The piezoelectric effect can be further broken down into two different processes. When the conversion is from a mechanical input to electrical output, it is described as the direct piezoelectric effect (see Figure 2) [16]; the mechanical input is usually a force that causes internal stresses that deform the microstructure. Conversely, when the conversion is from an electrical input to a mechanical output, it is described as the indirect piezoelectric effect (see Figure 3) [16]; a common electrical input is exposure to an electric field which causes the electric dipoles to align themselves (called polarization) in such a way that repels the field [15]. The relationship between the polarization of piezoelectric materials and the applied electric field can be seen in Figure 4. Since vibrational energy harvesting requires the conversion of vibrations, which are essentially alternating compressive and tensile forces, into electric charges, they implement the direct piezoelectric effect and should be fabricated in a manner that enhances this property.

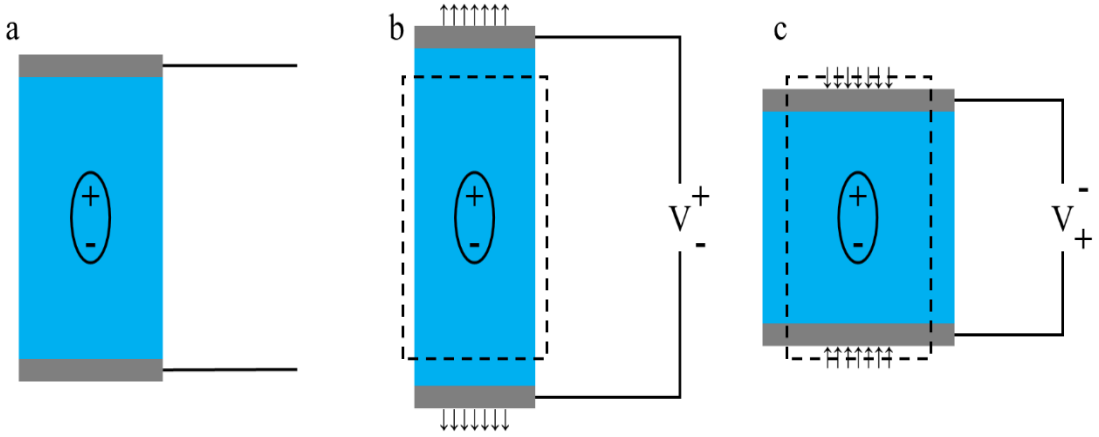

Figure 2. A demonstration of the direct piezoelectric effect with a piezoelectric material that is (a) not exposed to a mechanical input, (b) exposed to a tensile force, and (c) exposed to a compressive force.

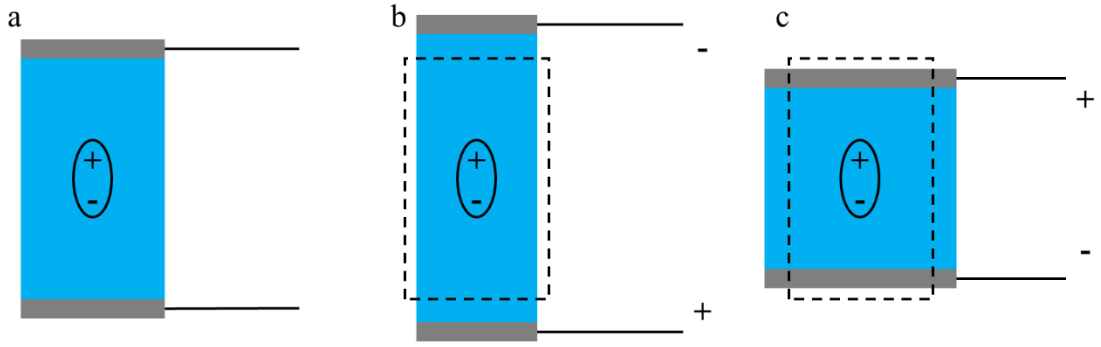

Figure 3. A demonstration of the indirect piezoelectric effect with a piezoelectric material that is (a) not exposed to an electrical input, (b) exposed to an electric field with the opposite polarity, and (c) exposed to an electric field with the same polarity.

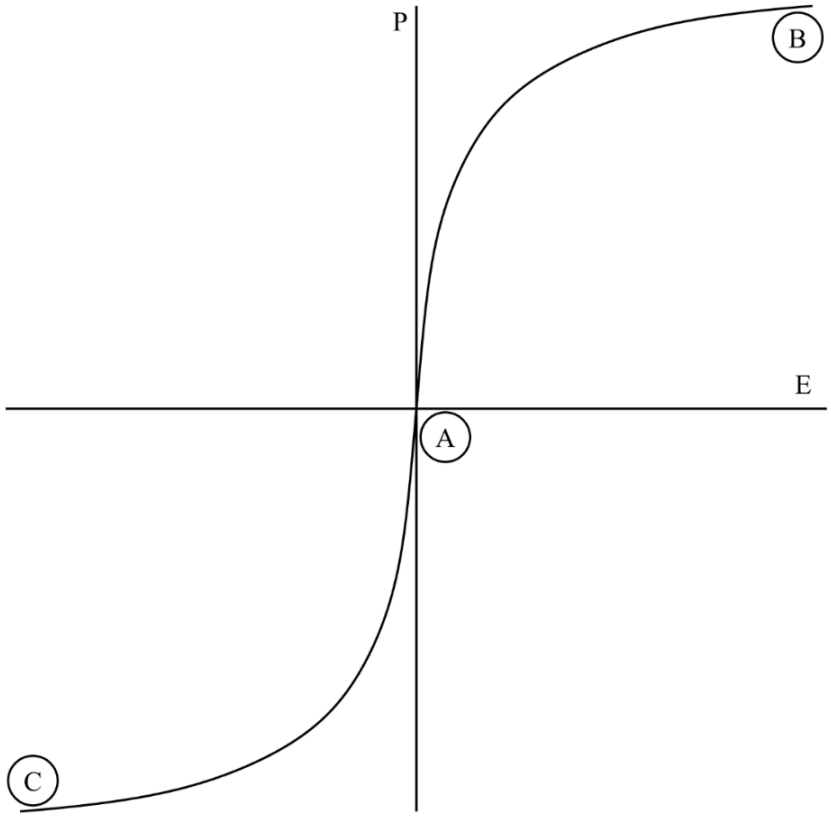

Figure 4. The polarization curve for piezoelectric materials where the electric dipoles are unaligned at state A, are being polarized at state B and C. The x-axis is the applied electric field (E), and the y-axis is the polarization of the electric dipoles (P).

Piezoelectric Strain Coefficients

A common method to measure the performance of a piezoelectric material is to measure the amount of electrical charges produced per unit force applied. These measurements are called the piezoelectric strain coefficients and are often recorded in pC/N. These values will change, however, depending on the orientation of the force applied with respect to the orientation of the electric dipoles within the piezoelectric materials. The highest amount of electrical charges will be produced when the force is being applied in the direction of the electric dipole alignment; therefore, it is common to measure this specific strain coefficient. The piezoelectric strain coefficients are noted by the letter d followed by the direction of the dipole alignment unit vector number (usually denoted as 3) and the unit vector number of the force (usually either 1 or 3). Therefore, the strain coefficient with the force and the electric dipole alignment in the same direction is d_{33}. Similarly, the strain coefficient for when the force is applied orthogonal to the electric dipole alignment is d_{31}.

Ferroelectricity

In addition to piezoelectric materials, there is another group of materials called ferroelectric materials that can exhibit the piezoelectric effect but only under specific circumstances. This difference is caused by the summation of the polarity of their electric dipoles following a hysteresis curve (see Figure 5). In other words, ferroelectric materials can maintain their electric dipoles without the need of an external force to deform their microstructures, but they also will not initially demonstrate the piezoelectric effect without some type of processing [17-18].

The phenomenon that allows ferroelectric materials to maintain their electric dipoles is caused by their microstructure naturally lacking symmetry [18]. Figure 6 provides an example of one such microstructure called a perovskite which has an ABX_3 chemical composition. It should be noted, however, that Figure 6 provides two cross-

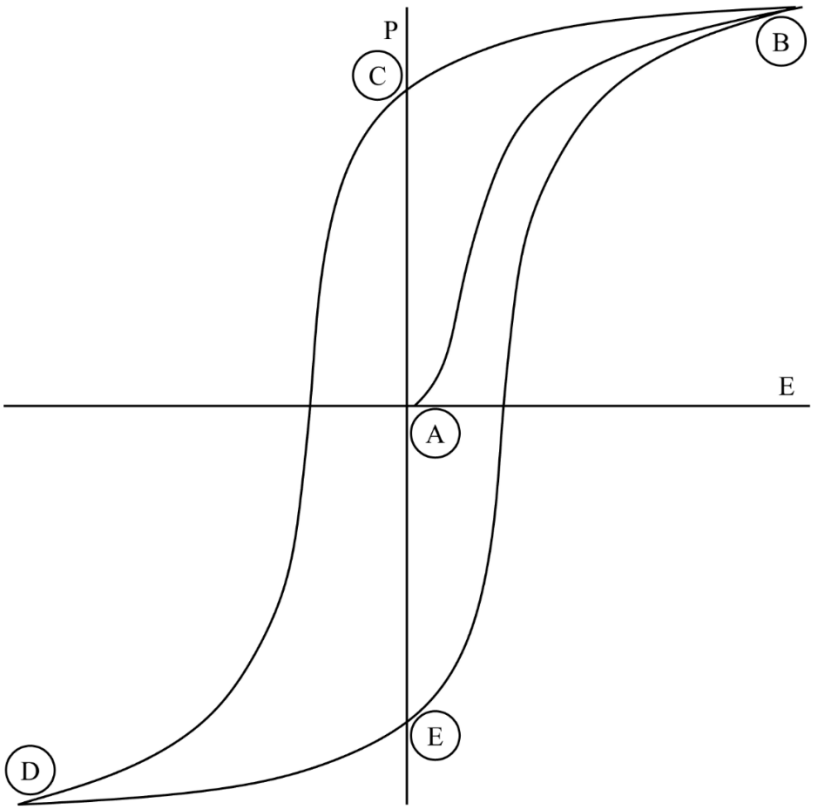

Figure 5. The ferroelectric hysteresis curve where the dipoles are unaligned at state A, are being polarized at state B, have a remnant polarization at state C, are reversing their alignment at state D, and have a reversed remnant polarization at state E. The x-axis is the applied electric field (E), and the y-axis is the polarization of the electric dipoles (P).

sectional views because the geometry is dependent on the temperature of the perovskite. Perovskites only function as ferroelectric materials below a specific temperature. This temperature is called the Curie temperature, and it is defined as the temperature at which the microstructure of any given ferroelectric material becomes symmetric [17-18]; therefore, it is the temperature at which ferroelectrics can no longer maintain their electric dipoles without an external force. A few examples of perovskites are barium titanate (BT), lead zirconium titanate (PZT), and calcium titanate (CT), and they tend to have superior piezoelectric properties when compared to piezoelectric materials [2]; however, this statement is only true if ferroelectric materials are first exposed to a strong magnetic field in a process called poling [17].

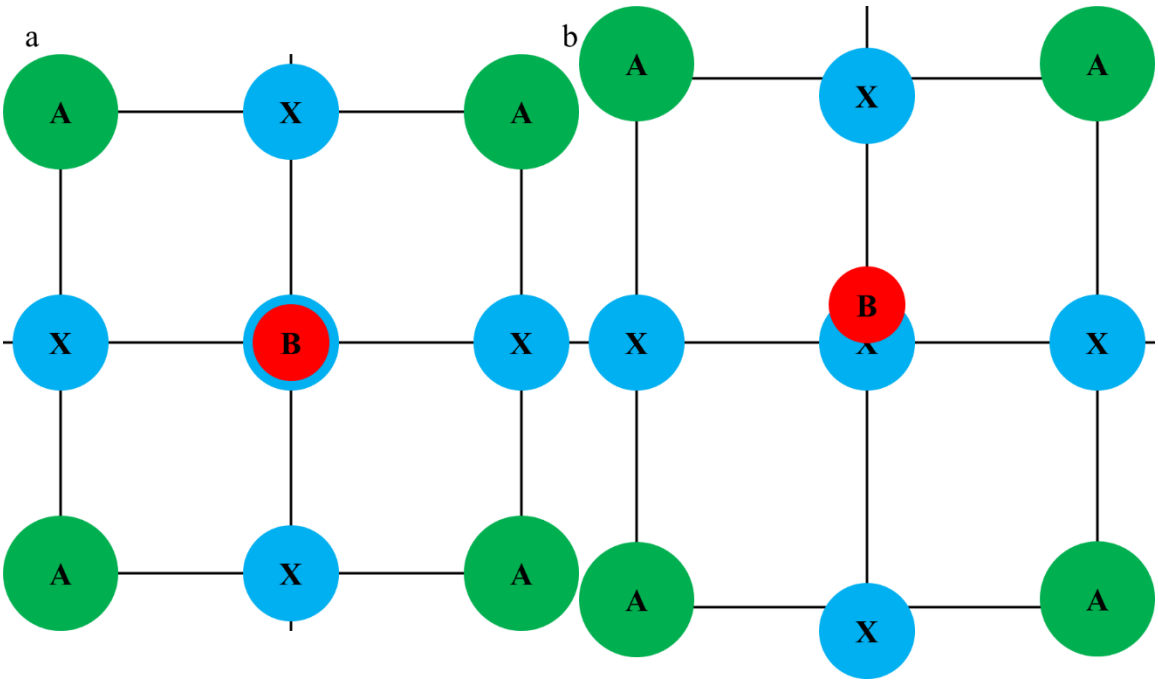

Figure 6. An example of a ferroelectric microstructure (perovskite with an ABX_3 composition) showing (a) the symmetry at temperatures higher than the Curie temperature, and (b) the lack of symmetry and displacement of the ions at temperatures below than the Curie temperature.

Poling

Ferroelectric materials are often polycrystalline ceramics, so they lack a single continuous matrix of ionic bonds. Instead, ferroelectric materials contain numerous independent monocrystalline sections of material called grains that interact with each other at grain boundaries (see Figure 7) [19]. Since each grain is separate from each other, they have their own microstructure alignment which in turn provides each grain with its own electric dipole alignment (see Figure 8a). The alignment of each grain is essentially random, so the net electric dipole (also called polarization) of the entire ferroelectric material is initially zero [17,19]. This state of zero polarization can also be seen in Figure 5 at point A.

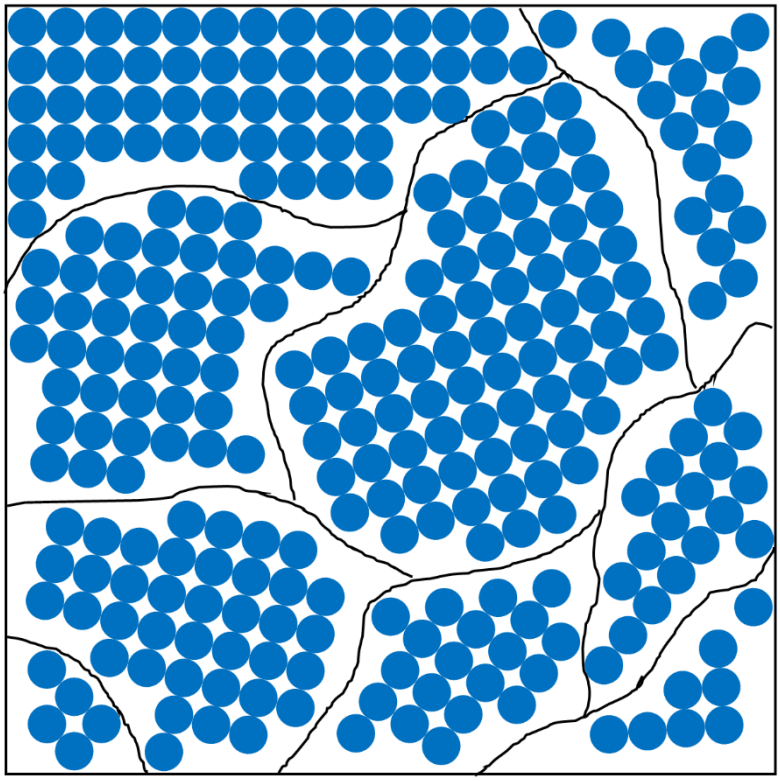

Figure 7. The different alignments of the microstructures of the grains of polycrystalline materials.

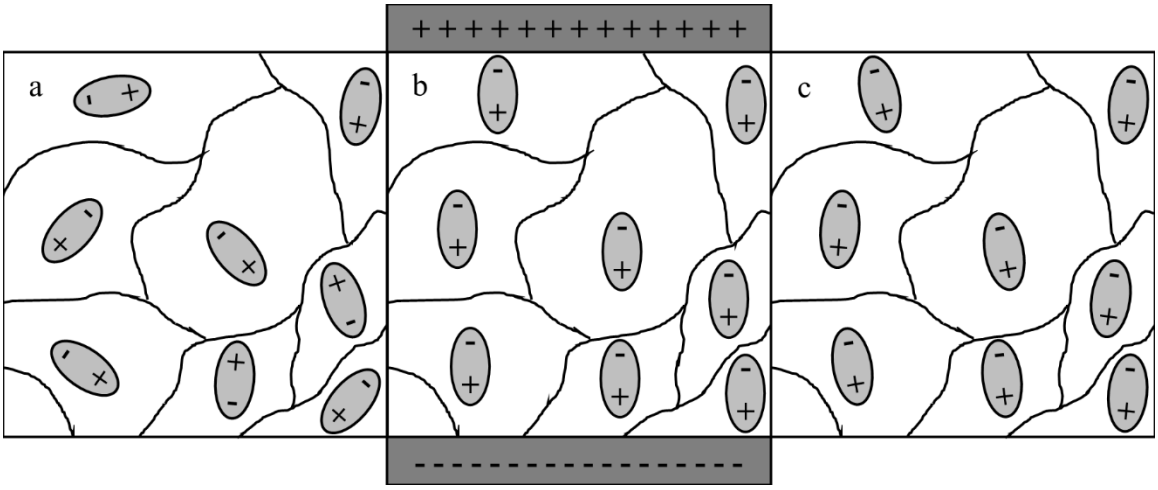

Figure 8. Depictions of (a) the unaligned electric dipoles, (b) the poling process aligning the electric dipoles, and (c) the remnant polarization after poling in ferroelectric materials.

A zero net polarization prevents ferroelectric materials from demonstrating the piezoelectric effect, so the electric dipoles need to be aligned in a process called poling (see Figure 8b). This process implements the indirect piezoelectric effect of each grain by exposing ferroelectric materials to a strong electric field which aligns each electric dipole in the same direction [15]. This process is also shown in Figure 5 from state A where there is no polarization to state B where the applied electric field induces a net polarization. Then, once the ferroelectric materials are removed from the electric field, the electric dipoles relax slightly which leaves a remnant polarization (see Figure 7c). The remnant polarization is also shown in Figure 5 at state C where there is a polarization with no electric field [19]; it is at this point that the ferroelectric materials are considered poled.

Furthermore, poled ferroelectric materials will maintain their polarization, but the magnitude of the polarization can still change from an external force. For example, if poled ferroelectric materials are exposed to a vibrational force, then the material is constantly expanding and contracting. These alternating deformations in the materials' microstructure repeatedly elongate and contract the aligned electric dipoles which in turn produces an electrical output that is constantly increasing and decreasing (i.e. an alternating voltage) [20]. Additionally, the net alignment of the electric dipoles can be reversed, if the ferroelectric materials are exposed to a strong electric field with the opposite polarity of the electric field originally used for poling. This reversal of the polarization process is shown in Figure 5 from state C where there is a positive remnant polarization to state D where there is a negative polarization. Then, in a similar manner to the original poling process, the polarization relaxes to its new remnant polarization shown in Figure 5 at state E where there is a negative remnant polarization. Additionally, if the ferroelectric materials are poled again with the original poling electric field, the net polarization returns to where it was during the first poling process shown in Figure 5 at

state B. These poling reversal processes can be repeated continuously, and the polarization will not return to zero (i.e. state A in Figure 5) but will follow the hysteresis curve shown in Figure 5. If the ferroelectric materials need to be reset to their zero polarization, then they should be heated above their Curie temperature and then cooled back down.

Corona discharge poling. Poling ferroelectric composites requires a strong electric field which can be a problem with conventional contact poling methods. The strength of the electric field produced by these methods may not be strong enough, and they tend to cause dielectric breakdown within the composite [21-23]. To overcome these challenges, researchers have been using corona discharge plasma as a method to pole piezoelectric composites [21].

Corona discharge plasma is caused by charging a metal needle with a high voltage. The charges build up on the needle and jump an air gap to a grounded dissimilar metal base plate. As the charges move through the air, they ionize the gases and produce a plasma [24]. A piezoelectric composite can then be added to this system between the needle and the base plate. This addition exposes the composite to a high voltage that poles the composite without causing dielectric breakdown [21] (see Figure 9).

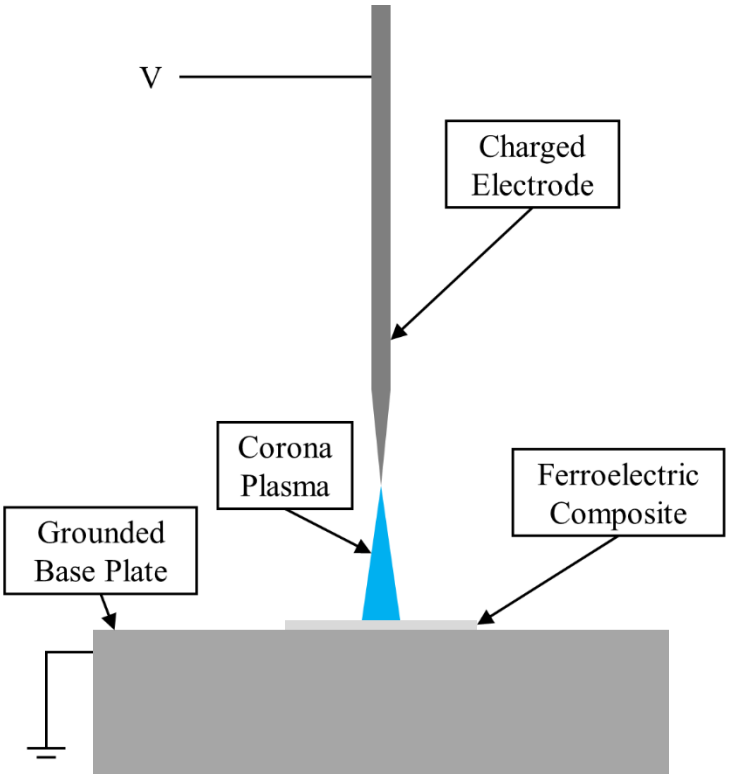

Figure 9. The corona plasma poling setup.

LITERATURE REVIEW

Researchers are always testing new methods to enhance the performance of the piezoelectric energy harvesters [1]. These methods include modifying the geometries of the materials, tailoring the energy harvester to have a natural frequency close to the source frequency, and incorporating different materials to fabricate composites [8,10]. S. Jeong et al, for example, found that texturing bismuth-sodium titanate-barium titanate (BNT-BT) increased the power generation of their energy harvesters [8], and A. Koka et al found that BT nanowires were superior to their zinc oxide (ZnO) nanowire counterparts [25]. Researchers also found that changing the size of the particles used can change the properties; S. Banerjee et al found that decreasing the particle size of aluminum inclusions in composites from micron-sized to nano-sized particles decreased the piezoelectric strain coefficients. They noted that this was likely due to agglomerations, change in the contact resistance, and excess air voids [6]. These methods are not mutually exclusive, however, and many researchers have chosen to work with composites to implement the advantages of different materials and structures [9,14,26].

Energy Harvesting Composites

Most piezoelectric materials are ceramics and are, consequently, incapable of handling the high stresses caused by intense vibrations without fracturing [12,14]. One method to overcome this problem is to develop energy harvesting composites that contain a flexible polymer that is capable of withstanding the intense vibrations.

Two-Phase Composites

A simple energy harvesting composite contains a piezoelectric or ferroelectric ceramic (the first-phase) and a flexible polymer (the second-phase). Usually the first-phase is dispersed into the second-phase, and the second-phase is used as a continuous

polymer matrix. This configuration allows for the polymer to flex with the vibrations without fracturing and for the piezoelectric or ferroelectric ceramic to convert the stresses that are transferred to it through the polymer matrix into an electrical output [1,14,26-28]. The downside of using a two-phase energy harvester, however, is that now only a fraction of the energy harvester can convert the vibrations into useful energy. This loss in performance can be reduced if an appropriate third component is introduced into the composite [6].

Even though two-phase composites have their challenges, researchers are still developing them and enhancing their properties. J. Park et al, for example, found that a two-phase composite mixture of BT and an elastomer with high mechanical strength could produce a peak voltage of 2 V and a peak current of 40 nA from an additive manufacturing process [26]. In addition, C. Bowland et al found that hydrothermally grown BT on carbon fibers produced multifunctional composites capable of producing a voltage of 23.5 mV [14].

Three-Phase Composites

Energy harvesting composites with a third component often have superior properties as compared to their two-phase counterparts. These third components are usually highly conductive materials, such as metal powders, graphene, and carbon nanotubes, because the conductive fillers increase the amount of charge carriers within the polymer matrix which enhances the electrical output [12,28,29-30]. Y. Wang et al, for example, found that adding CNTs to a BT composite with a polymer matrix greatly improved the output voltage density to 7.3 V/cm^2 and the output current density to 3.3 nA/cm^2 [11].

The third component, however, does not have to be conductive. If researchers wish to develop composites that are multifunctional instead of fully optimizing them for

one application, then any material can be implement as the third component [14]. One example is to add a semiconductor into the composite that is used to harvest energy from light. In this case, these three-phase composites could be incorporated into a solar panel to harvest both the vibrations from the wind and the light from the sun.

Material Selection

A challenge with many of the well-studied and high performing piezoelectric and ferroelectric materials (i.e. lead zirconium titanate) is the environmental concern due to their lead content [2-3,7,9,25]. As a result, researchers have been shifting towards implementing lead-free materials, such as BT, BNT-BT, ZnO, polyvinylidene difluoride (PVDF), and Potassium-Sodium Niobate (KNN), which can possess similar properties when compared to other lead-based piezoelectric materials [1,8-9]. Therefore, lead-free materials should be used to fabricate vibrational energy harvesters, since they can perform just as well as lead-based materials but also be incorporated into more applications.

Barium Titanate ($BaTiO_3$)

BT is a lead-free ferroelectric material with a perovskite microstructure (see Figure 10) [25]. It has a relatively low Curie temperature as compared to other ferroelectric materials of 105°C, but it possesses a relatively high piezoelectric constant [28]. This makes it ideal for a high-performance lead-free energy harvester with a relatively low operating temperature [25].

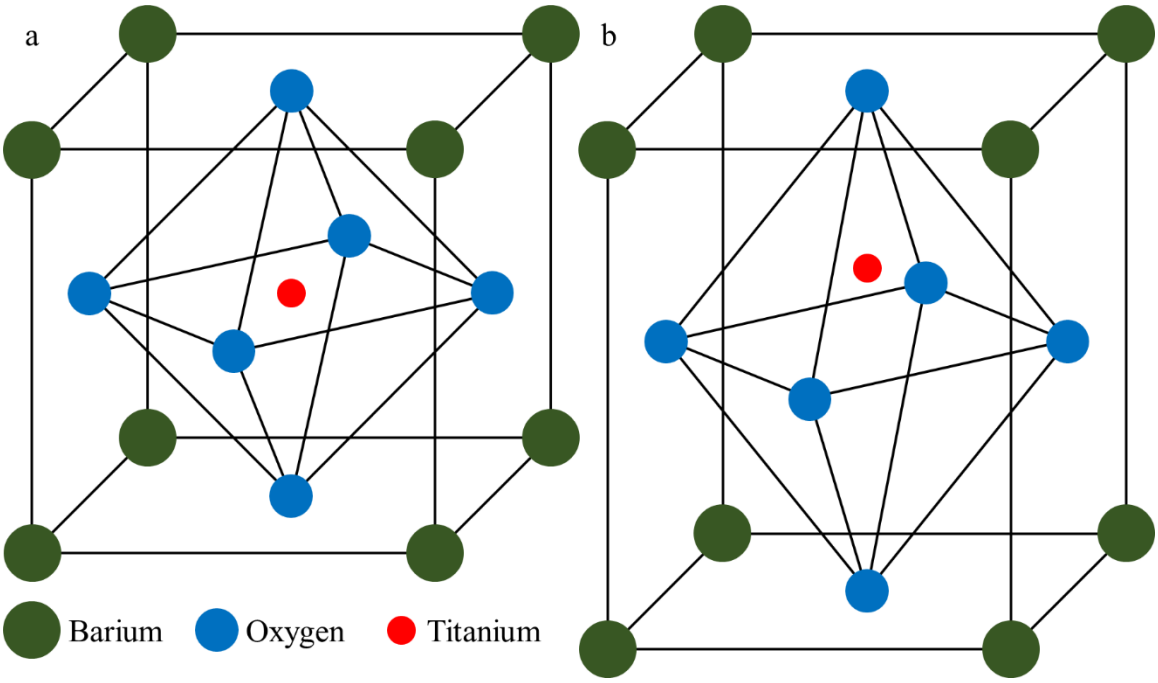

Figure 10. The microstructure of barium titanate showing (a) the symmetry at temperatures greater than the Curie temperature, and (b) the lack of symmetry and displacement of the titanium ion at temperature lower than the Curie temperature.

Zinc Oxide (ZnO)

ZnO is a lead-free semiconductor with a wurtzite microstructure (see Figure 11) that is used frequently in solar cells for the n-type layer [31-32]. Therefore, a composite that uses ZnO as the third component could be incorporated into a solar cell to harvest both the light energy from the sun, as well as vibrational energy from the surrounding environment. In addition, ZnO is also a weak piezoelectric due to its microstructure consisting of alternating layers of negatively charge oxygen ions and positively charged zinc ions (see Figure 11b). These layers of alternating charges are what create an electric dipole within the microstructure.

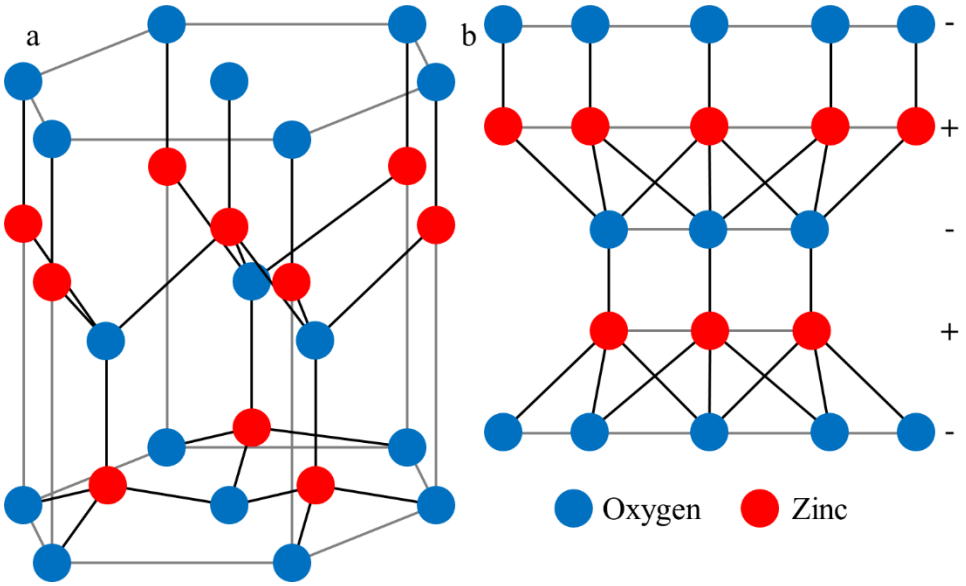

Figure 11. (a) A depiction of the Wurtzite microstructure of zinc oxide, and (b) a front view of the microstructure showing the alternating planes of differently charged ions.

METHODOLOGY

Three-phase multifunctional composites were fabricated using a solution-based technique. The ferroelectric material was micron-sized BT particles, the polymer matrix was a two-part epoxy (Ep), and the third inclusion was nano-sized ZnO particles. The BT particles varied from 1 μm to 4 μm, whereas the ZnO particles varied from 40 nm to 100 nm.

Fabrication Procedure

The volume fraction of BT was held constant at 0.40, the moles of BT and ZnO per liter of solution was held constant at 6.2 mol/L, and the ZnO volume fraction was varied from 0.01 to 0.10 in increments of 0.01. The volume fraction of BT was chosen so that the composites would be mostly epoxy. This provided the composites with a higher flexibility, while also possessing a significant amount of energy harvesting material. Similarly, the volume fractions of ZnO were chosen so that no less than fifty percent of the composites was the epoxy. The ZnO was also incremented so the effect of increasing the third-phase could be determined. The moles of particles per liter of solution was held constant to maintain constant distribution of particles in the solution during fabrication.

The required quantity of ZnO for each volume fraction was measured and added to the required volume of ethanol in a beaker. Parafilm was used to seal the beaker, and the ZnO-ethanol mixture was sonicated for 1 h. After sonication, the required quantity of BT was measured and added to the beaker. The beaker was then sealed with parafilm and sonicated again for 30 min. Afterwards, the required volume of epoxy resin was measured and added to the beaker. The beaker was then sealed and sonicated for 1 h. Finally, the required volume of epoxy hardener was measured and added to the beaker. The beaker was then sealed with parafilm and sonicated for 10 min. The required

quantities used are listed in Table 1, and a schematic of the fabrication procedure is shown in Figure 12.

Table 1. The quantities of zinc oxide, barium titanate, epoxy resin, epoxy hardener, and ethanol used to fabricate each composite based on the volume fraction of zinc oxide (VF of ZnO)

VF of ZnO	0.01	0.02	0.03	0.04	0.05	0.06	0.07	0.08	0.09	0.10
ZnO (g)	0.22	0.45	0.67	0.90	1.12	1.34	1.57	1.79	2.01	2.24
$BaTiO_3$ (g)	9.36	9.36	9.36	9.36	9.36	9.36	9.36	9.36	9.36	9.36
Resin (ml)	2.08	2.05	2.01	1.98	1.94	1.91	1.87	1.84	1.80	1.77
Hardener (ml)	0.28	0.27	0.27	0.26	0.26	0.25	0.25	0.25	0.24	0.24
Ethanol (ml)	5.98	6.55	7.13	7.70	8.28	8.85	9.43	10.0	10.6	11.2

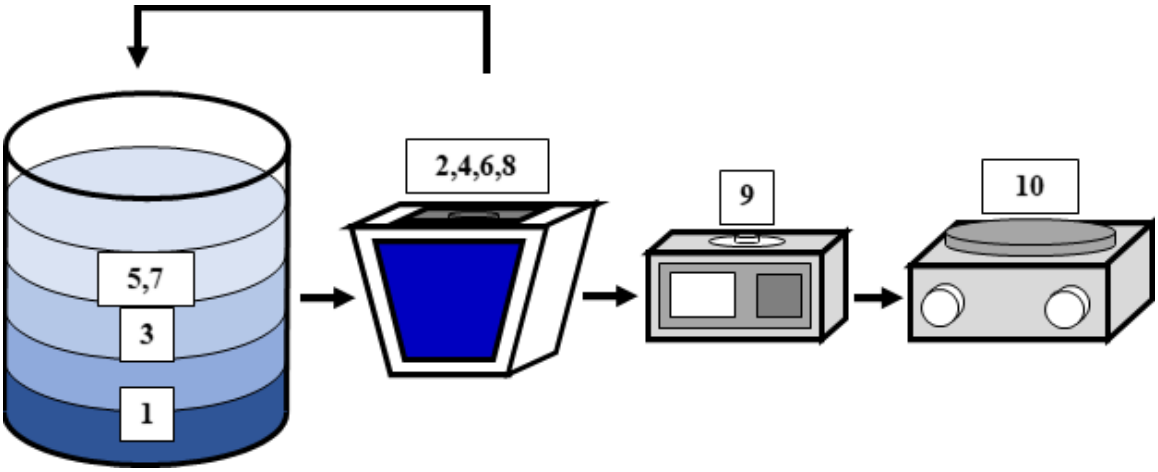

Figure 12. A schematic of the fabrication procedure: (1) addition of ethanol and ZnO to a beaker, (2) sonication for 1 h, (3) addition of BT to the beaker, (4) sonication for 30 min, (5) addition of epoxy resin to beaker, (6) sonication for 1 h, (7) addition of epoxy hardener to the beaker, (8) sonication for 10 min, (9) spin-coating of 1 ml of solution onto stainless steel substrates for 2 min, and (10) curing of composites on a hot plate for 8 h.

After the final sonication, 1 ml of the solution was applied to a 24 mm x 24 mm x 0.10 mm flexible stainless-steel substrate and allowed to rest for 1.5 min. The solution was then spincoated at 800 rpm for 2 min, and the completed samples were cured for 8 h

at 75°C on a hot plate. A modified Ultravolt high voltage generator was used to pole the composites using a contactless corona plasma discharge method at a voltage of 4.6 kV.

Measurementation and Post Processing

A Keysight E4990A Impedance Analyzer was used to test the electrical and dielectric properties of the composites from a frequency range of 20 Hz to 10 MHz. The composites were clamped between a point electrode and a plane electrode using the electrode setup provided by Keysight; the stainless-steel substrates were in contact with the plane electrode, and the dial on the setup was turned until a specific force was applied; the same force was applied to all samples. Furthermore, a Piezotest PiezoMeter System PM300 was used to test the piezoelectric strain coefficients at a frequency of 110 Hz and with a force of 3.5 N. A VEGA3 TESCAN scanning electron microscope (SEM) was used to analyze the surface morphology and the particle distribution.

ImageJ was used to count the total number and to calculate the cross-sectional area of the exposed particles in the SEM micrographs. A MATLAB program was then used to count the number of particles with a cross-sectional area of 0.050 μm^2 or less, which corresponds to ZnO agglomerations based on the approximate diameter of the ZnO nanoparticles provided by the manufacturer. The MATLAB program then calculated the percentage of ZnO agglomerations by using Equation 1:

$$\%\ ZnO\ Agglomerations = N_{ZnO}/N_{Part} \qquad \textbf{Equation 1}$$

where N_{ZnO} is the number of ZnO agglomerations and N_{Part} is the total number of particles.

An additional MATLAB program was used to group, normalize, and graph the electrical data. All MATLAB programs used are provided in the Appendices.

RESULTS AND DISCUSSION

Figure 13 shows a few of the final fabricated composites that were poled and ready for testing. Figure 14 shows the relative size of the composites with respect to a nickel; the composites are 24 mm x 24 mm squares and 36 µm thick. Figure 15 shows the flexibility of the fabricated composites.

Figure 13. Some of the final fabricated and poled samples ready for testing.

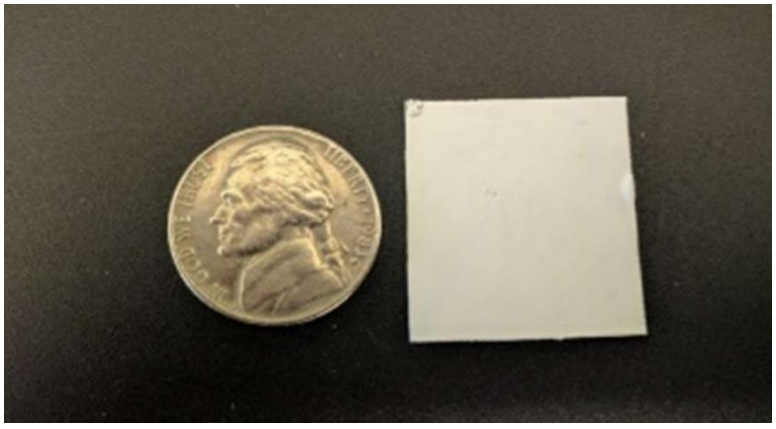

Figure 14. The relative size of the composites as compared to a nickel.

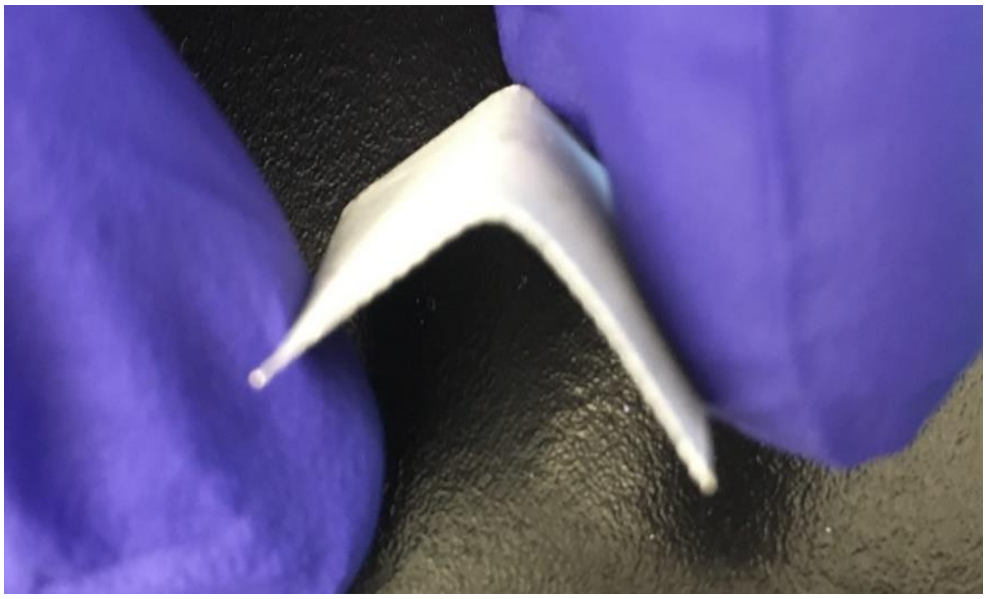

Figure 15. A demonstration of the flexibility of the composites (shows a 90° bend).

Electrical Properties (20 Hz to 10 MHz)

The data from the electrical and dielectric testing shows that the impedance (magnitude), resistivity, and dielectric constant of the composites decrease as frequency increases from 20 Hz to 10 MHz (see Figures16, 17, and 19); in addition, the conductivity of the composites increases as frequency increases (see Figure 18). These relationships hold true for all volume fractions of ZnO. These relationships are also consistent with what is expected. At higher frequencies, the impedance analyzer is applying more energy to the composites which would make it easier for the electrons to flow. Therefore, it is expected that the impedance and resistivity would decrease with increasing frequency, which matches the results. In addition, it is expected that the conductivity of the composites would increase with increasing frequency, which also matches the results, and the inverse relationship between resistivity and conductivity can be easily seen in Figures 17 and Figure 18.

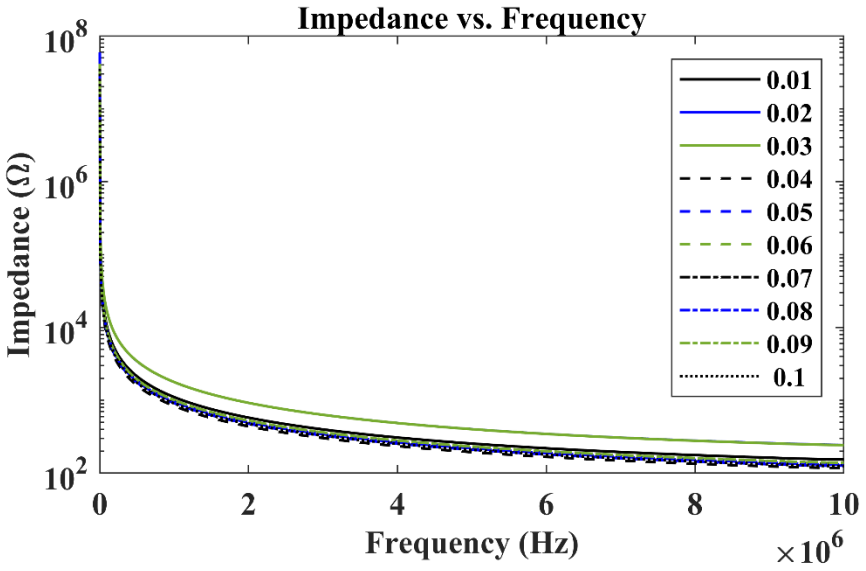

Figure 16. The average impedance of the composites for each volume fraction of zinc oxide with respect to frequency.

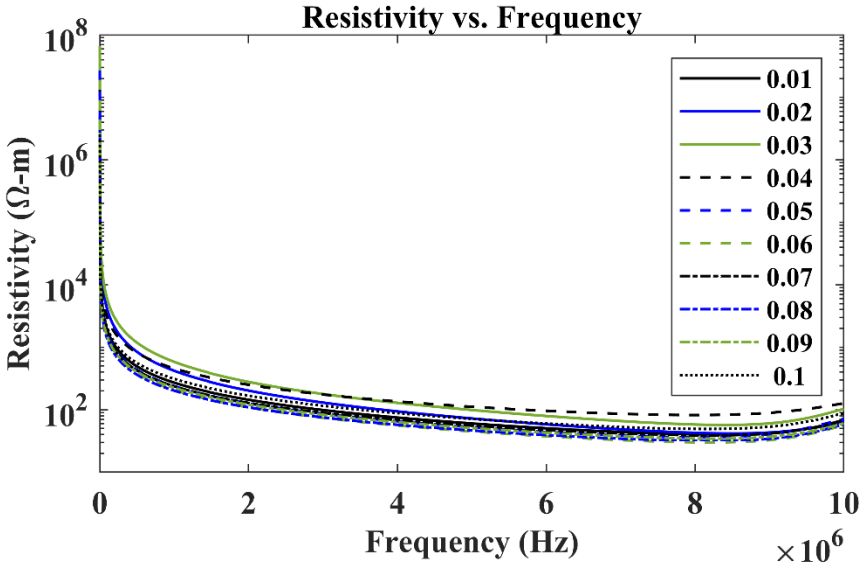

Figure 17. The average resistivity of the composites for each volume fraction of zinc oxide with respect to frequency.

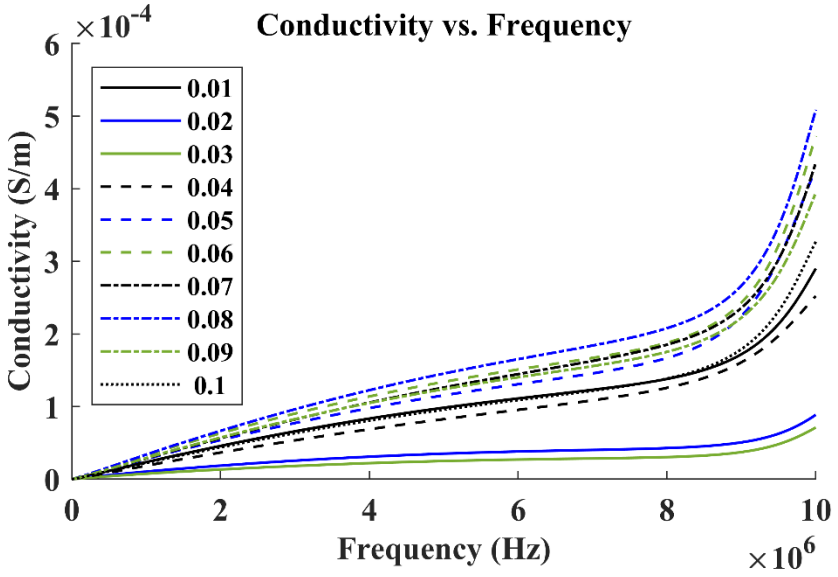

Figure 18. The average conductivity of the composites for each volume fraction of zinc oxide with respect to frequency.

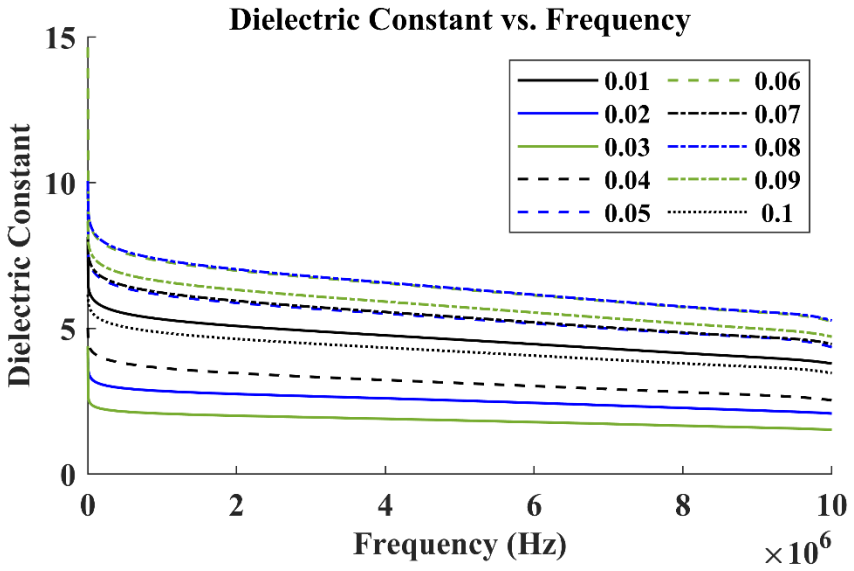

Figure 19. The average dielectric constant of the composites for each volume fraction of zinc oxide with respect to frequency.

Electrical Properties (1 MHz)

Figures 20-23 show the relationship between the electrical and dielectric properties and the volume fractions of ZnO of the composites at a frequency of 1 MHz. At this frequency, the impedance (magnitude) increases from 1106 Ω to 1778 Ω, the resistivity increases from 270.9 Ω-m to 583.5 Ω-m, the conductivity decreases from 0.2347×10^{-5} S/m to 7.507×10^{-6} S/m, and the dielectric constant decreases from 5.313 to 2.078 when the volume fraction increases from 0.01 to 0.03. For volume fractions larger than 0.03, however, the electrical and dielectric performance of the composites return to near the performance of the composites with a volume fraction of 0.01. For example, Figures 20-23 show that at these higher volume fractions, the average impedance (magnitude) is 938.0 Ω, the average resistivity is 268.1 Ω-m, the average conductivity is 2.754 x 10-5 S/m, and the average dielectric constant is 6.020. These averages are less than 20% different than the values for a volume fraction of 0.01. These regressions in the electron transport properties are a result of the interactions of the three-phases in the composites; more specifically, the interactions between the other phases and the ZnO nanoparticles. Since the quantity of ZnO nanoparticles varies the most for all volume fractions of ZnO tested, the contact resistances between the ZnO and the BT (ZnO-BT) and between the ZnO and the epoxy (ZnO-Ep) vary the most. Conversely, since the volume fraction of BT is constant, the contact resistance between the BT and the epoxy (BT-Ep) is constant. Therefore, at the smaller volume fractions of ZnO (i.e. volume fractions at or below 0.03), the number of contact points within the composites increases with increasing volume fractions of ZnO (see Figure 24); in return, the higher number of contact points increases the ZnO-BT and the ZnO-Ep contact resistances, as well as the impedance and resistivity of the composites as a whole. At higher volume fractions of ZnO, however, the ZnO nanoparticles agglomerate more frequently, which significantly reduces the number of contact points within the composites (see Figure 24). This

reduction in the number of contact points causes the impedance (magnitude) and resistivity of the composites to regress to a state very near the performance of the 0.01 volume fraction composites. This similarity in performance is a result of the 0.01 volume fraction composites and the higher volume fraction composites having a similar number of contact points.

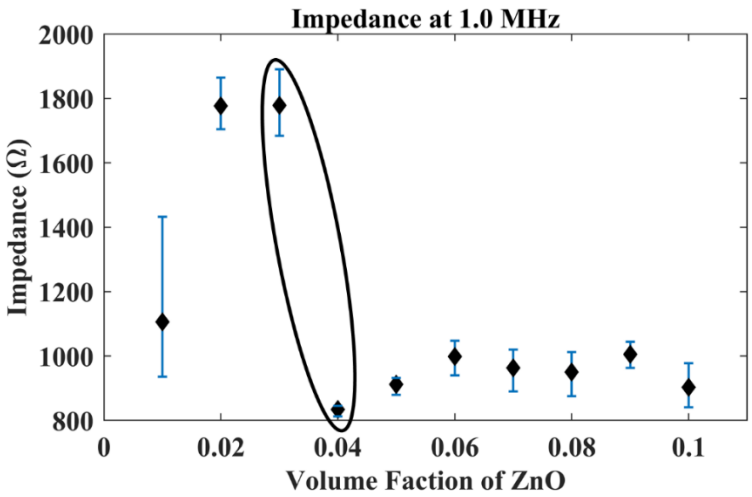

Figure 20. The average impedance (magnitude) of the composites for each volume fraction of zinc oxide at a frequency of 1 MHz.

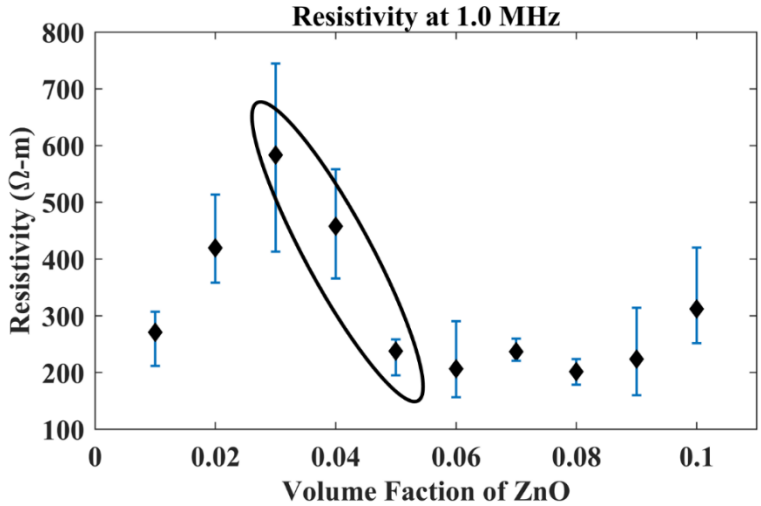

Figure 21. The average resistivity of the composites for each volume fraction of zinc oxide at a frequency of 1 MHz.

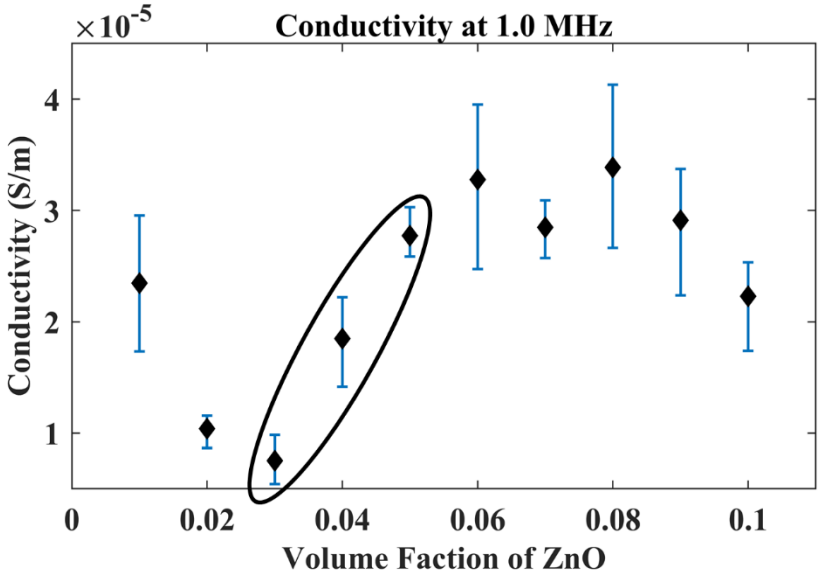

Figure 22. The average conductivity of the composites for each volume fraction of zinc oxide at a frequency of 1 MHz.

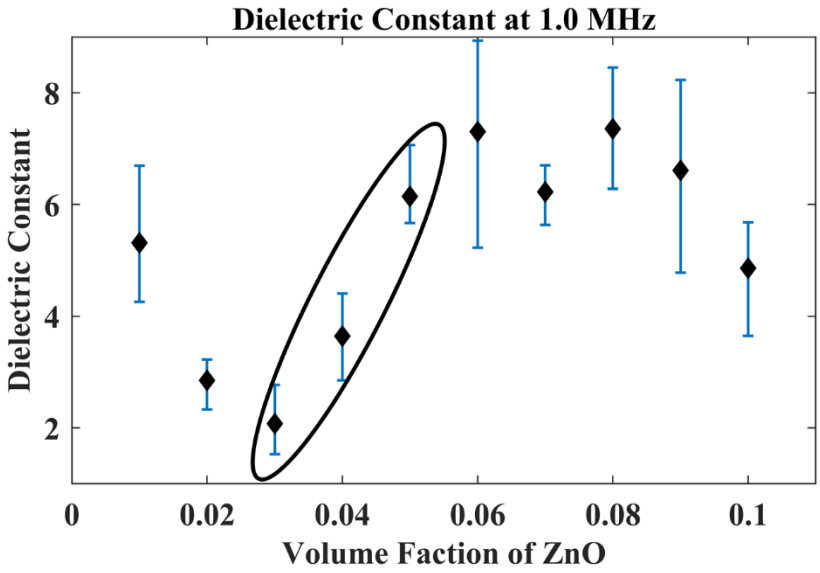

Figure 23. The average dielectric constant of the composites for each volume fraction of zinc oxide at a frequency of 1 MHz.

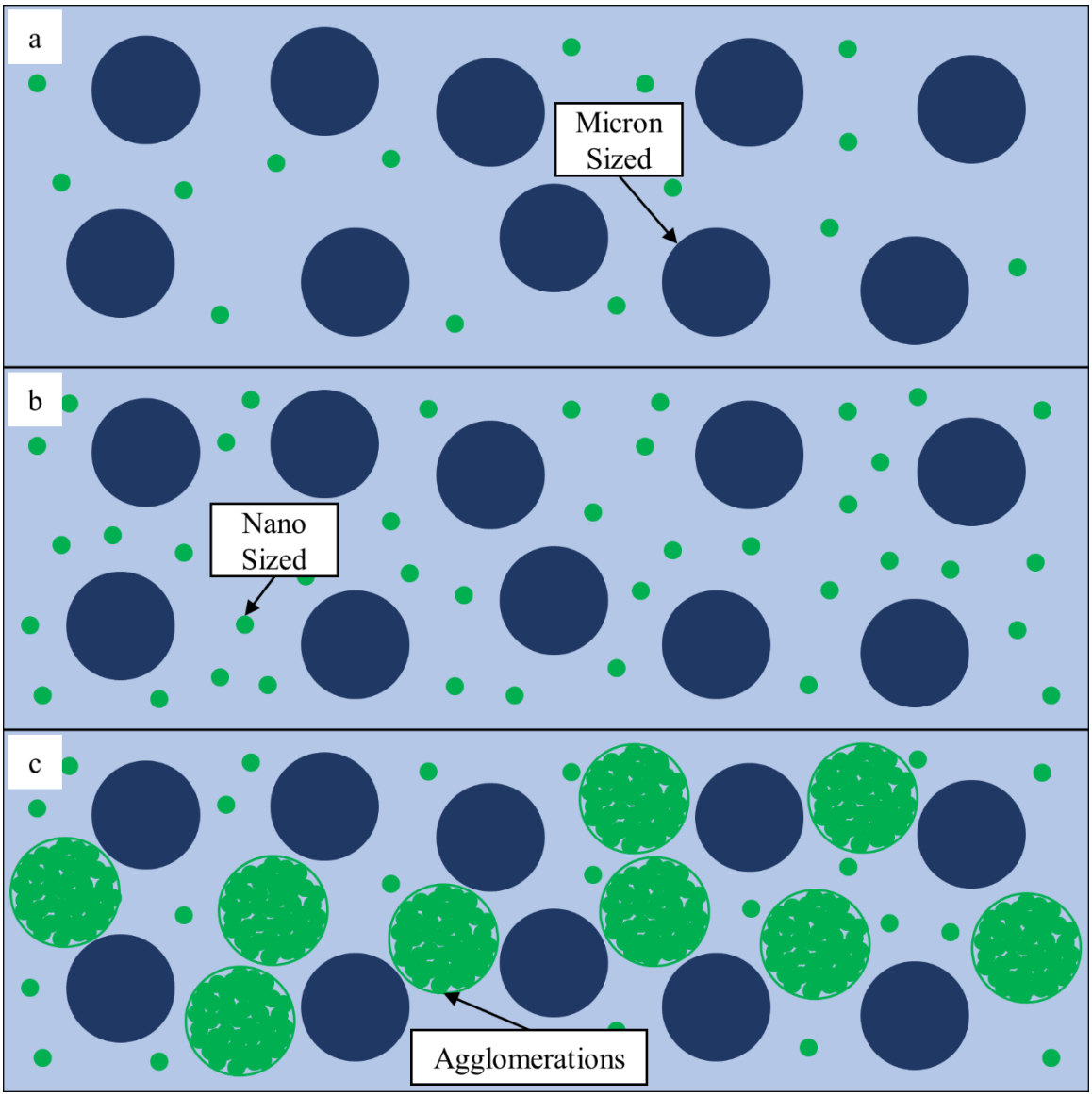

Figure 24. A depiction of how the number of contact points decreases within the composites with (a) a small volume fraction of zinc oxide and a small number of contact points (i.e. volume fraction of 0.01), (b) a small volume fraction of zinc oxide and a large number of contact points (i.e. a volume fraction of 0.03), and (c) a large volume fraction of zinc oxide and a small number of contact points (i.e. volume fraction of 0.10).

In addition, due to the inverse relationship between resistivity and conductivity, the conductivity of the composites follows the same trend as the resistivity but inversed (see Figure 22). The conductivity of the composites decreases as the volume fraction of ZnO increases from 0.01 to 0.03 and then regress, thereafter, to a state very near the

performance of the 0.01 volume fraction composites. The dielectric constant also follows this trend due to the nature of the effective (complex) relative permittivity of composites which is given by Equation 2 [33]:

$$\varepsilon_e^* = \varepsilon' - j\varepsilon_e'' \qquad \textbf{Equation 2}$$

where ε_e^* is the effective (complex) relative permittivity, ε' is the dielectric constant, and ε_e'' is the effective dielectric loss. Equation 2 is comparable to the relative complex permittivity equation (Equation 3) [33]:

$$\varepsilon^* = \varepsilon' - j\varepsilon'' \qquad \textbf{Equation 3}$$

where ε^* is the relative complex permittivity and ε'' is the dielectric loss, except that the effective (complex) relative permittivity equation (Equation 2) does not neglect the static electrical conductivity. Equation 2 accounts for static electrical conductivity by defining the effective dielectric loss as [33]:

$$\varepsilon_e'' = \varepsilon'' + \sigma/\omega\varepsilon_o \qquad \textbf{Equation 4}$$

where σ is the conductivity, ω is the frequency of oscillation of the electric field, and $\varepsilon_o$is the permittivity of a vacuum. Equation 4 can then be substituted into Equation 2 to get Equation 5 [33]:

$$\varepsilon_e^* = \varepsilon' - j(\varepsilon'' + \sigma/\omega\varepsilon_o) \qquad \textbf{Equation 5}$$

which can then be rearranged to solve for the dielectric constant to get Equation 6:

$$\varepsilon' = \varepsilon_e^* + j(\varepsilon'' + \sigma/\omega\varepsilon_o) \qquad \textbf{Equation 6}$$

which shows that the dielectric constant has a proportional relation with the effective (complex) relative permittivity, the dielectric loss, and the conductivity. Therefore, it follows that if the conductivity of the composites increases, then the dielectric constant of the composites would increase as well, which can be seen in Figures 22 and 23. Figures 18 and 19, however, appear to show the opposite with the conductivity increasing and the dielectric constant decreasing as the frequency increases. This is because the dielectric constant is inversely proportional to the frequency of oscillation (see Equation 6) which shows that the frequency of oscillation has a greater influence on the dielectric constant than the conductivity.

Piezoelectric Strain Coefficients (d_{33} and d_{31})

The piezoelectric strain coefficient, d_{33}, of the composites follows a similar trend. Figure 25 shows that d_{33} increases from 0.120 pC/N to 0.168 pC/N when the volume fraction increases from 0.01 to 0.03. For volume fractions greater than 0.03, d_{33} values drop close to the piezoelectric properties for a volume fraction of 0.01. The average of the d_{33}'s for the larger volume fractions is 0.118 pC/N which is a percent difference of 1.67%. Figure 26 shows that d_{31} of the composites are mostly similar except for volume fractions of 0.02 and 0.05. The average of the d_{31}'s for all volume fractions is 0.154 pC/N and the standard deviation is 0.091 pC/N.

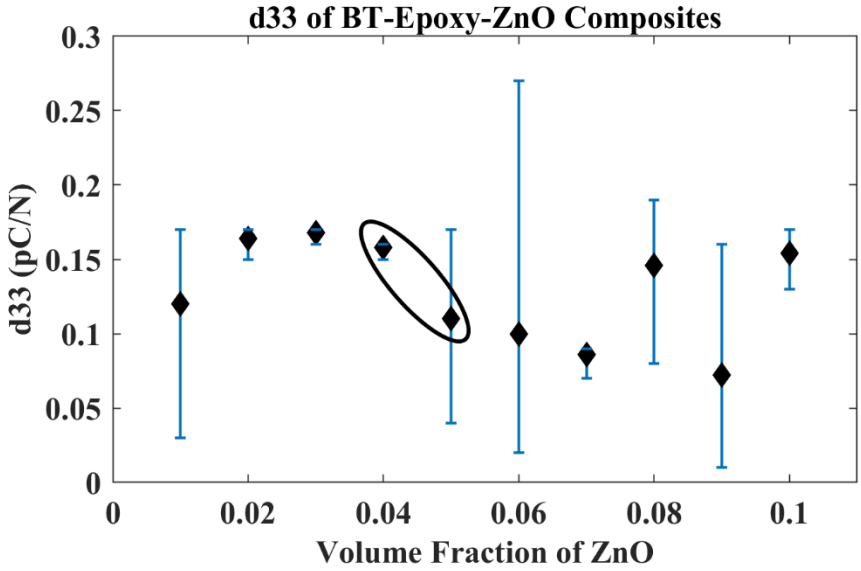

Figure 25. The average piezoelectric strain coefficient, d_{33}, for each volume fraction of zinc oxide.

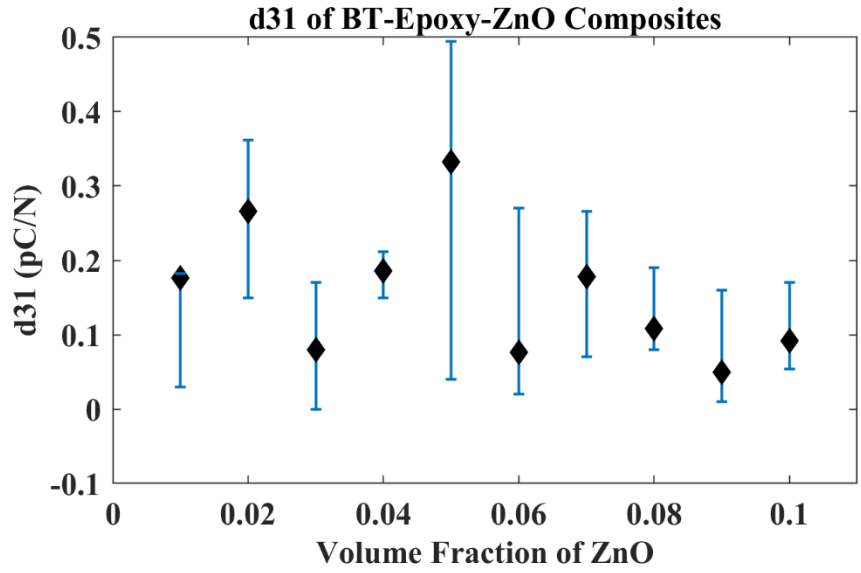

Figure 26. The average piezoelectric strain coefficient, d_{31}, for each volume fraction of zinc oxide.

Scanning Electron Microscope Micrographs

Figures 27-36 show the SEM micrographs of the surface of the composites; they were taken at a voltage of 30 kV, a working distance of 7.50 mm, and a magnification of 40 kx. Figures 37-46 are micrographs of the fractured surface of the composites; they

were taken at a voltage of 30 kV, a working distance of 7.50 mm, and a magnification of 53.3 kx; however, the composite with a volume fraction of 0.03 is an exception, since it was taken at a magnification of 80.0 kx.

Figures 27-36 were used to analyze the particle distribution on the surface of the composites. A visual inspection of the composites shows that the nano-sized ZnO particles are rare in the micrographs of volume fractions that are 0.03 or less and common in the micrographs of volume fractions that are larger than 0.03; Figure 47 provides examples of how the ZnO agglomerations and the BT particles appear in the SEM micrographs, and post-processing of these images with ImageJ validates this relationship.

Figures 37-46 were used to determine if the agglomerations of ZnO nanoparticles were present throughout the composites and that the agglomerations increased in frequency. A visual inspection of the composites confirms that the agglomerations are present, and that they increase with increasing volume fractions of ZnO.

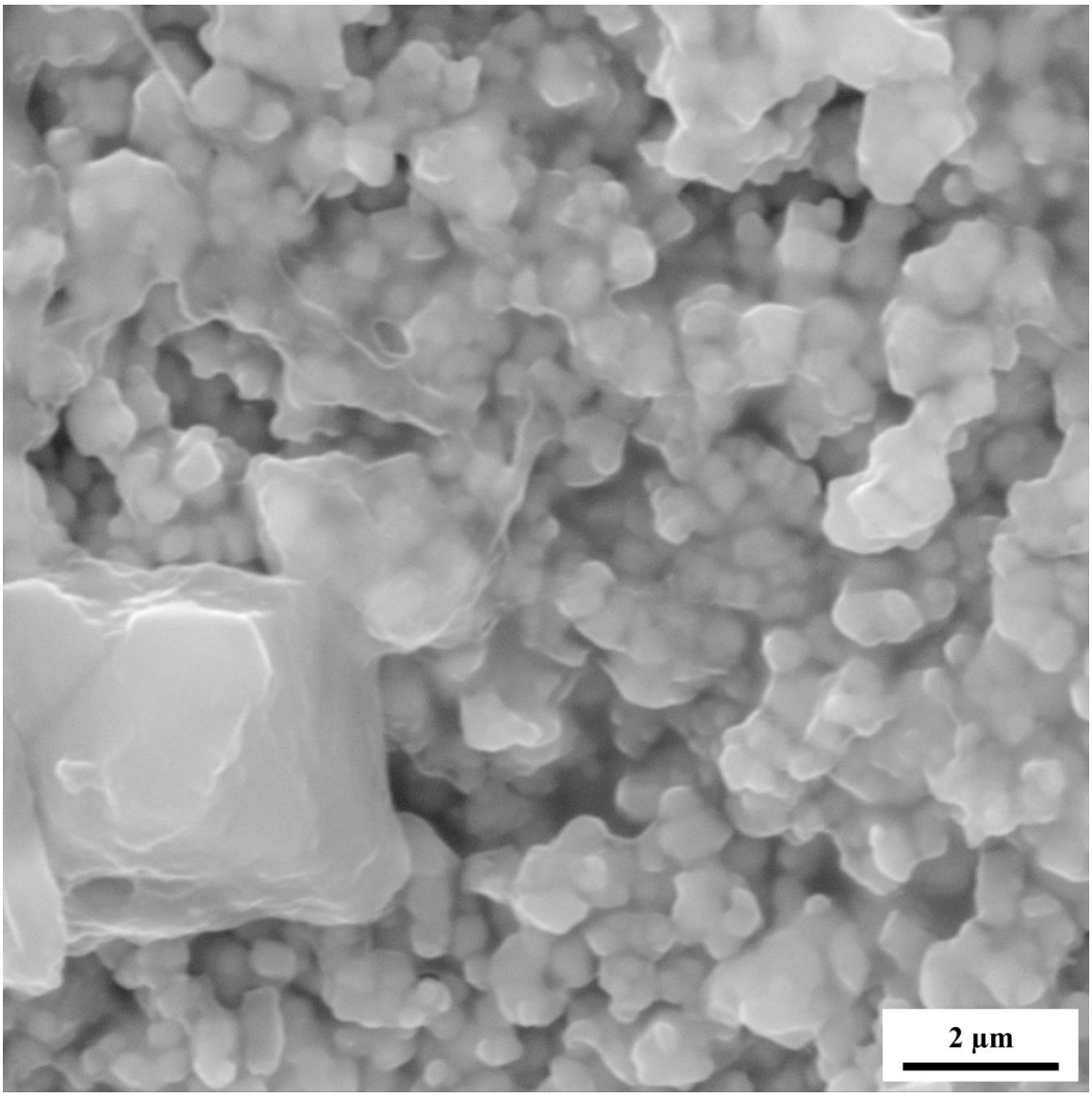

Figure 27. SEM micrograph of the surface of a composite with a volume fraction of zinc oxide of 0.01 at a magnification of 40.0 kx, a working distance of 7.50 mm, and voltage of 30.0 kV.

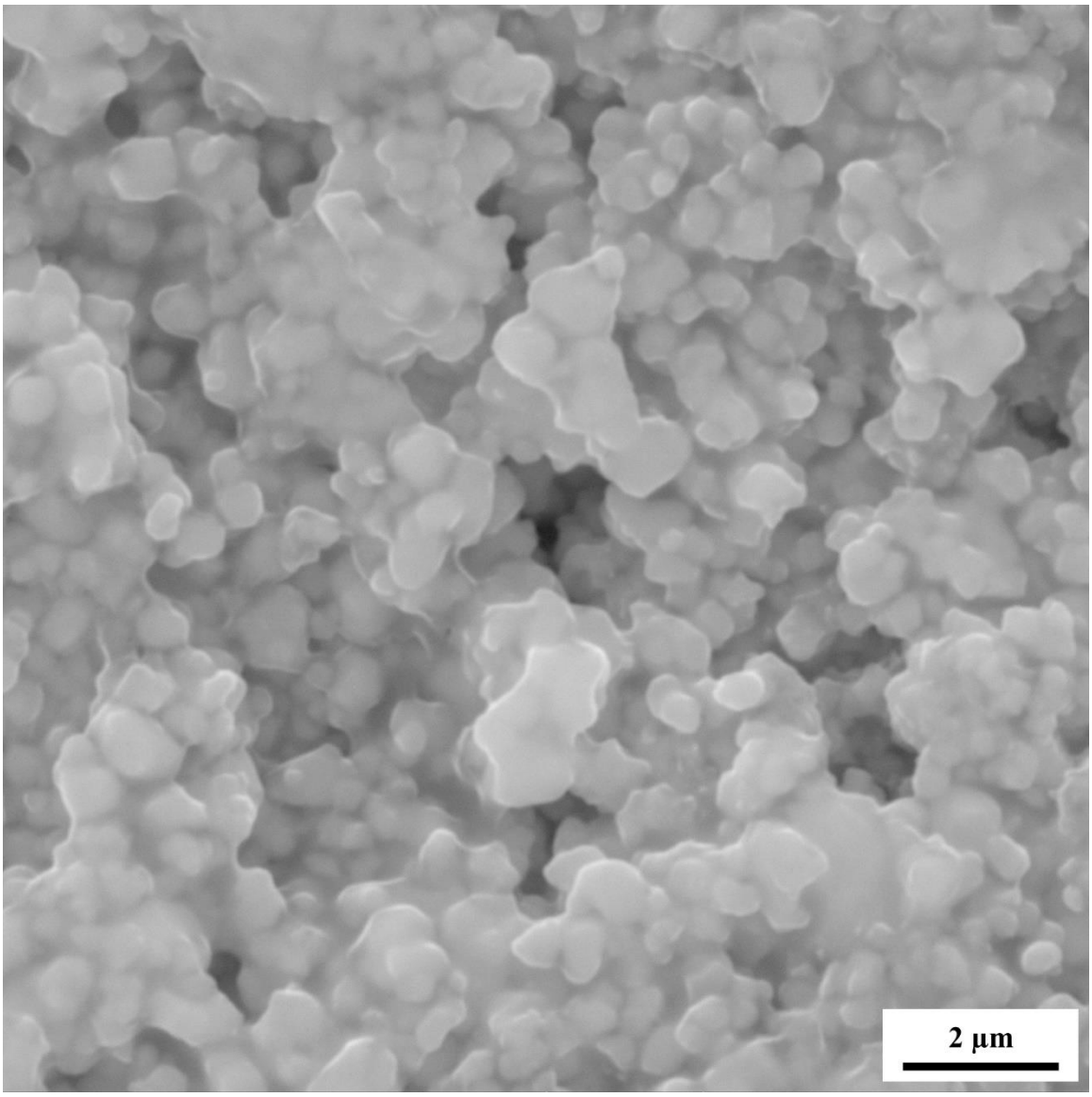

Figure 28. SEM micrograph of the surface of a composite with a volume fraction of zinc oxide of 0.02 at a magnification of 40.0 kx, a working distance of 7.50 mm, and voltage of 30.0 kV.

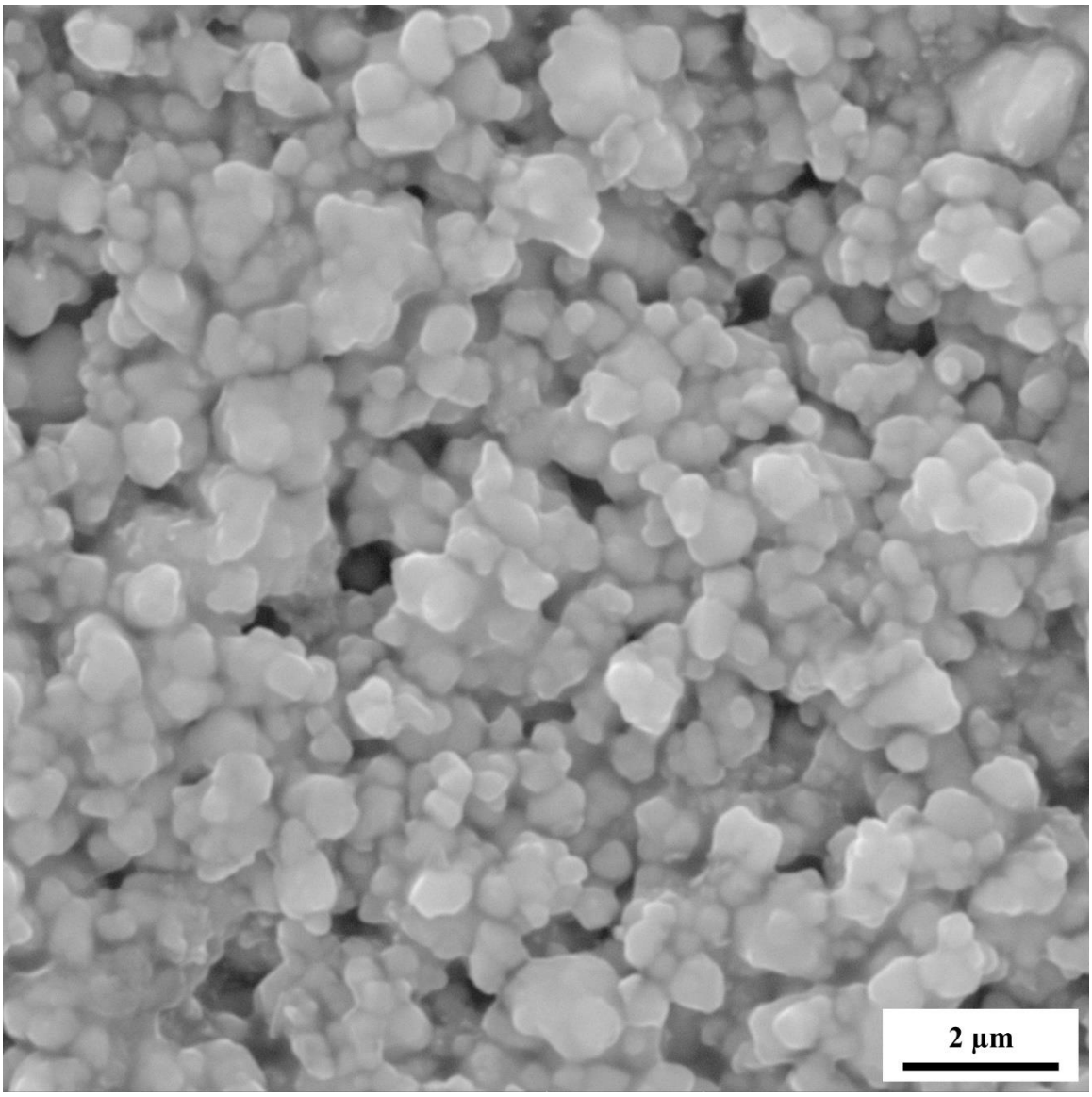

Figure 29. SEM micrograph of the surface of a composite with a volume fraction of zinc oxide of 0.03 at a magnification of 40.0 kx, a working distance of 7.50 mm, and voltage of 30.0 kV.

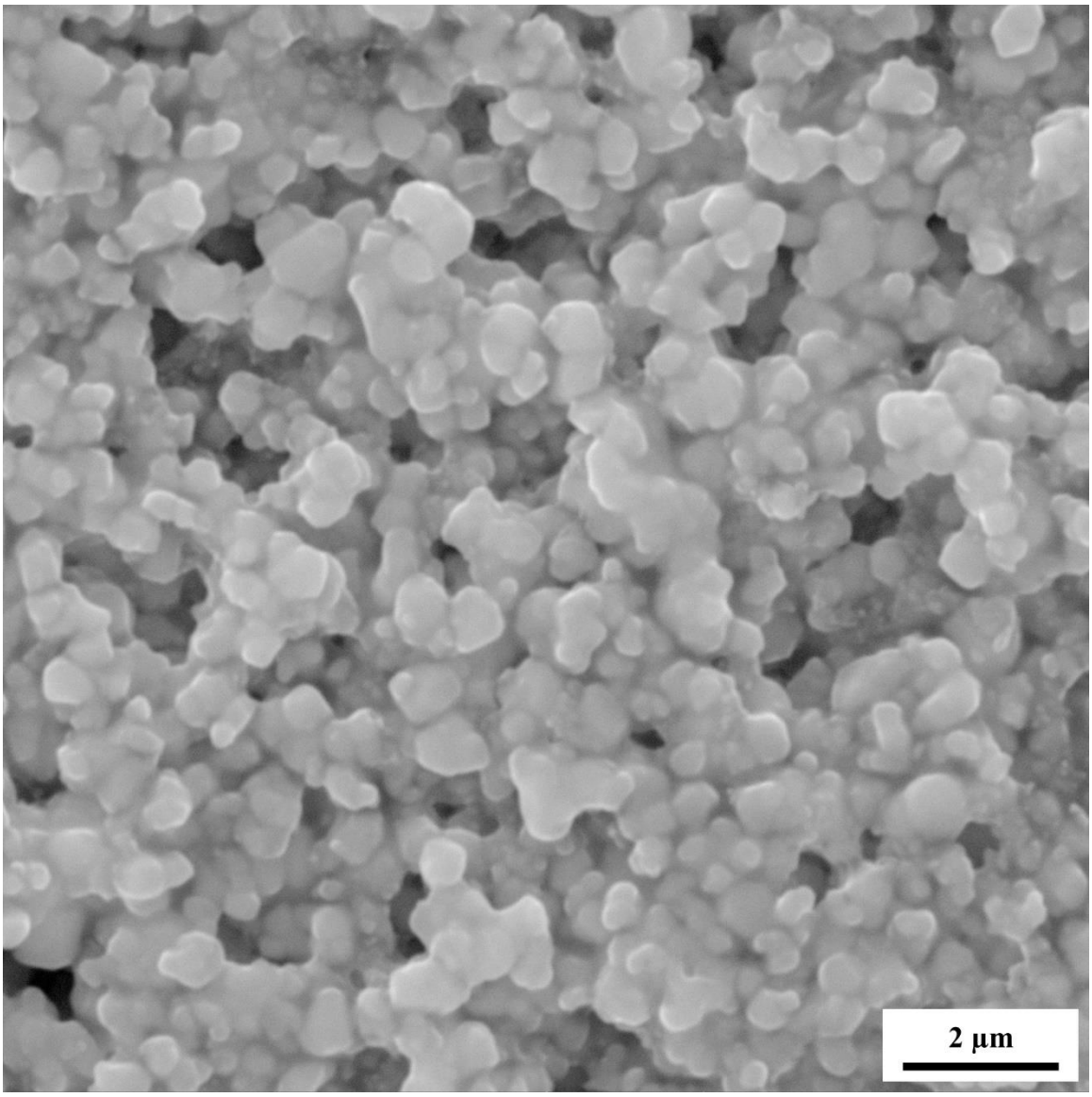

Figure 30. SEM micrograph of the surface of a composite with a volume fraction of zinc oxide of 0.04 at a magnification of 40.0 kx, a working distance of 7.50 mm, and voltage of 30.0 kV.

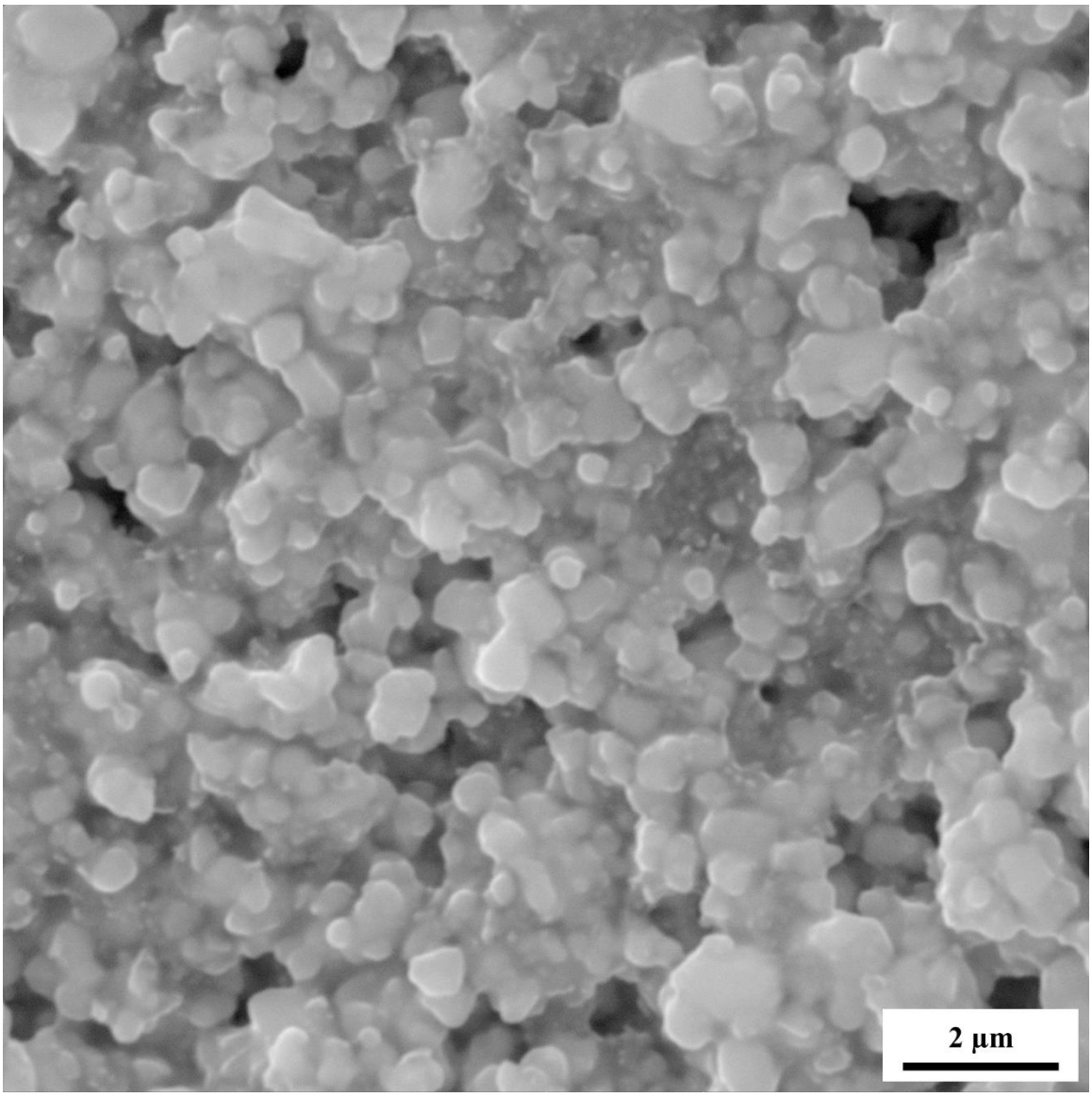

Figure 31. SEM micrograph of the surface of a composite with a volume fraction of zinc oxide of 0.05 at a magnification of 40.0 kx, a working distance of 7.50 mm, and voltage of 30.0 kV.

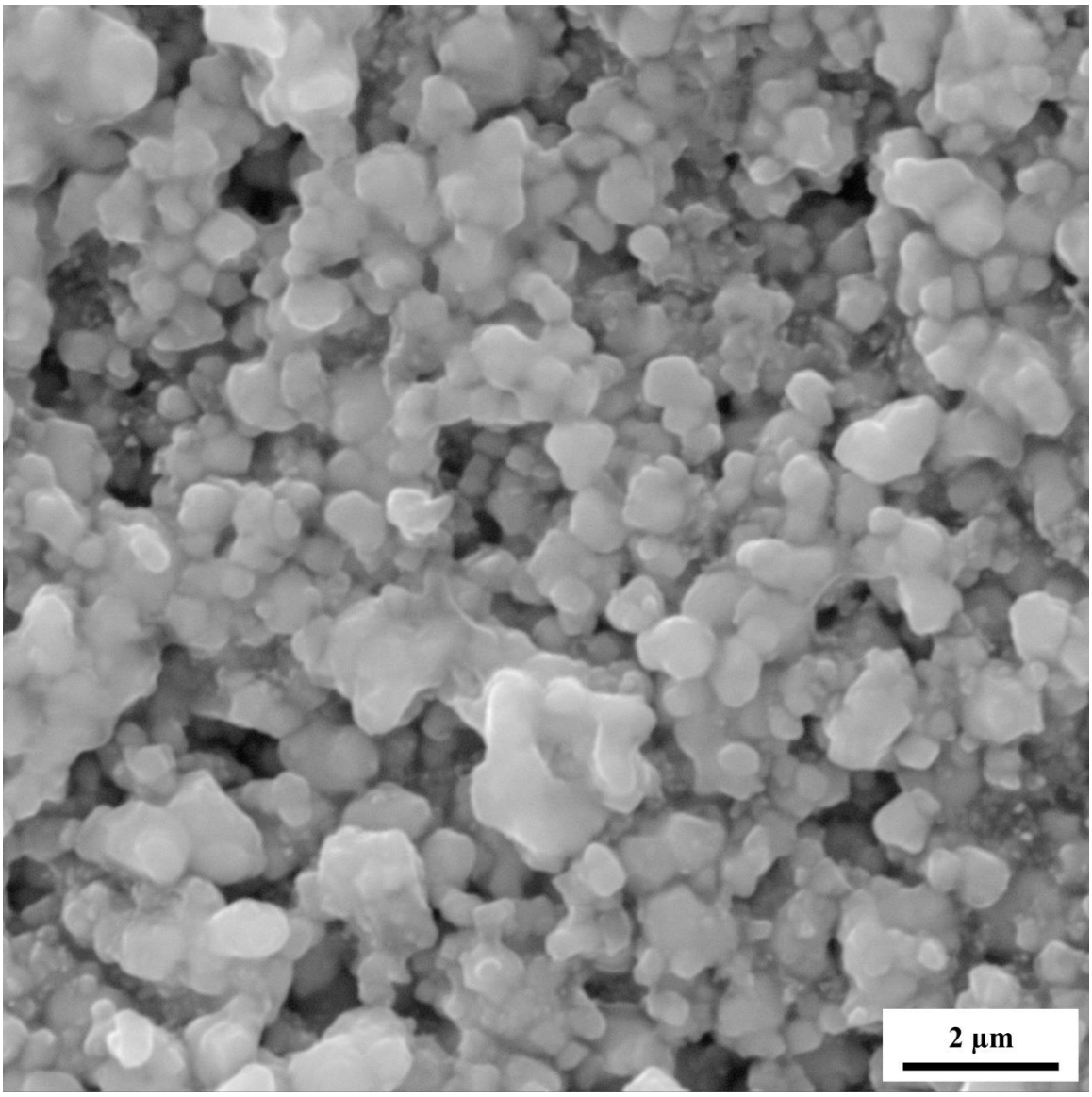

Figure 32. SEM micrograph of the surface of a composite with a volume fraction of zinc oxide of 0.06 at a magnification of 40.0 kx, a working distance of 7.50 mm, and voltage of 30.0 kV.

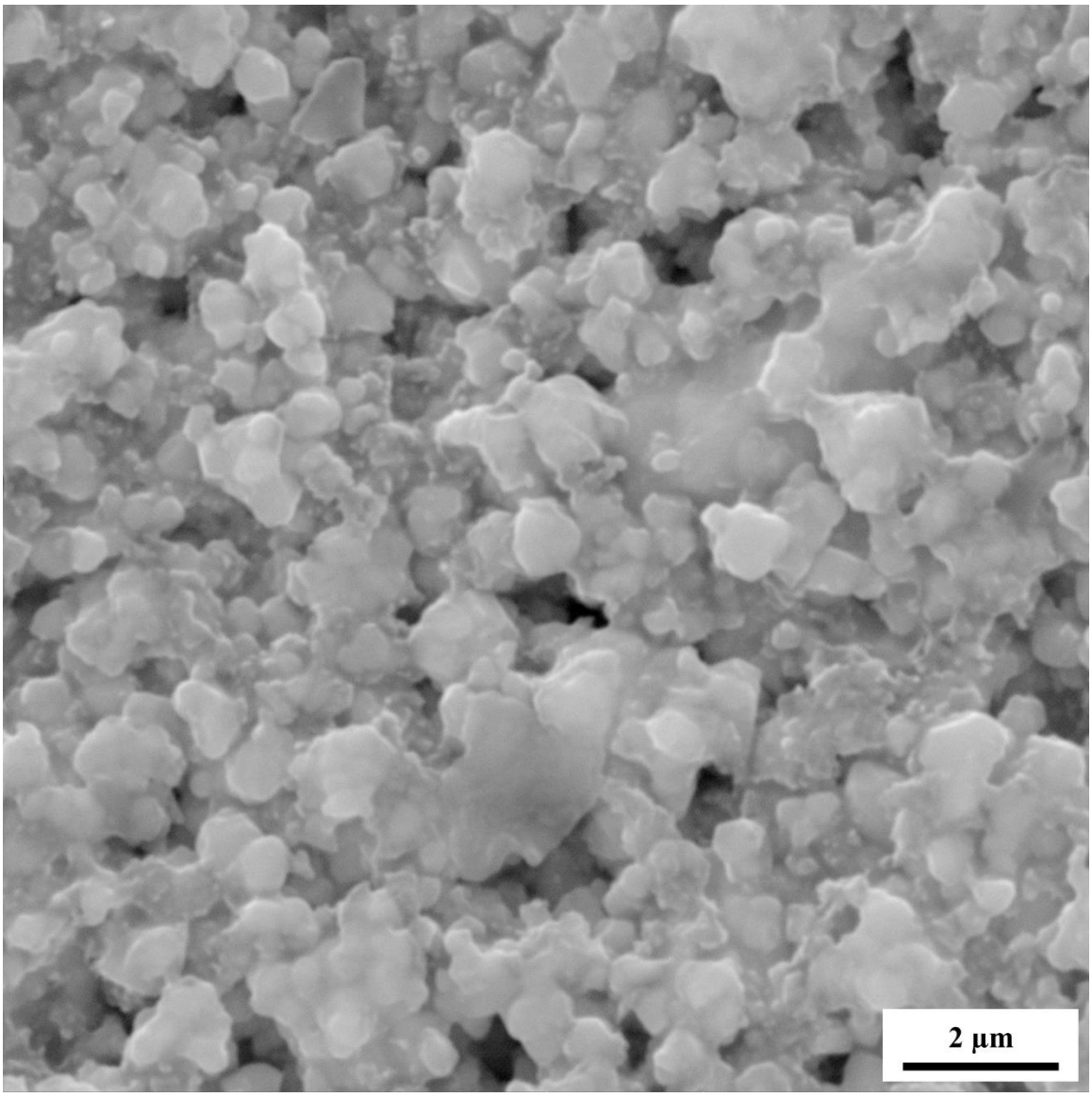

Figure 33. SEM micrograph of the surface of a composite with a volume fraction of zinc oxide of 0.07 at a magnification of 40.0 kx, a working distance of 7.50 mm, and voltage of 30.0 kV.

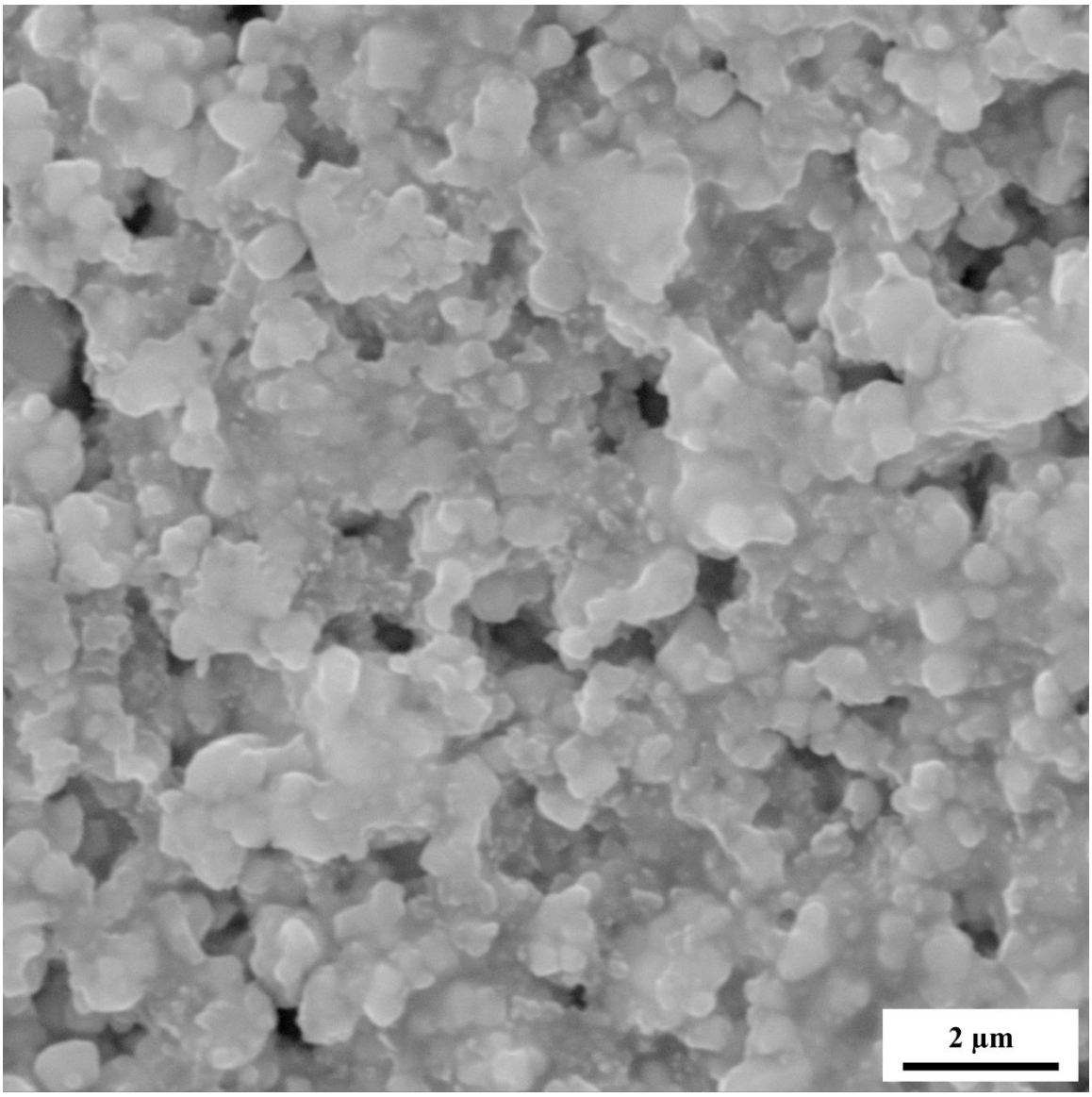

Figure 34. SEM micrograph of the surface of a composite with a volume fraction of zinc oxide of 0.08 at a magnification of 40.0 kx, a working distance of 7.50 mm, and voltage of 30.0 kV.

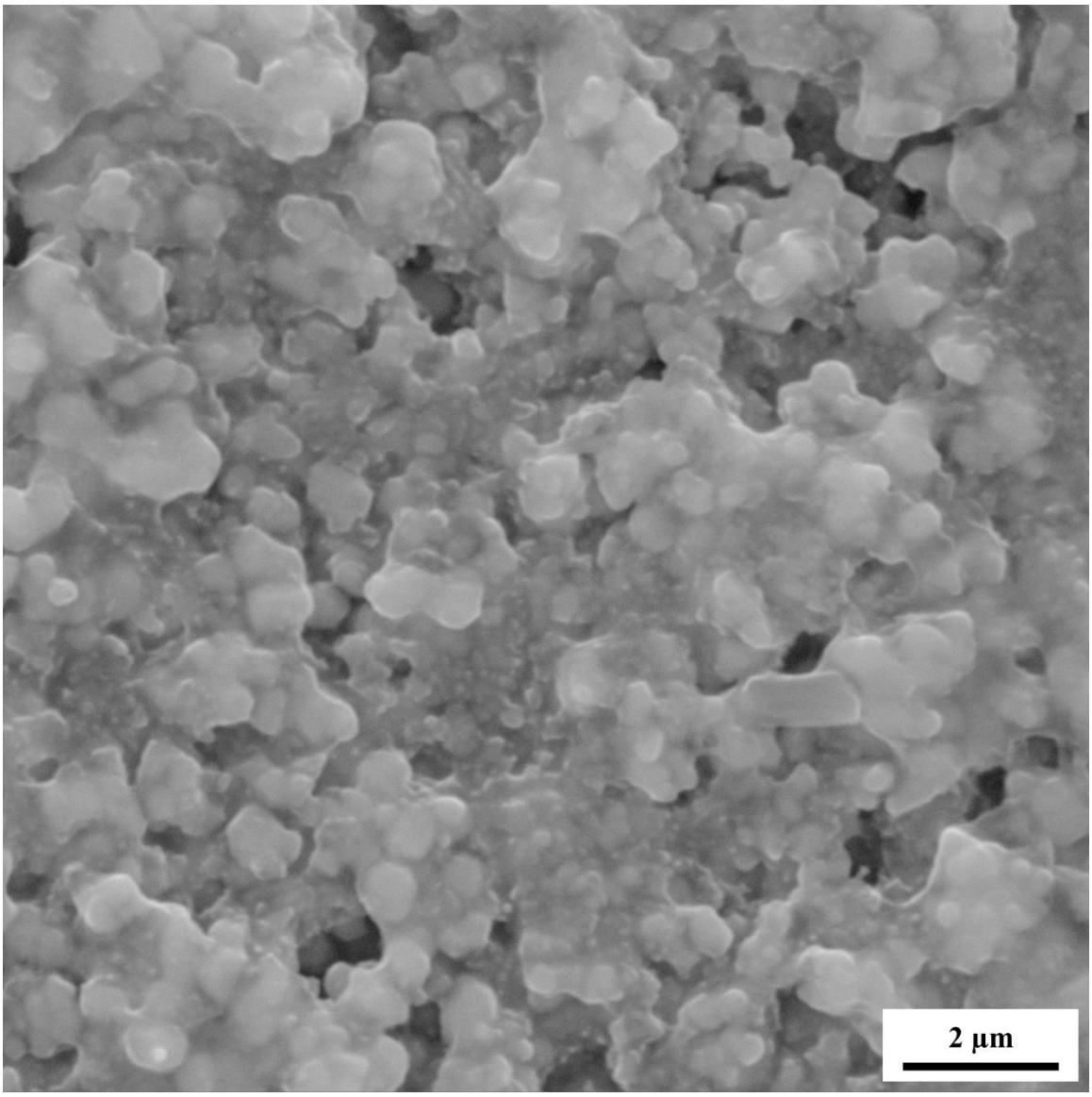

Figure 35. SEM micrograph of the surface of a composite with a volume fraction of zinc oxide of 0.09 at a magnification of 40.0 kx, a working distance of 7.50 mm, and voltage of 30.0 kV.

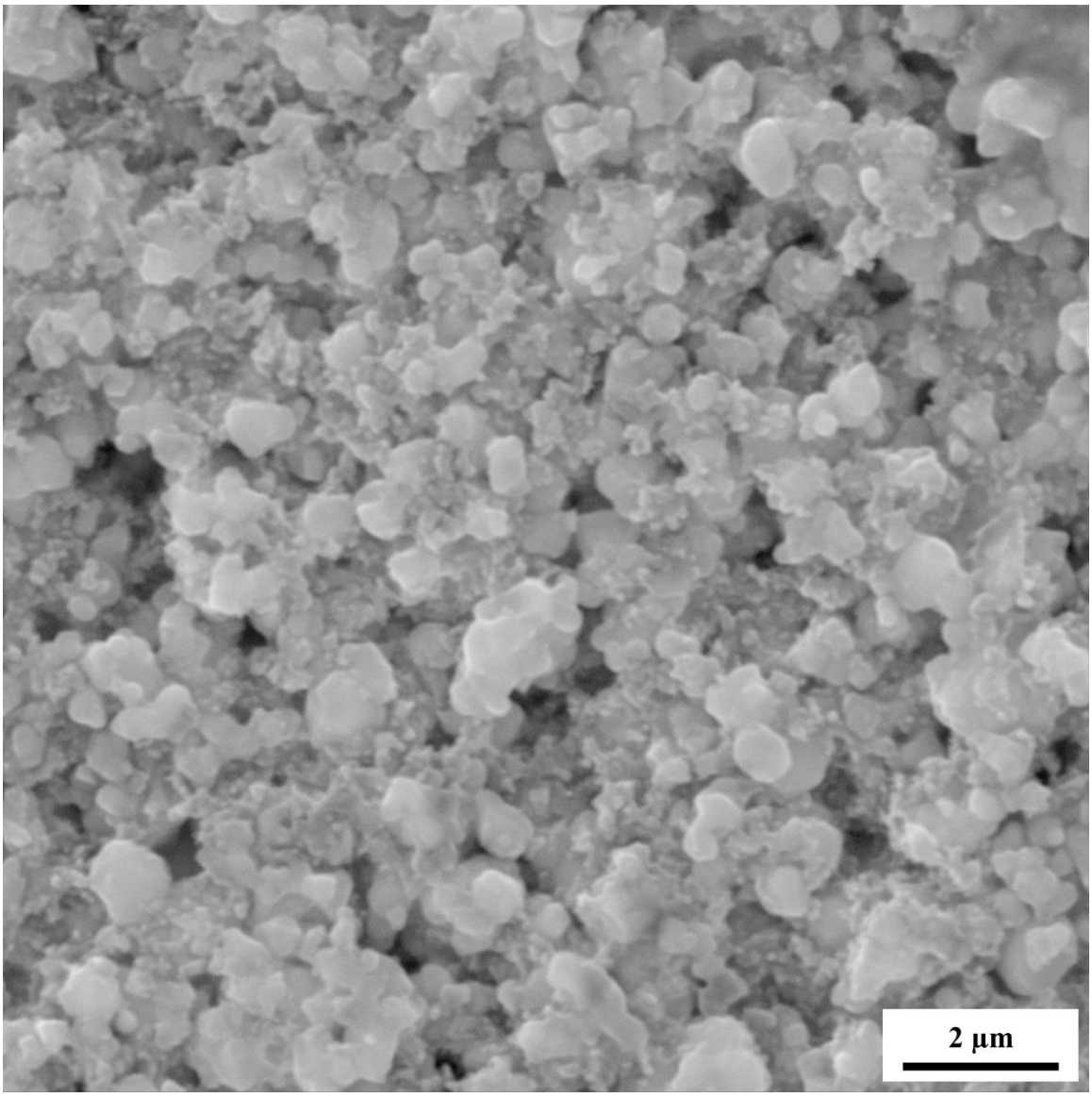

Figure 36. SEM micrograph of the surface of a composite with a volume fraction of zinc oxide of 0.10 at a magnification of 40.0 kx, a working distance of 7.50 mm, and voltage of 30.0 kV.

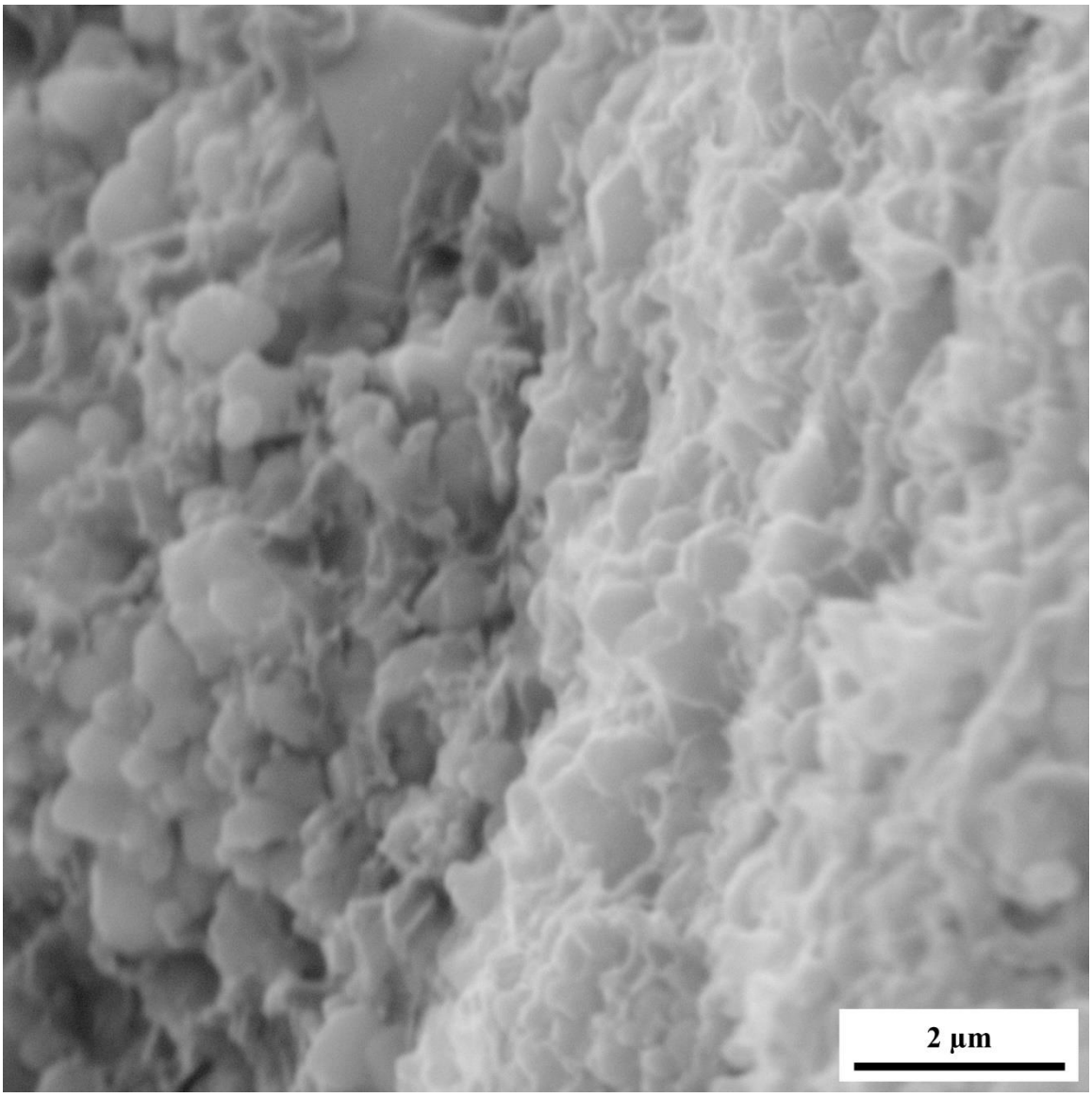

Figure 37. SEM micrograph of the fractured surface of a composite with a volume fraction of zinc oxide of 0.01 at a magnification of 53.3 kx, a working distance of 7.50 mm, and voltage of 30.0 kV.

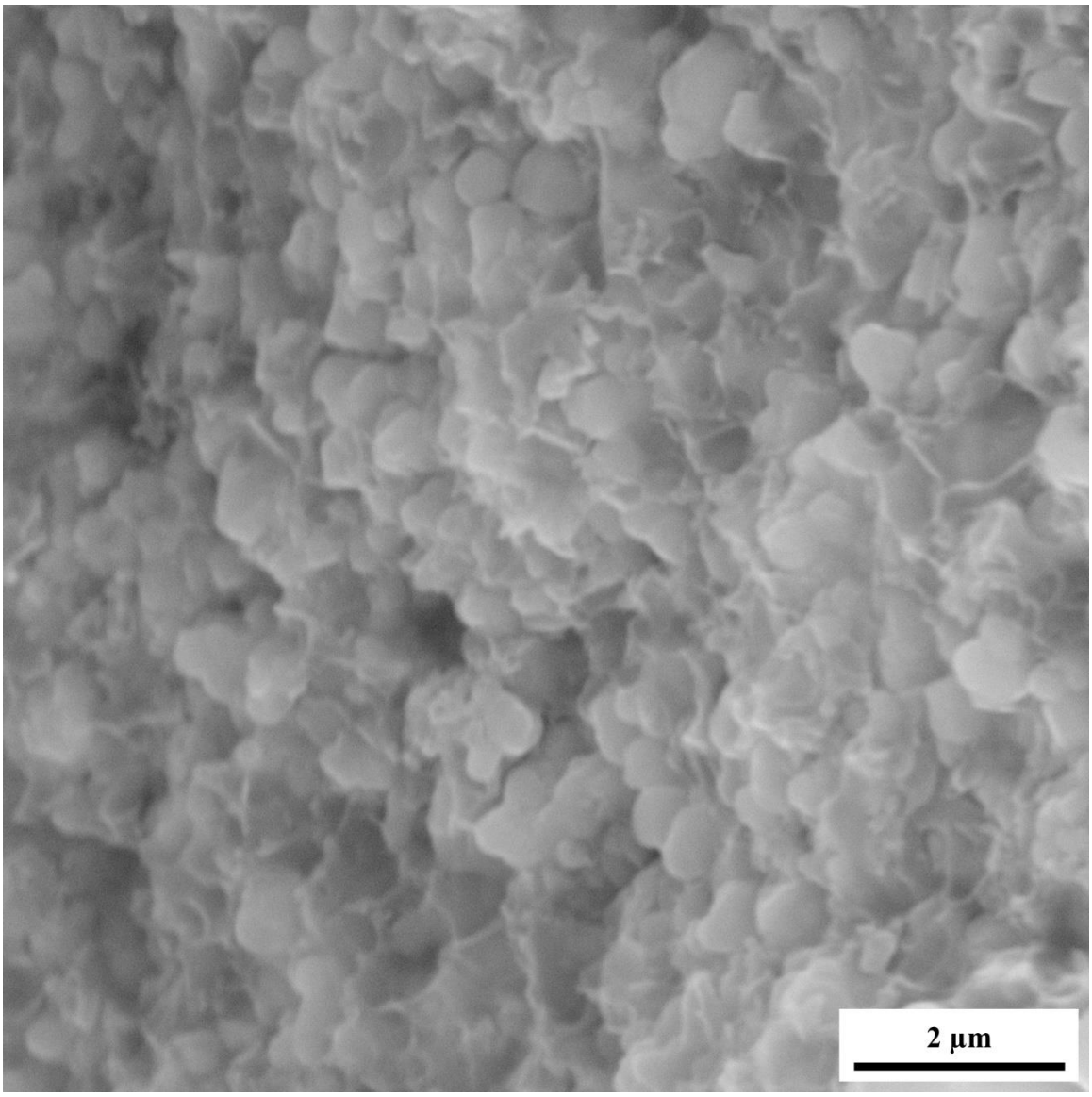

Figure 38. SEM micrograph of the fractured surface of a composite with a volume fraction of zinc oxide of 0.02 at a magnification of 53.3 kx, a working distance of 7.50 mm, and voltage of 30.0 kV.

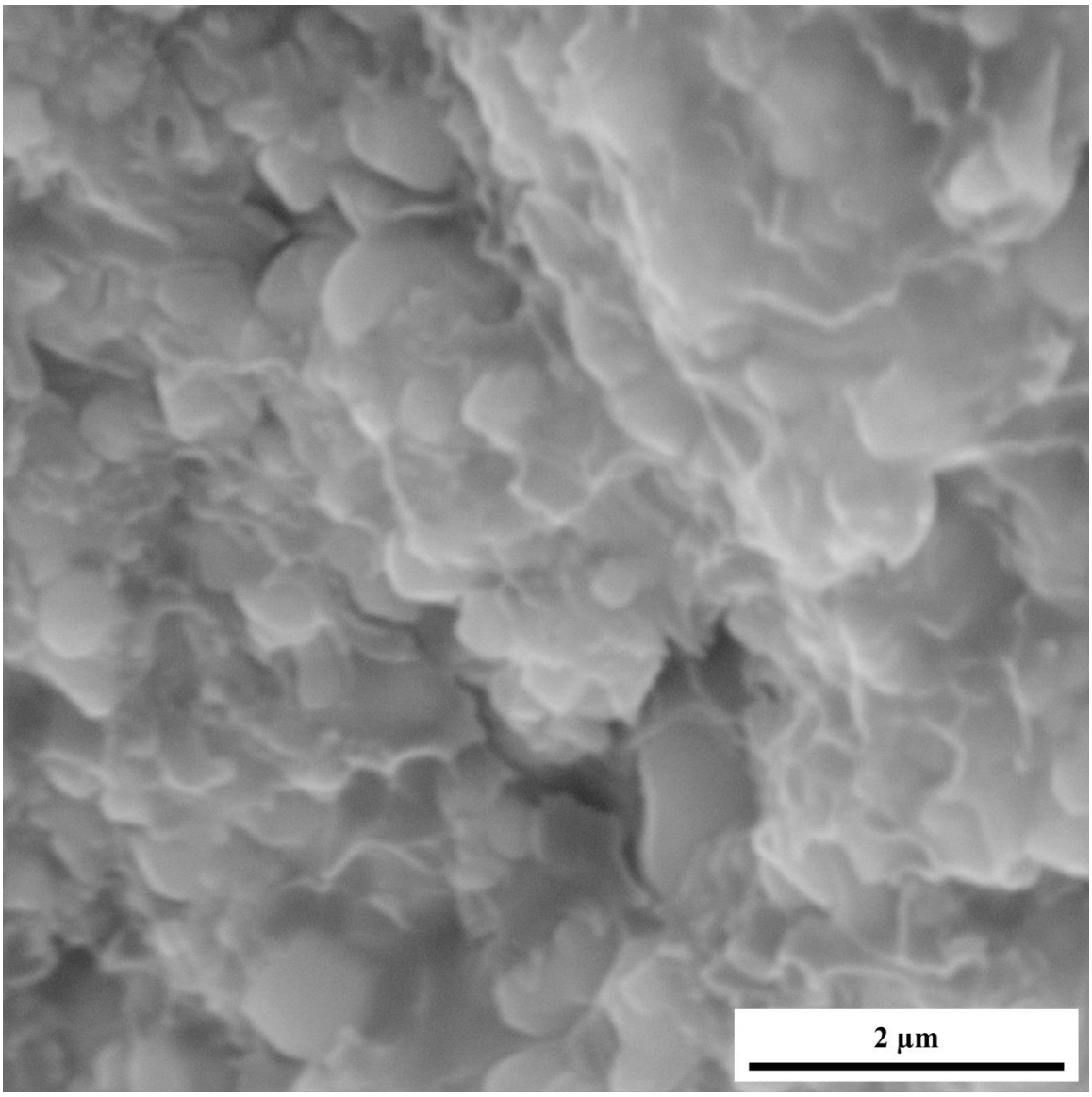

Figure 39. SEM micrograph of the fractured surface of a composite with a volume fraction of zinc oxide of 0.03 at a magnification of 80.0 kx, a working distance of 7.50 mm, and voltage of 30.0 kV.

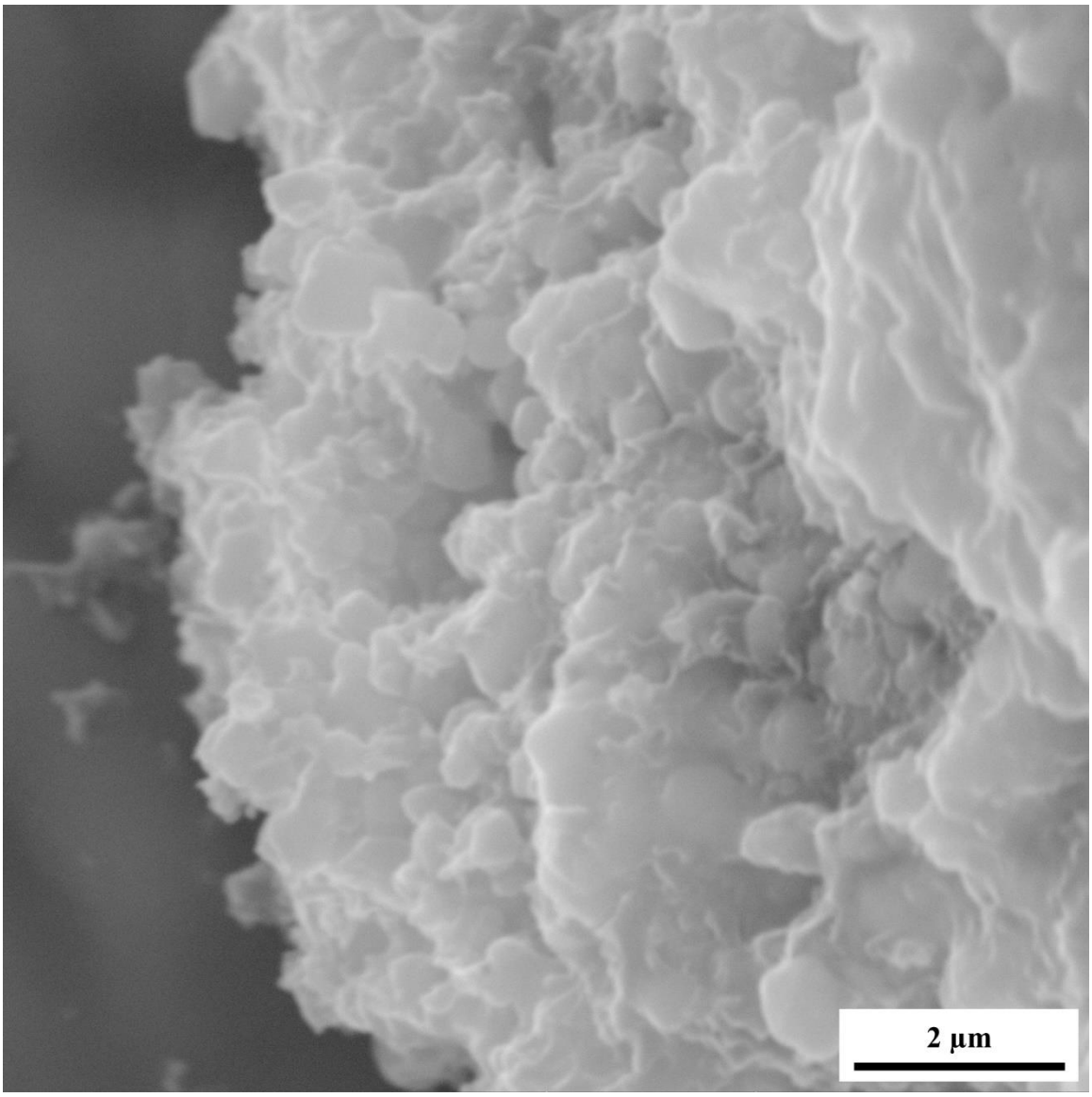

Figure 40. SEM micrograph of the fractured surface of a composite with a volume fraction of zinc oxide of 0.04 at a magnification of 53.3 kx, a working distance of 7.50 mm, and voltage of 30.0 kV.

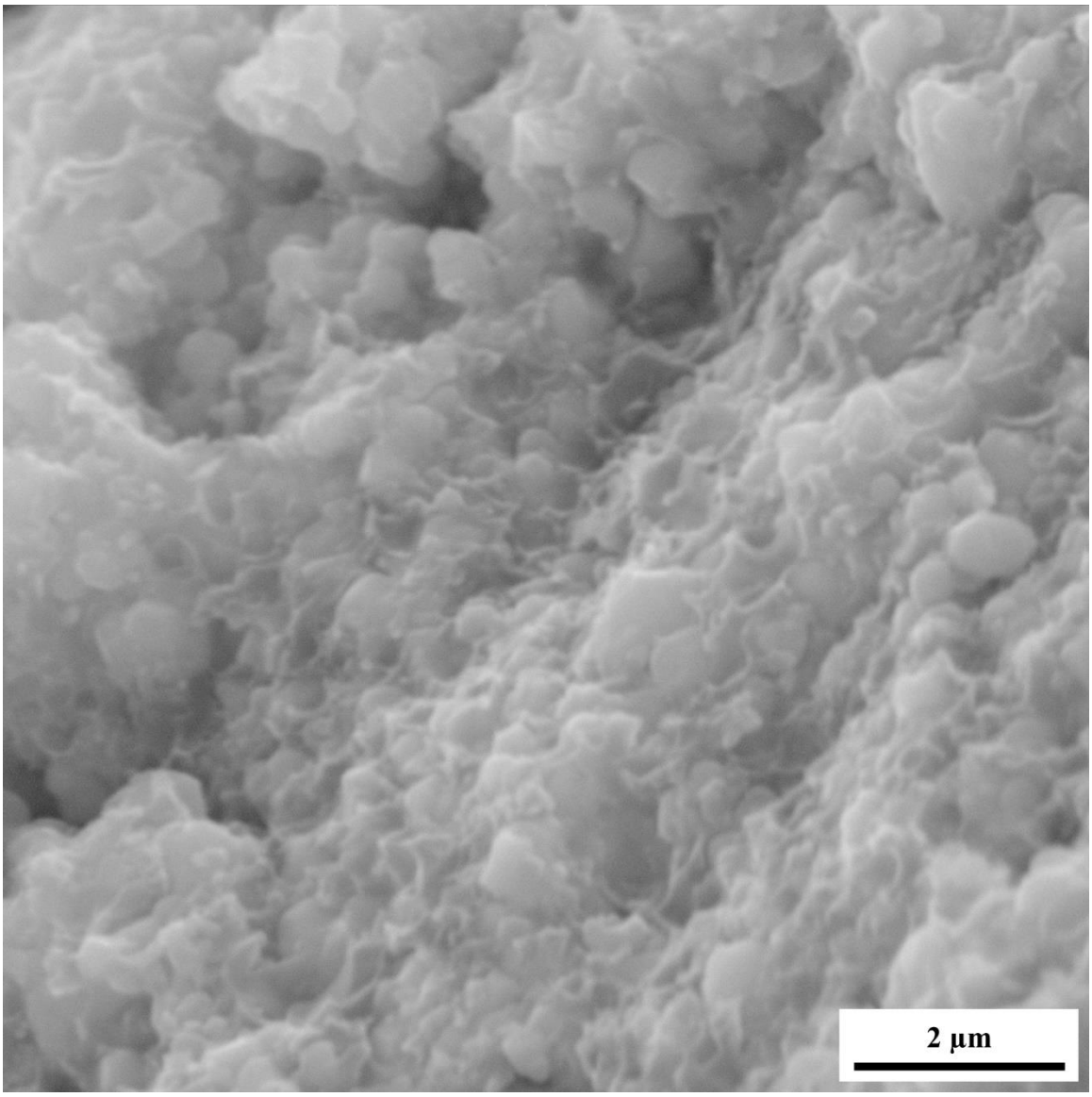

Figure 41. SEM micrograph of the fractured surface of a composite with a volume fraction of zinc oxide of 0.05 at a magnification of 53.3 kx, a working distance of 7.50 mm, and voltage of 30.0 kV.

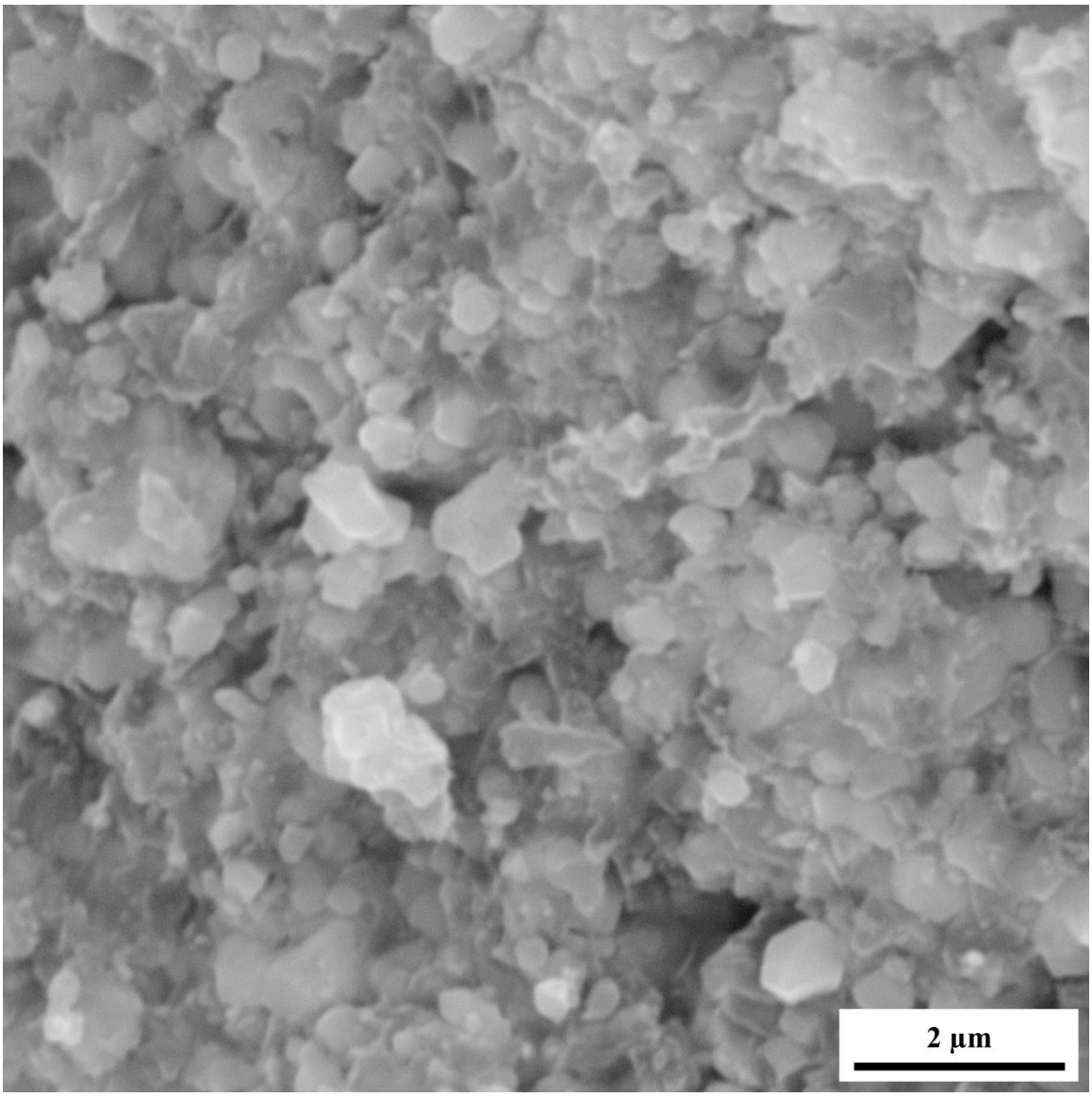

Figure 42. SEM micrograph of the fractured surface of a composite with a volume fraction of zinc oxide of 0.06 at a magnification of 53.3 kx, a working distance of 7.50 mm, and voltage of 30.0 kV.

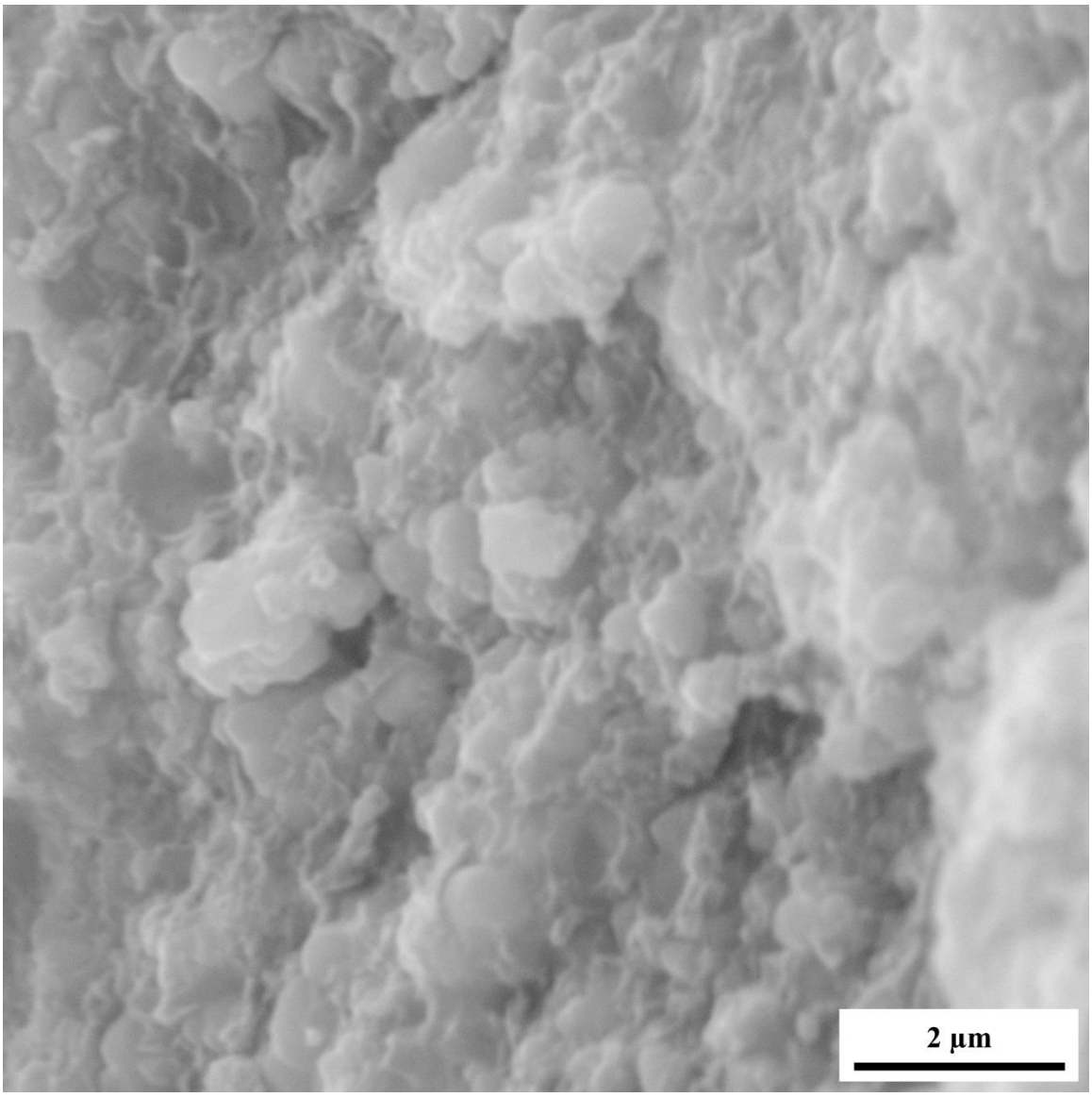

Figure 43. SEM micrograph of the fractured surface of a composite with a volume fraction of zinc oxide of 0.07 at a magnification of 53.3 kx, a working distance of 7.50 mm, and voltage of 30.0 kV.

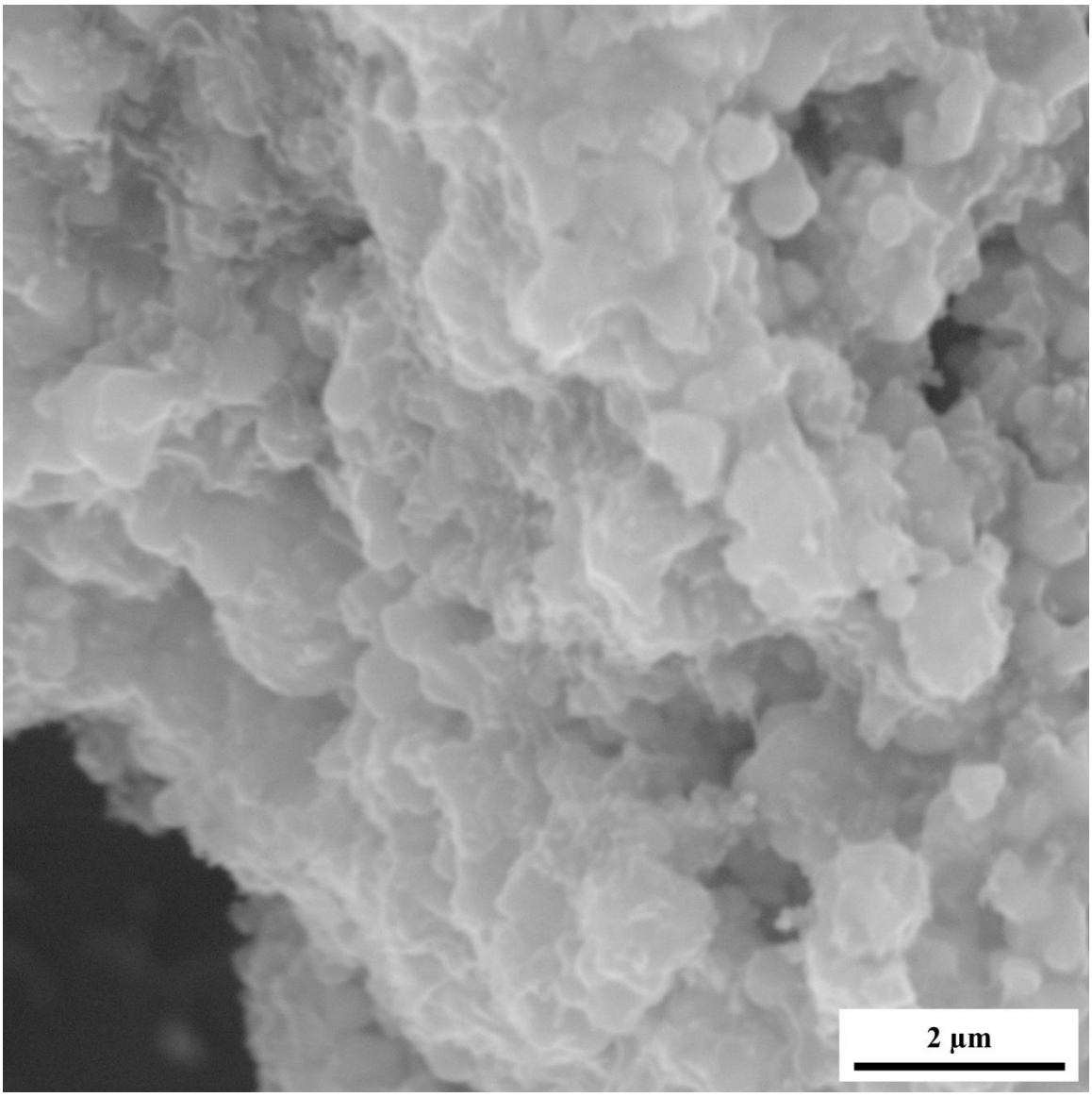

Figure 44. SEM micrograph of the fractured surface of a composite with a volume fraction of zinc oxide of 0.08 at a magnification of 53.3 kx, a working distance of 7.50 mm, and voltage of 30.0 kV.

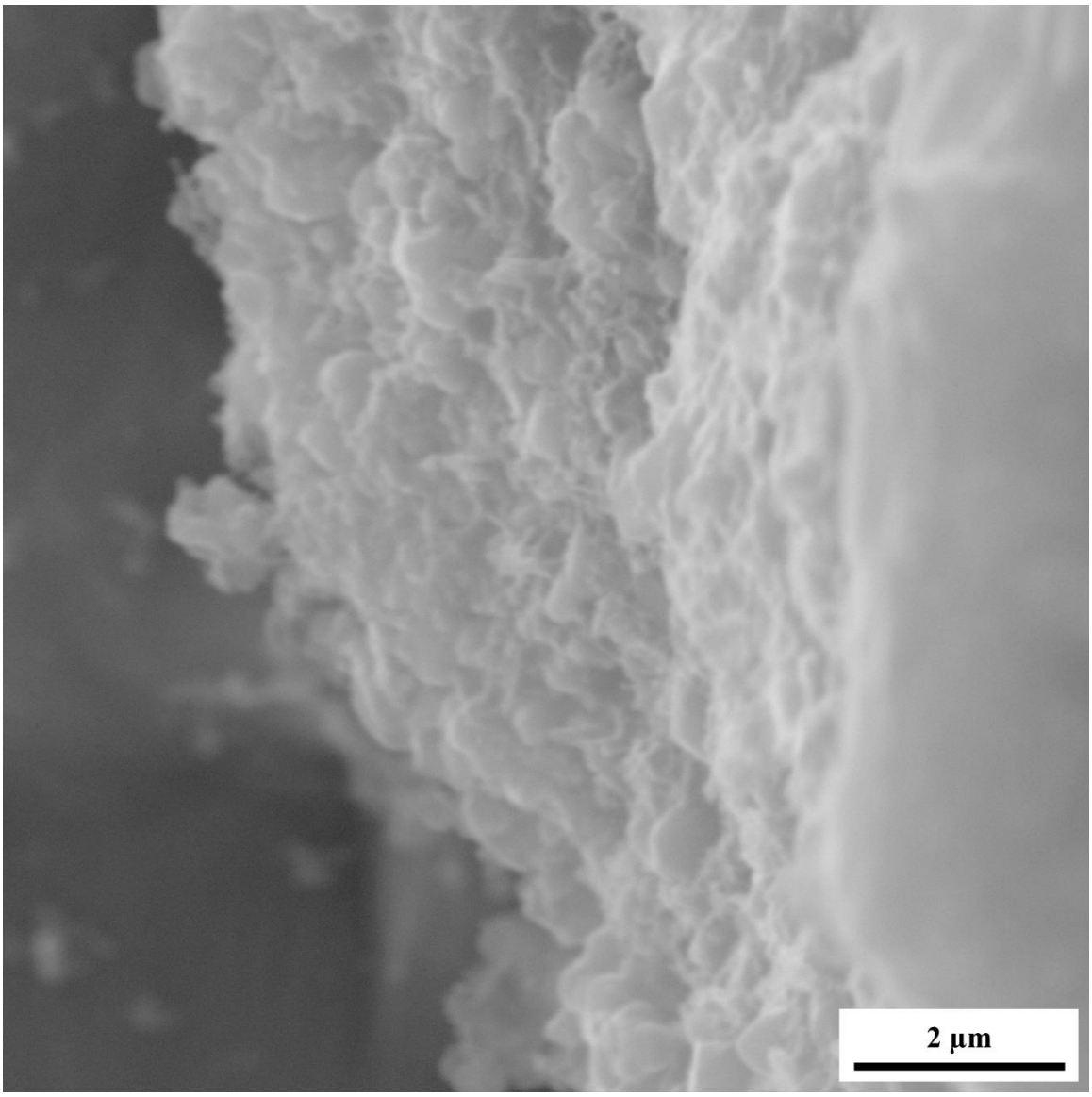

Figure 45. SEM micrograph of the fractured surface of a composite with a volume fraction of zinc oxide of 0.09 at a magnification of 53.3 kx, a working distance of 7.50 mm, and voltage of 30.0 kV.

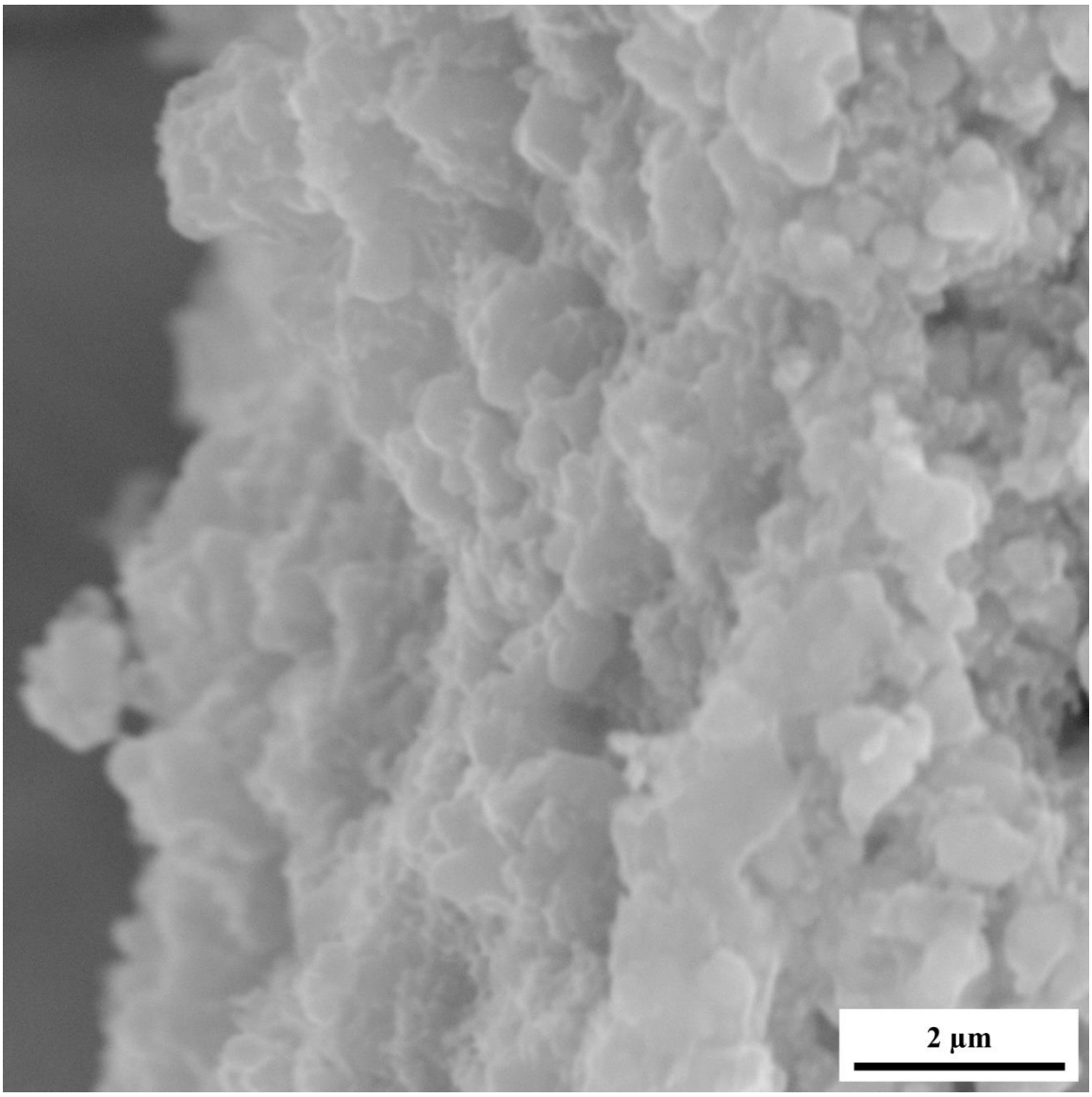

Figure 46. SEM micrograph of the fractured surface of a composite with a volume fraction of zinc oxide of 0.10 at a magnification of 53.3 kx, a working distance of 7.50 mm, and voltage of 30.0 kV.

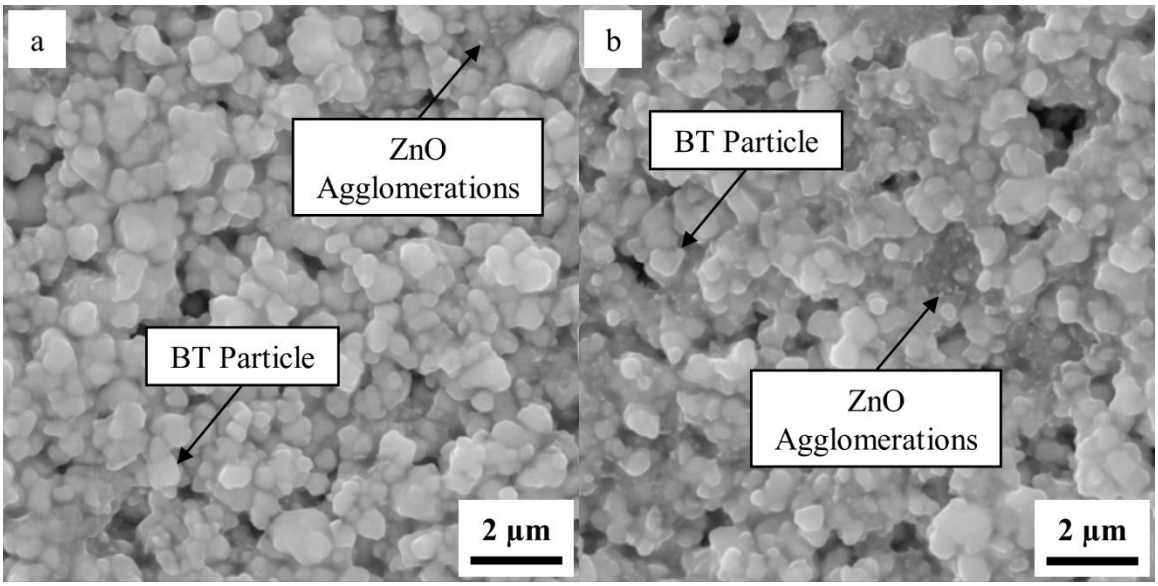

Figure 47. SEM micrographs with indications showing how the zinc oxide agglomerations and barium titanate particles appear in composites with a volume fraction of (a) 0.03 and (b) 0.05.

Figures 48-51 show the SEM micrographs of the cross-sections of the composites with a volume fraction of 0.01, 0.03, 0.04, and 0.10, respectively; they were taken at a voltage of 30 kV, a working distance of 7.50 mm, and a magnification of 9.33 kx. The micrographs were used to verify the thicknesses of the composites by comparison to the measured thicknesses with a micrometer. The thicknesses were 24.25 µm, 35.98 µm, 23.89 µm, and 46.08 µm for volume fractions of 0.01, 0.03, 0.04, and 0.10, respectively.

Supplemental SEM micrographs are provided in the Appendices.

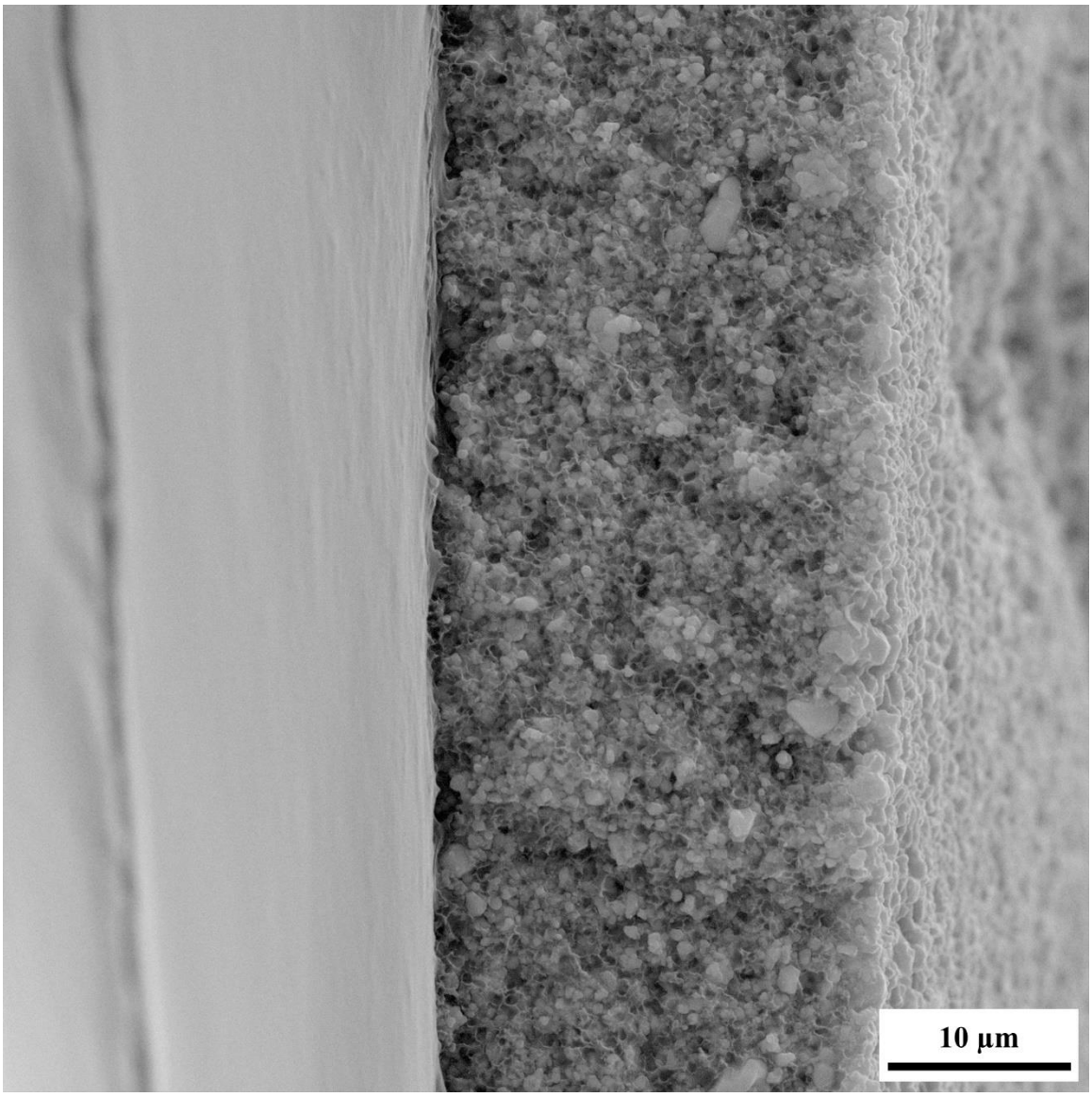

Figure 48. SEM micrograph of the cross-section of a composite with a volume fraction of zinc oxide of 0.01 at a magnification of 9.33 kx, a working distance of 7.50 mm, and voltage of 30.0 kV. The thickness of the composites is 24.25 µm.

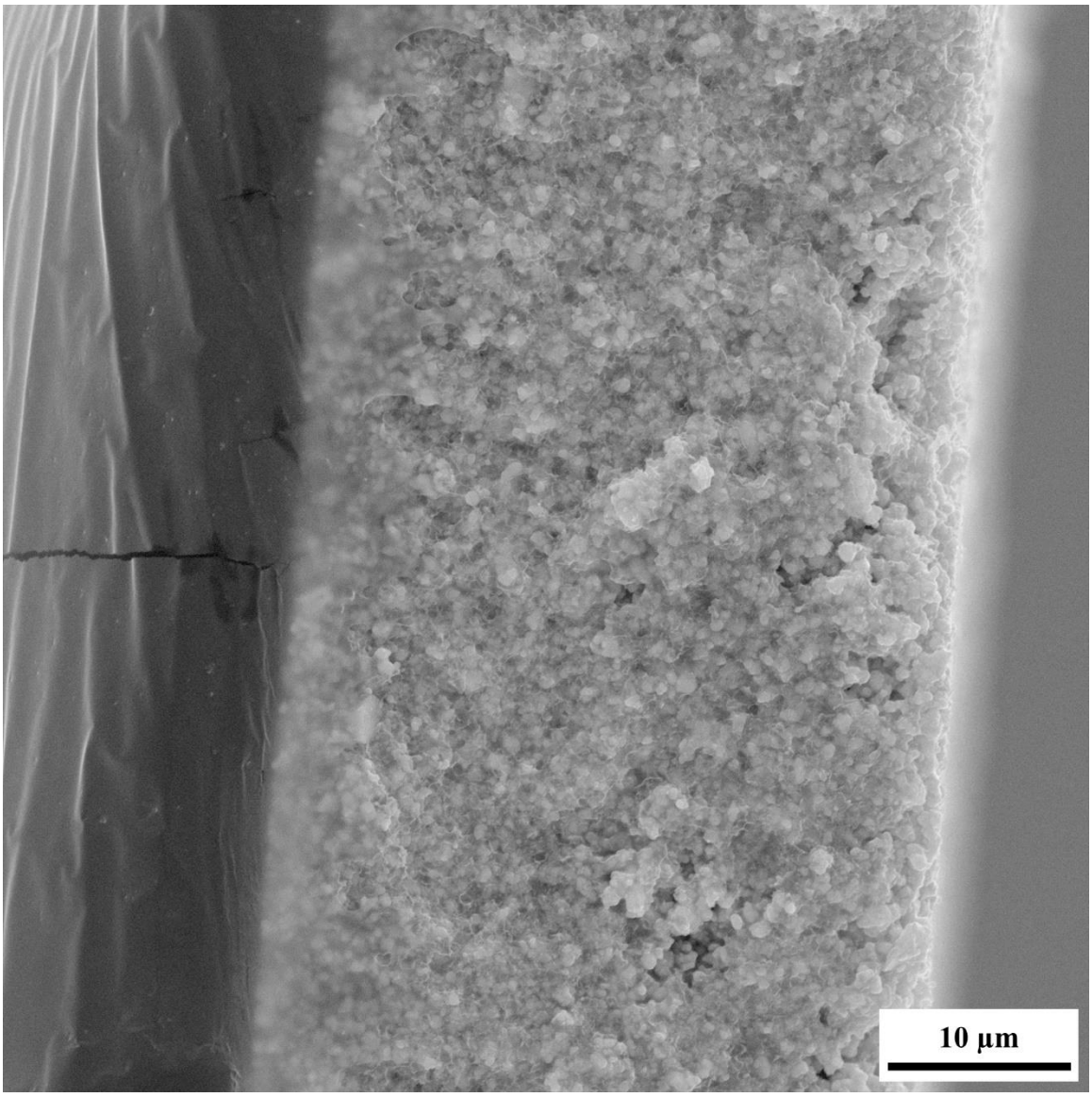

Figure 49. SEM micrograph of the cross-section of a composite with a volume fraction of zinc oxide of 0.03 at a magnification of 9.33 kx, a working distance of 7.50 mm, and voltage of 30.0 kV. The thickness of the composites is 35.98 µm.

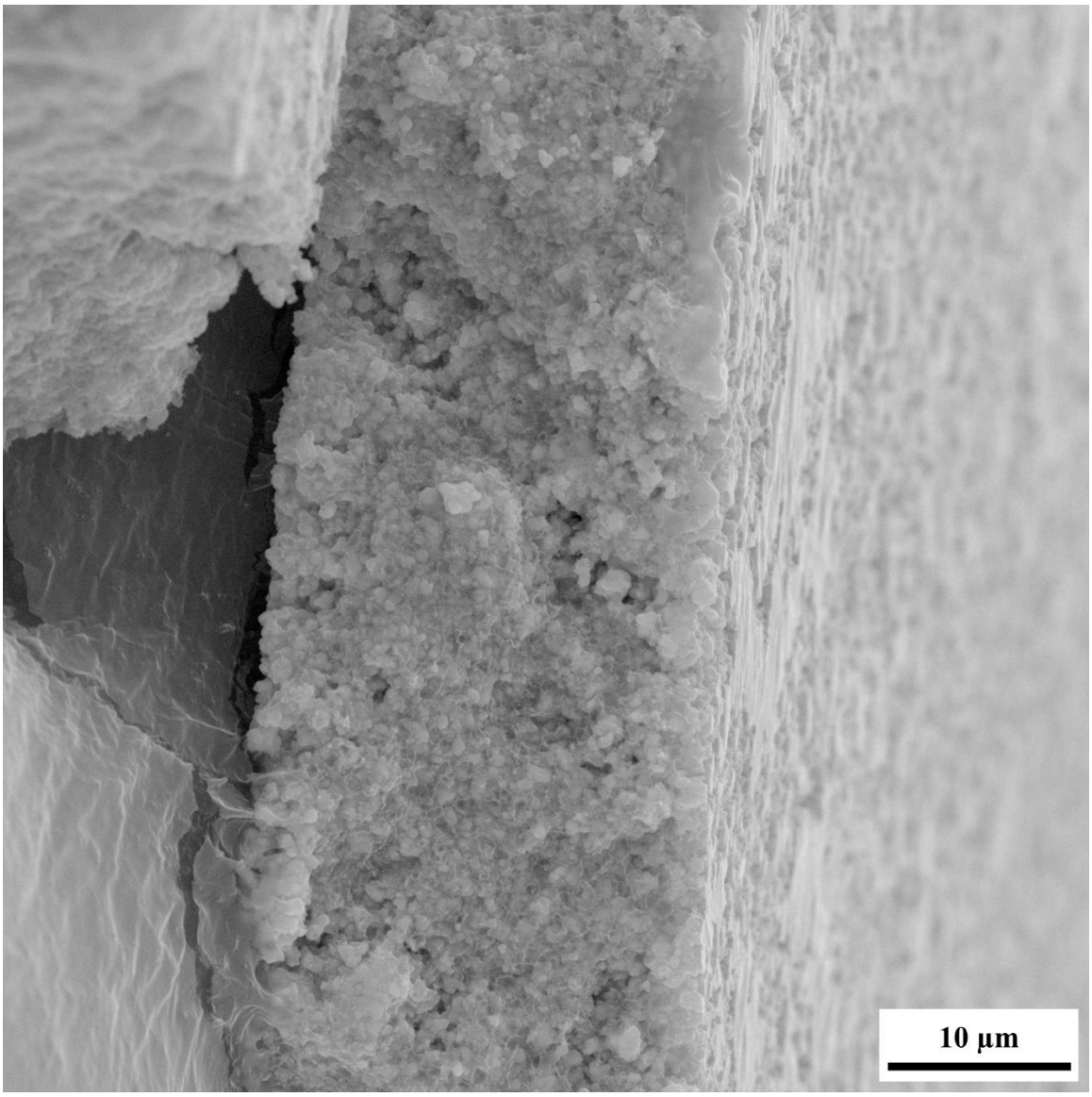

Figure 50. SEM micrograph of the cross-section of a composite with a volume fraction of zinc oxide of 0.04 at a magnification of 9.33 kx, a working distance of 7.50 mm, and voltage of 30.0 kV. The thickness of the composites is 23.89 µm.

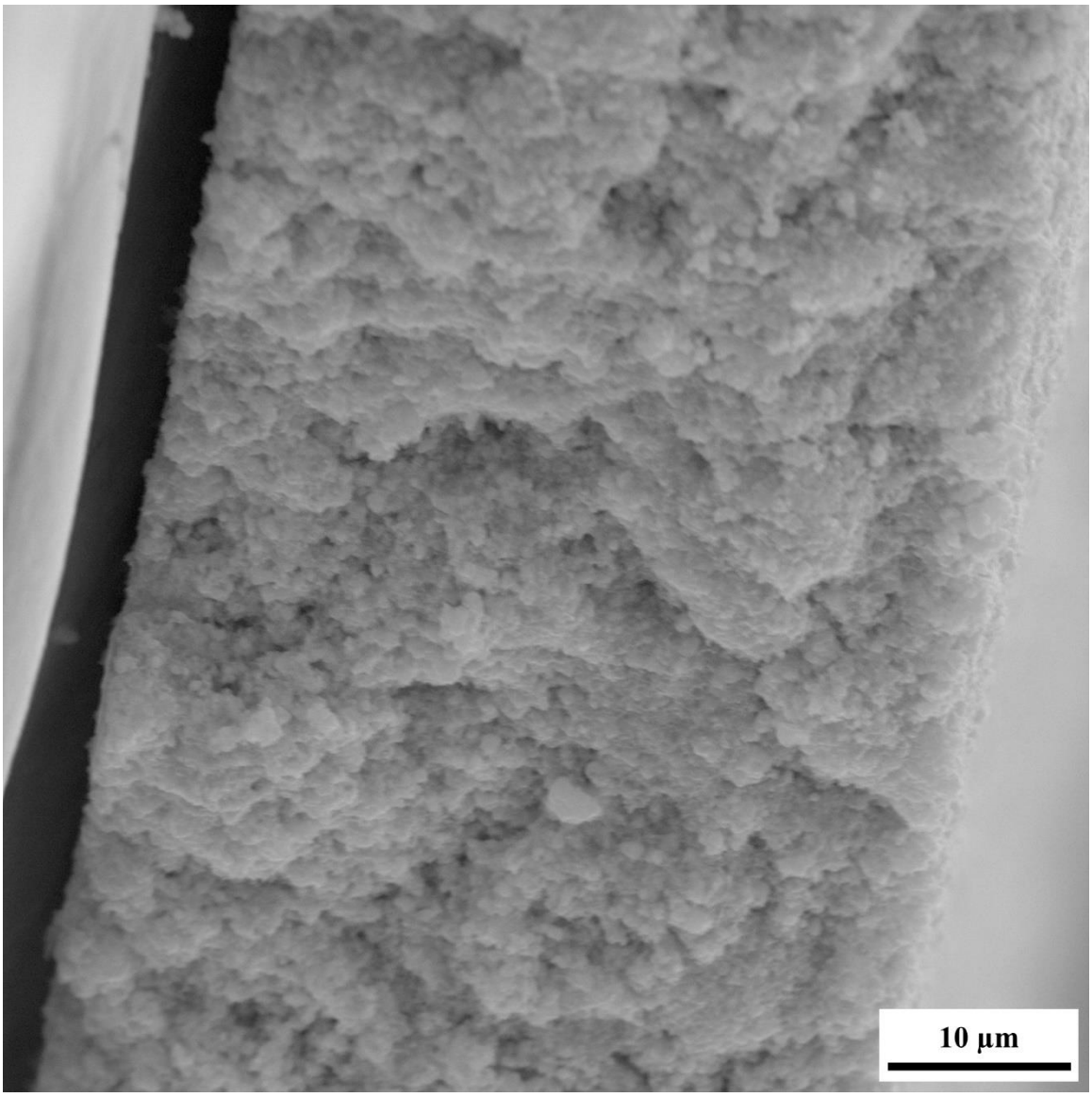

Figure 51. SEM micrograph of the cross-section of a composite with a volume fraction of zinc oxide of 0.10 at a magnification of 9.33 kx, a working distance of 7.50 mm, and voltage of 30.0 kV. The thickness of the composites is 46.08 µm.

Post Processing Results (Agglomerations)

Figure 52 shows the results of SEM micrograph post-processing, and the percentage of ZnO agglomerations for volume fractions of 0.03 or less is nearly constant with an average percentage of 22.0%. The percentage of agglomerations then increase from 24.32% to 46.96% for volume fractions of 0.04 and 0.10, respectively. The appearance of the nano-sized particles in the micrographs is a result of larger and more frequent agglomerations of ZnO in higher volume fractions. These agglomerations are caused by van der Waals forces between the nanoparticles during the solution-based fabrication and the curing of the composites [34-35]. This appearance further supports the relationship of the contact resistances of the three-phases, since the increase of agglomerations of the ZnO nanoparticles appear in the micrographs at the same volume fraction at which the electrical and dielectric properties of the composites begin to regress to the properties of the 0.01 volume fraction composites.

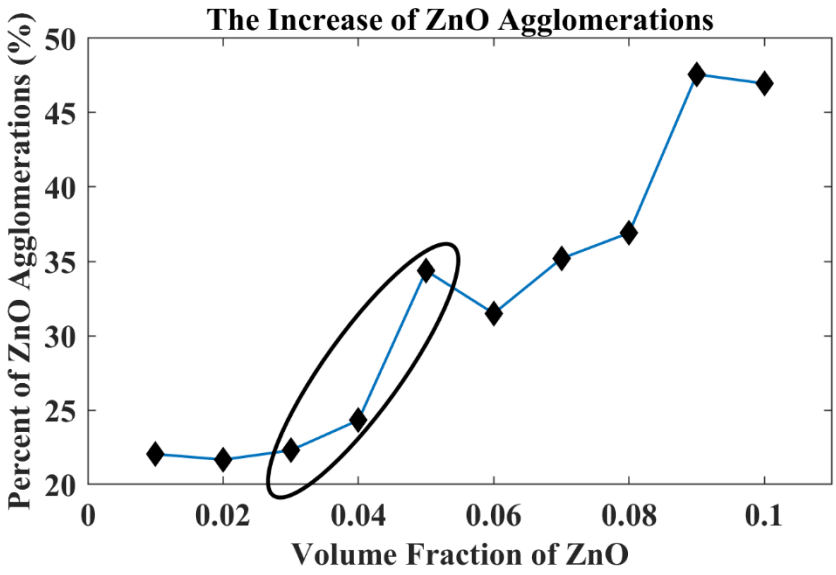

Figure 52. The percent of zinc oxide agglomerations for each volume fraction of zinc oxide from the post processing of the SEM micrographs with ImageJ.

CONCLUSION

Three-phase ZnO-BT-Ep multifunctional composites were fabricated. The volume fraction of micron-sized BT particles was held constant at 0.04, and the moles of particles per liter of solution was held constant at 6.2 mol/L. The volume fraction of the ZnO nanoparticles was varied from 0.01 to 0.10 in increments of 0.01. The impedance, resistivity, and dielectric constant of the composites decrease with increasing frequency, and the conductivity of the composites increases with frequency. At any specific frequency from 20 Hz to 10MHz, the impedance and resistivity of the composites increase, and the conductivity and dielectric constant decrease with increasing volume fractions ZnO from 0.01 to 0.03. At volume fractions of 0.04 or greater, the electrical and dielectric performance of the composites regress to the performance of the composites with a volume fraction of 0.01. This regression is due to the contact resistance of the three-phases in the composites decreasing as the number of ZnO agglomerations increases. Analysis and postprocessing of the SEM micrographs support this relationship because the ZnO agglomerations mostly appear in the composites with volume fractions of ZnO that are 0.04 or larger.

Future Work

Piezoelectric energy harvesters are moving towards wearable technologies as a method of using human motion to power or charge small hand-held devices; therefore, future work in this field would be to fabricate energy harvesting fibers that can be woven into textiles. A proposed method to achieve this is to electrospin BT particles that are embedded in a polymer to produce thin flexible fibers. The volume fraction of BT in the fibers can be varied from 0.10 to 0.70 to determine which volume fractions of BT can be electrospun while also maintaining flexibility. A small loom can then be used to weave small square textiles that can be sandwiched between two plate electrodes for testing. The

electrical and piezoelectric properties of the textiles would be tested using the same methods as for the spincoated composites.

REFERENCES

REFERENCES

[1] J. Nunes-Pereira, V. Sencadas, V. Correia, J. Rocha, S. Lanceros-Méndez, "Energy harvesting performance of piezoelectric electrospun polymer fibers and polymer/ceramic composites," *Sensors and Actuators A: Physical*, vol. 196, pp. 55-62, 2013.

[2] Saqib Siddiqui, Do-Il Kim, Le Thai Duy, Minh Triet Nguyen, Shoaib Muhammad, Won-Sub Yoon, Nae-Eung Lee, "High-performance flexible lead-free nanocomposite piezoelectric nanogenerator for biomechanical energy harvesting and storage," *Nano Energy*, vol. 15, pp. 177-185, 2015.

[3] D. Shin, J. Koh, "Comparative study on storing energy for (Ba,Zr)TiO_3 and CuO-(Ba,Zr)TiO_3 ceramics for piezoelectric energy harvesting applications," *Ceramics International*, vol. 43, pp. S649-S654, 2017.

[4] V. Vivekananthan, N. Alluri, Y. Purusothaman, A. Chandrasekhar, S. Kim, "A flexible, planar energy harvesting device for scavenging road side waste mechanical energy via the synergistic piezoelectric response of $K_{0.5}Na_{0.5}NbO_3$-$BaTiO_3$/PVDF composite films," *Nanoscale*, Vol. 9, pp. 15122-15130, 2017.

[5] C. Sun, J. Shi, X. Wang, "Fundamental study of mechanical energy harvesting using piezoelectric nanostructures," *Journal of Applied Physics*, vol. 108, no. 034309, pp. 1-11, 2010.

[6] S. Banerjee, K. Cook-Chennault, "An investigation into the influence of electrically conductive particle size on electromechanical coupling and effective dielectric strain coefficients in three phase composite piezoelectric polymers," *Composites: Part A*, vol. 43, pp. 1612-1619, 2012.

[7] F. Wang, Y. Mai, D. Wang, R. Ding, W. Shi, "High quality barium titanate nanofibers for flexible piezoelectric device applications," *Sensors and Actuators A*, vol. 233, pp. 195-201, 2015.

[8] S. Jeong, D. Lee, M. Kim, D. Im, I. Kim, K. Cho, "Properties of piezoelectric ceramic with textured structure for energy harvesting," *Ceramics International*, vol. 38S, pp. S369–S372 , 2011.

[9] Y. Wang, X. Zhang, X. Guo, D. Li, B. Cui, K. Wu, J. Yun, J. Mao, L. Xi, Y. Zuo, "Hybrid nanogenerator of $BaTiO_3$ nanowires and CNTs for harvesting energy," *Journal of Material Science*, vol. 53, pp. 13081-13089, 2018.

[10] A. Matos, J. Guedes, K. Jayachandran, H. Rodrigues, "Computational model for power optimization of piezoelectric vibration energy harvesters with material homogenization," *Computers and Structures*, vol. 192, pp. 144-156, 2017.

[11] D. Saravanos, A. Christoforou, "Impact Response of Adaptive Piezoelectric Laminated Plates," *American Institute of Aeronautics and Astronautics Journal*, vol. 40, no. 10, pp. 2087-2095, 2002.

[12] C. Geng, J. Wang, Q. Zhang, Q. Fu, "New piezoelectric damping composites of poly(vinylidene fluoride) blended with clay and multi-walled carbon nanotubes," *Polymers International*, vol. 61, pp. 934-938, 2012.

[13] W. Kumar, A. Kumar, A. Bindal, "A MEMS structure for acoustic energy harvesting using a DPL type BAW resonator mounted over a SOI substrate," present at 2nd International Conference on Electronics and Communication Systems, Coimbatore, India, 2015.

[14] C. Bowland, M. Malakooti, H. Sodano, "Barium Titanate Film Interfaces for Hybrid Composite Energy Harvesters," *Applied Materials and Interfaces*, vol. 9, pp. 4057-4065, 2017.

[15] B. Jaffe, W. Cook, *Piezoelectric Ceramics*, New York, NY: Academic Press Inc., 1971.

[16] R. Newman, *Properties of Materials*, New York, NY: Oxford University Press, 2005.

[17] J. Roscow, Y. Zhang, M. Kraśny, R. Lewis, J. Taylor, C. Bowen, "Freeze cast porous barium titanate for enhanced piezoelectric energy harvesting," *Journal of Physics D: Applied Physics*, vol. 51, no. 225301, pp. 1-18, 2018.

[18] K. Uchino, *Ferroelectric Devices*, New York, NY: Marcel Dekker, 2000.

[19] Z. Shen, H. Yan, D. Gruner, L. Belova, Y. Sakamoto, J. Hu, C. Nan, T. Hoche, M. Reece, "Ferroelectric ceramics with enhanced remnant polarization by ordered coalescence of nano-crystals," *Journal of Materials Chemistry*, Vol. 22, pp. 23547-23552.

[20] Y. Liu, B. Li, W. Zhou, K. Chen, "Triggering piezoelectricity directly by heat to produce alternating electric voltage," *Applied Physics Letters*, Vol. 109, no. 113107, pp. 1-4, 2016.

[21] S. Banerjee, "An Experimental Investigation of Lead Zirconium Titanate-Epoxy-Multiwalled Carbon Nanotube Bulk and Flexible Thin Thick Film Composites," PhD Dissertation, Rutgers, The State University of New Jersey, New Brunswick, NJ, 2014.

[22] M. Dietze, M. Es-Souni, "Structural and functional properties of screen-printed PZT-PVDF-TrFE composites," *Sensors and Actuators A*, Vol. 143, pp. 329-334, 2008.

[23] K. Arlt, M. Wegener. “Piezoelectric PZT / PVDF-copolymer 0-3 Composites: Aspects on Film Preparation and Electrical Poling,” *IEEE Transactions on Dielectrics and Electrical Insulation,* Vol. 17, no. 4, pp. 1178-1184, 2010.

[24] N. Hasan, D. Antao, B. Farouk, “DC negative corona discharge in atmospheric pressure helium: transition from the corona to the ‘normal’ glow regime,” *Plasma Sources Science and Technology*, Vol. 23, no. 035013, pp. 1-16, 2014.

[25] A. Koka, Z. Zhou, H. Sodano, “Vertically aligned $BaTiO_3$ nanowire arrays for energy harvesting,” *Energy & Environmental Science*, vol. 7, pp. 288-296, 2014.

[26] J. Park, G. Lee, J. Yang, C. Kim, S. Ahn, “Flexible ceramic-elastomer composite piezoelectric energy harvester fabricated by additive manufacturing,” *Journal of Composite Materials*, vol. 50, no. 12, pp. 1573-1579, 2016.

[27] T. Zhou, J. Zha, R. Cui, B. Fan, J. Yuan, and Z. Dang, “Improving Dielectric Properties of $BaTiO_3$/Ferroelectric Polymer Composites by Employing Surface Hydroxylated $BaTiO_3$ Nanoparticles,” *Applied Material Interfaces*, Vol. 3, pp. 2184-2188, 2011.

[28] Z. Dang, S. Yao, J. Yuan, J. Bai, “Tailored Dielectric Properties based on Microstructure Change in BaTiO3-Carbon Nanotube/Polyvinylidene Fluoride Three-Phase Nanocomposites,” *J. Physical Chemistry C*, Vol. 114, pp. 13204-13209, 2010.

[29] W. Xue, H. Li, R. Dugnani, H. Rehman, C. Zhang, Y. Chen, H. Liu, “High loss factor piezoelectric damping composite with three-dimensional reduced graphene oxide as the conductive phase,” *Royal Society of Chemistry Advances*, vol. 8, pp. 12494-12502, 2018.

[30] T. Huang, S. Yang, P. He, J. Sung, S. Zhang, D. Li, Y. Meng, J. Zhou, H. Tang, J. Liang, G. Ding, X. Xie, “Phase-Separation-Induced PVDF/Graphene Coating on Fabrics toward Flexible Piezoelectric Sensors,” *Applied Material Interfaces*, vol. 10, pp. 30732, 2018.

[31] I. Bu, “Rapid synthesis of ZnO nanostructures through microwave heating process,” *Ceramics International*, vol. 39, pp. 1189-1194, 2013.

[32] F. Khaled, A. Bouloufa, K. Djessas, R. Mahamdi, I. Bouchama, “Aluminum doped zinc oxide wide band-gap n-type optical window for mc-Si superstrate solar cell,” *Vacuum*, vol. 120, pp. 14-18, 2015.

[33] R. Pal, *Electromagnetic, Mechanical, and Transport Properties of Composite Materials*, Boca Raton, FL: CRC Press, 2015.

[34] C. Kong, D. Yu, Q. Yao, S. Li, “Morphological changes of nano-Al agglomerates during reaction and its effect on combustion,” *Combustion and Flame*, vol. 165, pp. 11-20, 2016.

[35] M. Andio, P. Browning, P. Morris, S. Akbar, “Comparison of gas sensor performance of SnO2 nano-structures on microhotplate platforms,” *Sensors and Actuators B: Chemical*, Vol. 165, pp. 13-18, 2012.

APPENDICES

APPENDIX A: SUPPLEMENTAL SEM MICROGRAPHS

Figure 53-62 are SEM micrographs of the surface of the composites. The magnification is 2.67 kx, the working distance is 7.50 mm, and the voltage is 30.0 kV. The magnification is considerably less than the SEM micrographs used to determine the ZnO agglomerations. This makes it is difficult to see the ZnO agglomerations, but they can be used to better determine the quality of the samples. For example, Figure 54 has a small crack in the composite and has some valleys, whereas Figure 55 has a very smooth surface with little defects.

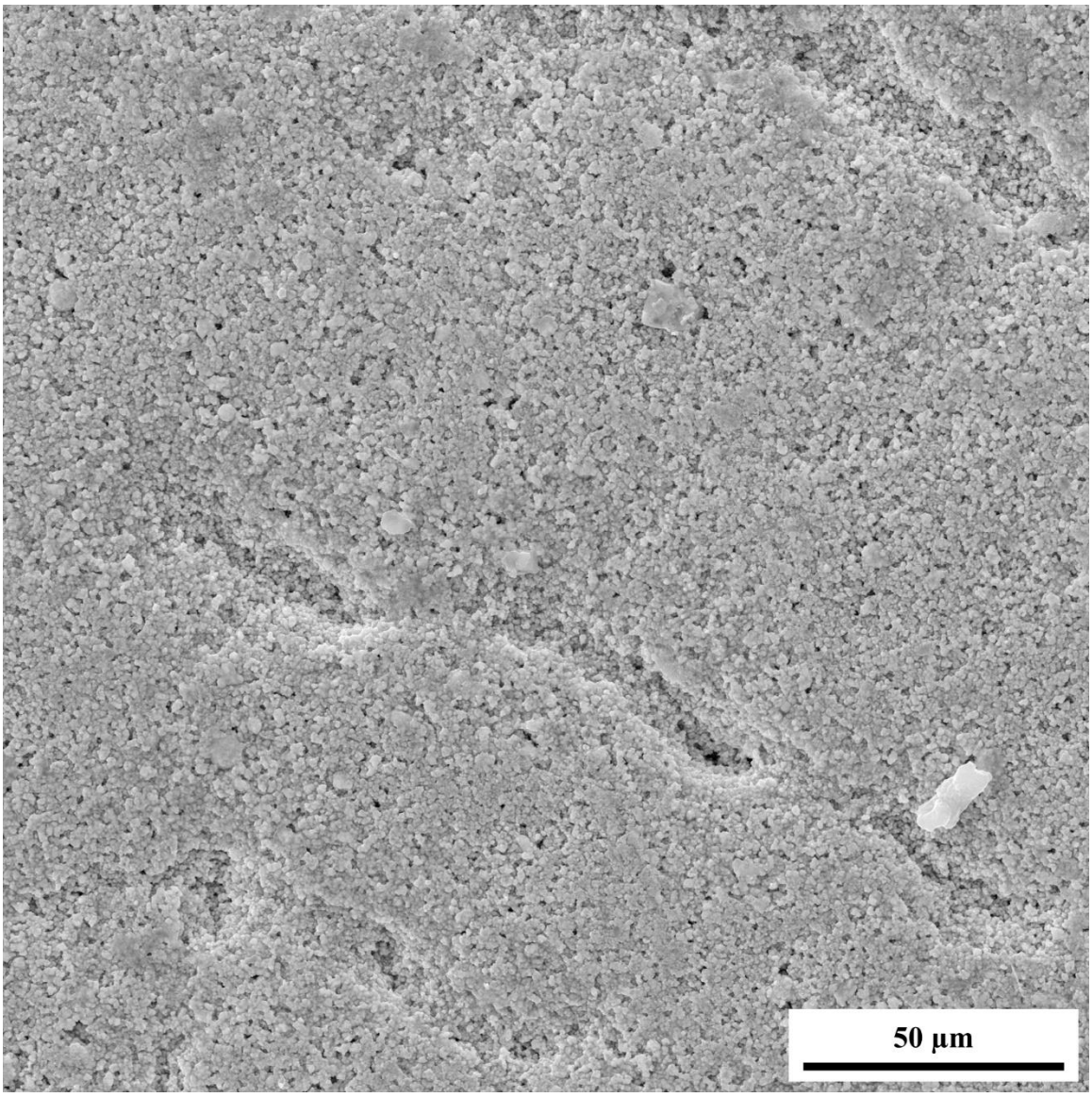

Figure 53. SEM micrograph of the surface of a composite with a volume fraction of zinc oxide of 0.01 at a magnification of 2.67 kx, a working distance of 7.50 mm, and voltage of 30.0 kV.

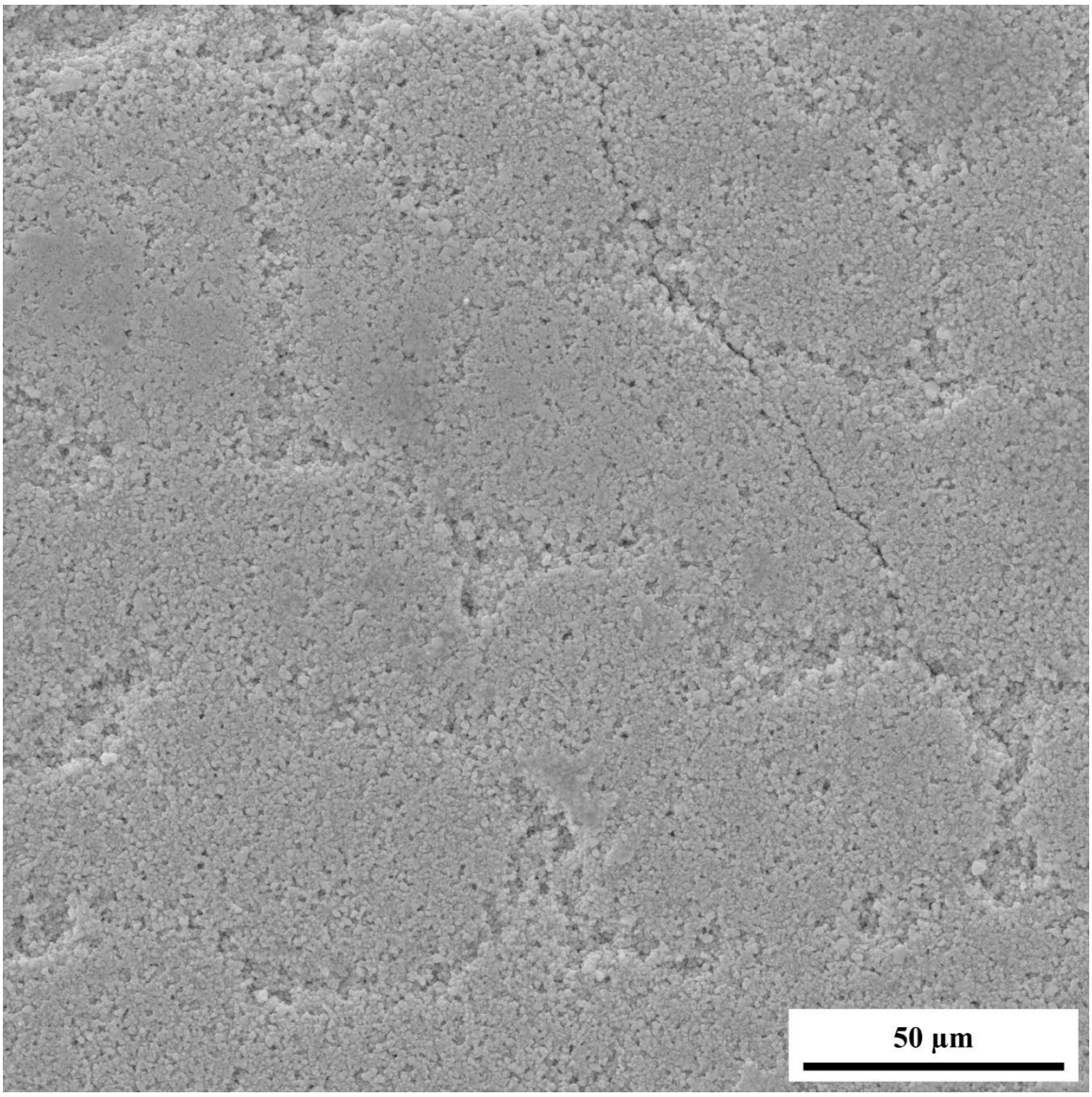

Figure 54. SEM micrograph of the surface of a composite with a volume fraction of zinc oxide of 0.02 at a magnification of 2.67 kx, a working distance of 7.50 mm, and voltage of 30.0 kV.

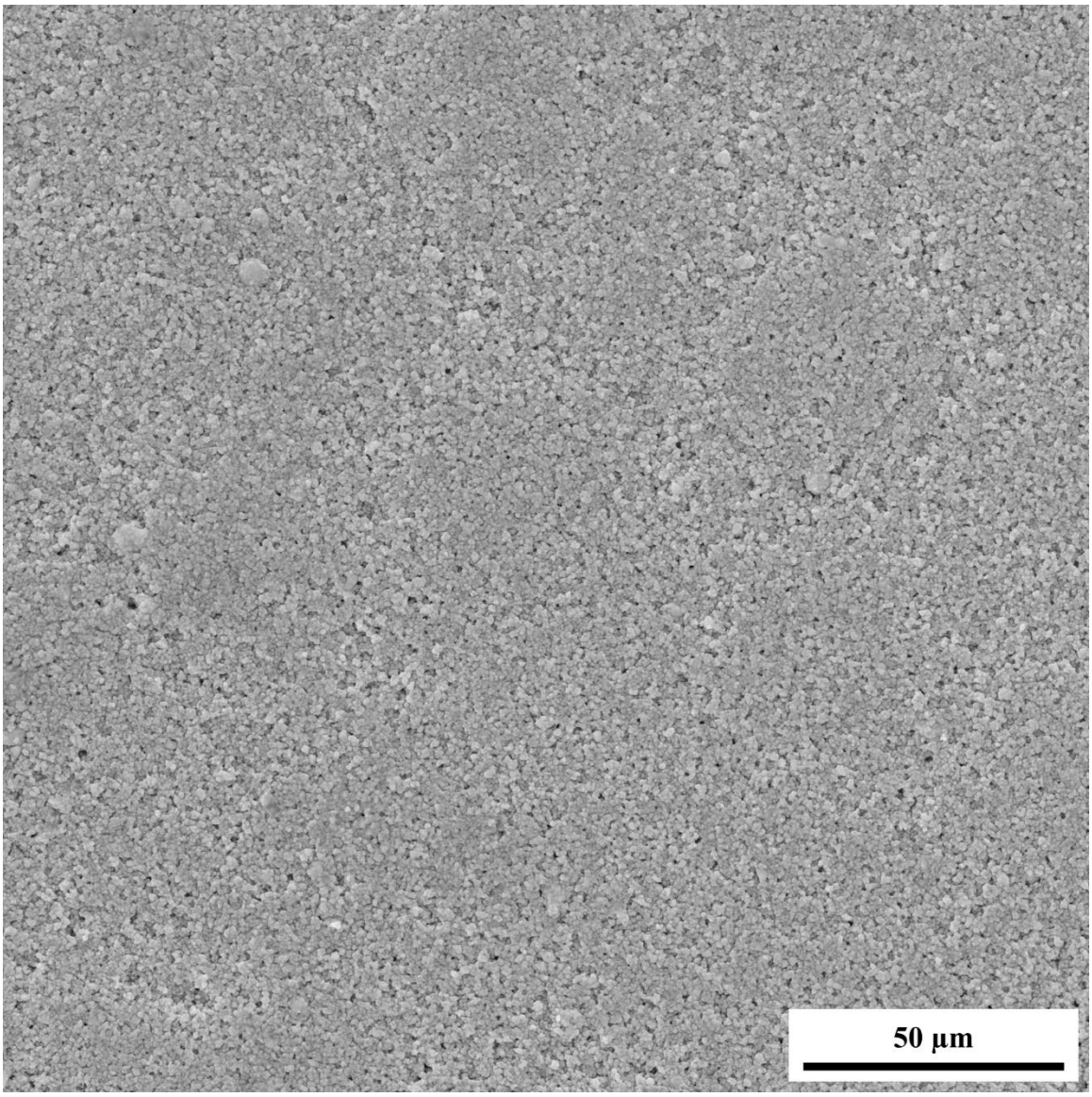

Figure 55. SEM micrograph of the surface of a composite with a volume fraction of zinc oxide of 0.03 at a magnification of 2.67 kx, a working distance of 7.50 mm, and voltage of 30.0 kV.

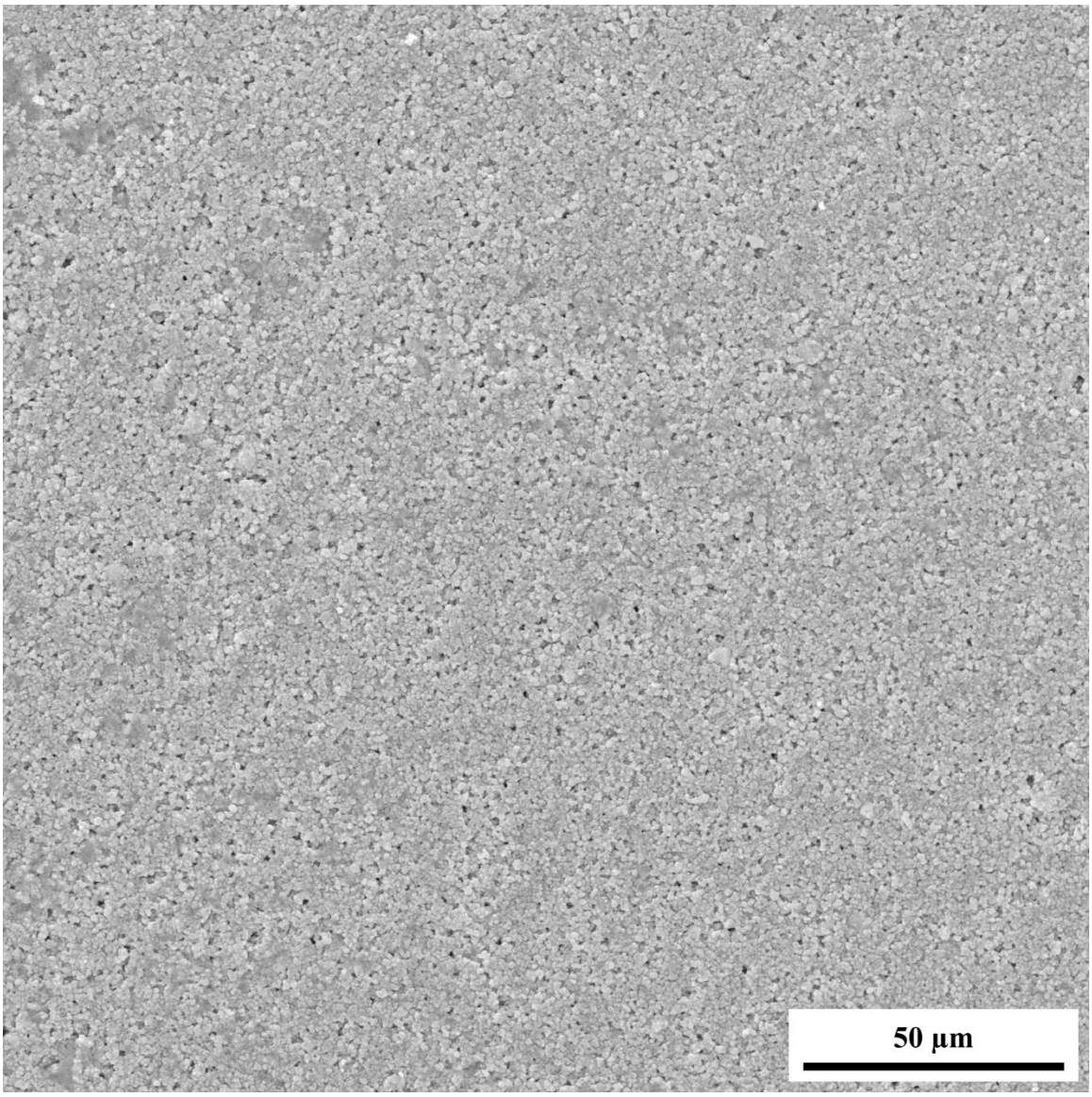

Figure 56. SEM micrograph of the surface of a composite with a volume fraction of zinc oxide of 0.04 at a magnification of 2.67 kx, a working distance of 7.50 mm, and voltage of 30.0 kV.

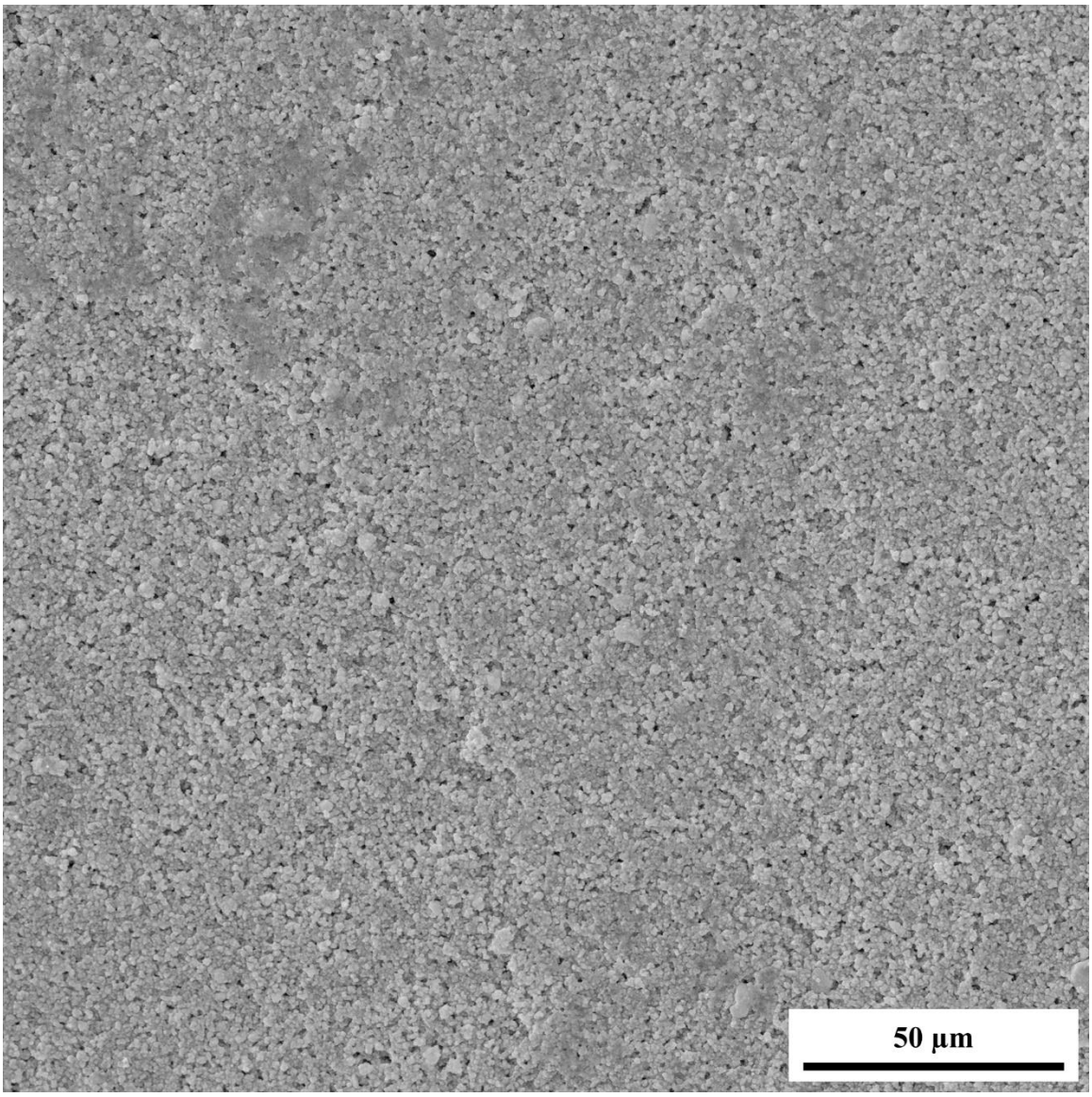

Figure 57. SEM micrograph of the surface of a composite with a volume fraction of zinc oxide of 0.05 at a magnification of 2.67 kx, a working distance of 7.50 mm, and voltage of 30.0 kV.

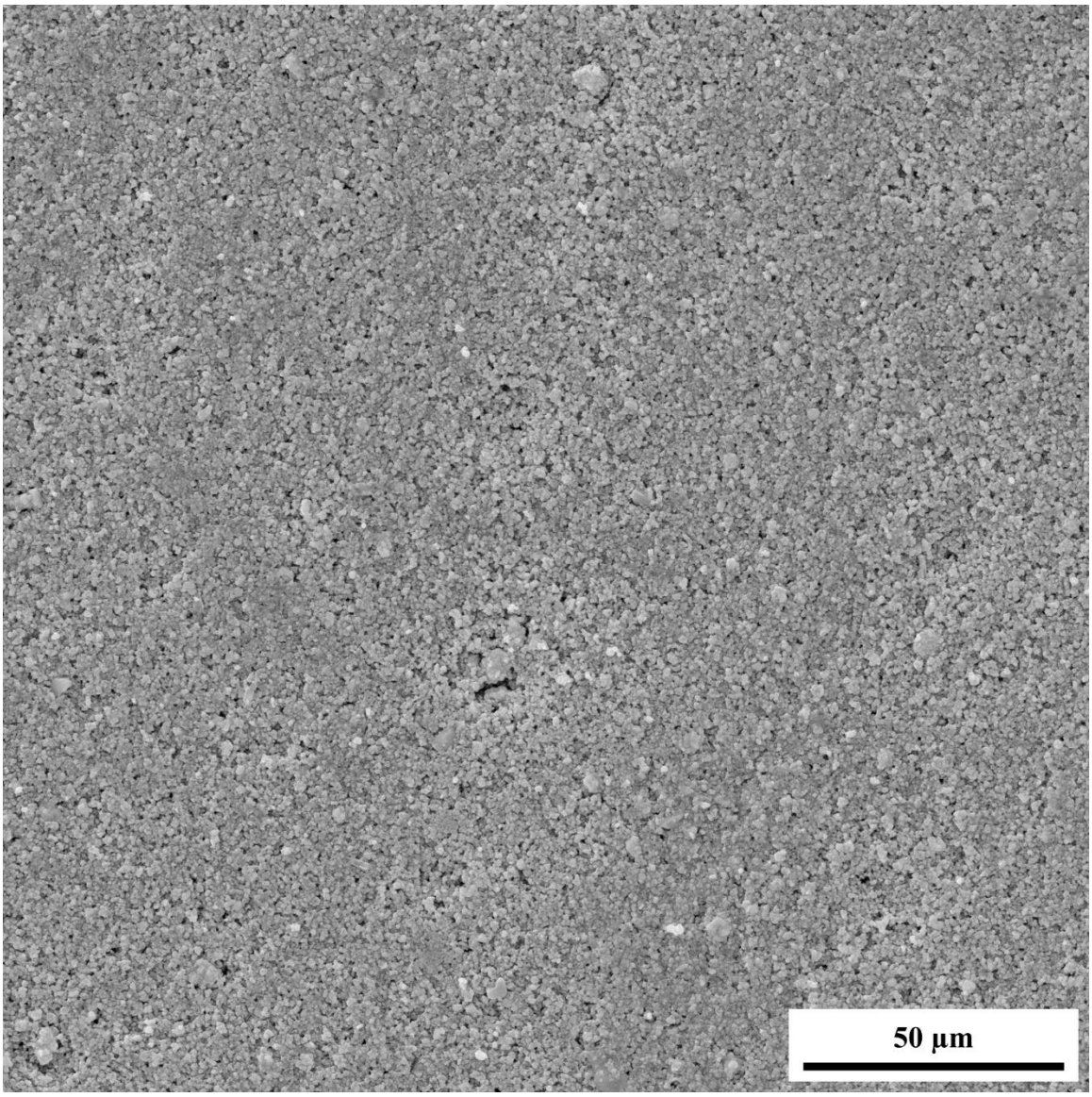

Figure 58. SEM micrograph of the surface of a composite with a volume fraction of zinc oxide of 0.06 at a magnification of 2.67 kx, a working distance of 7.50 mm, and voltage of 30.0 kV.

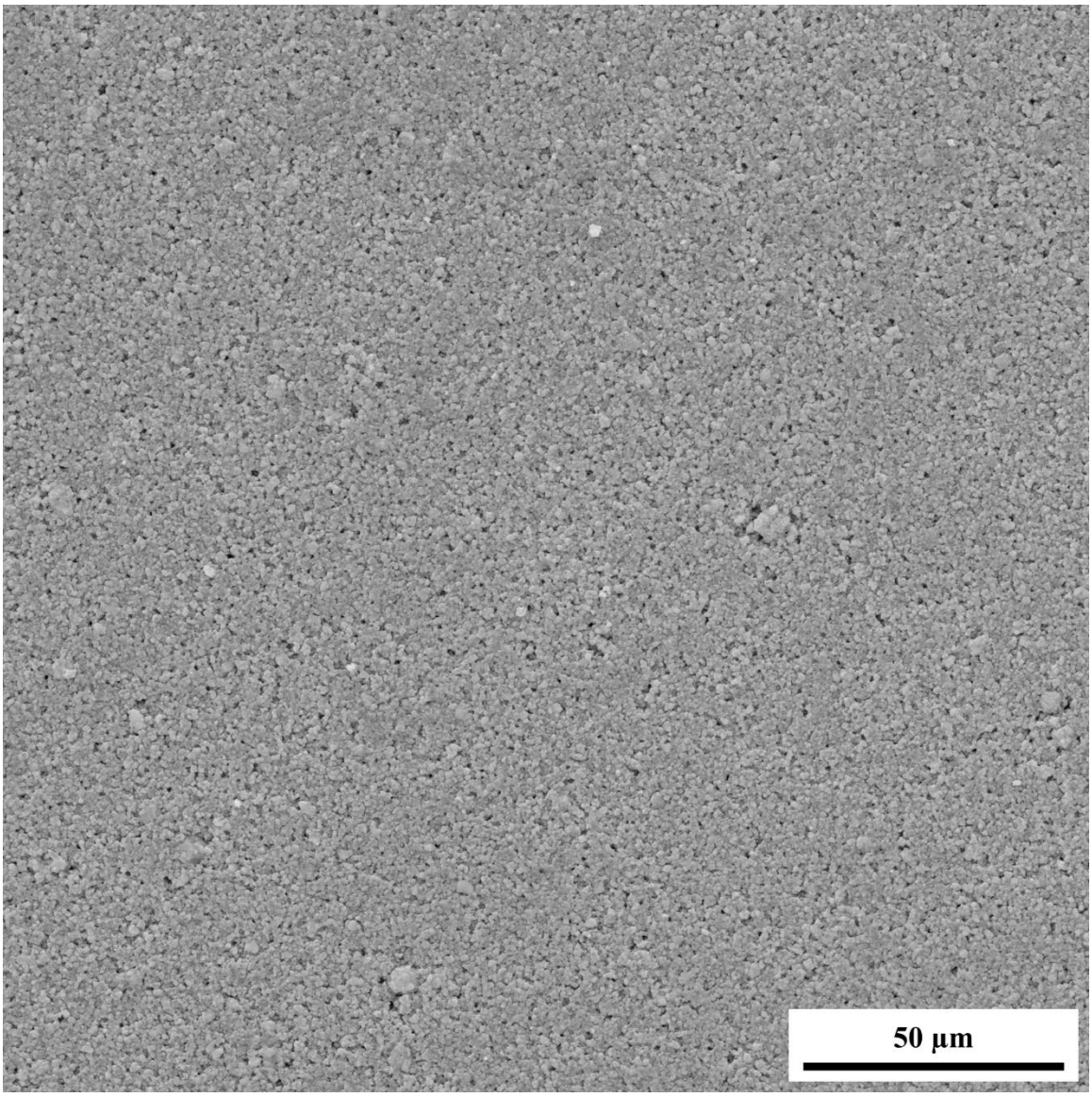

Figure 59. SEM micrograph of the surface of a composite with a volume fraction of zinc oxide of 0.07 at a magnification of 2.67 kx, a working distance of 7.50 mm, and voltage of 30.0 kV.

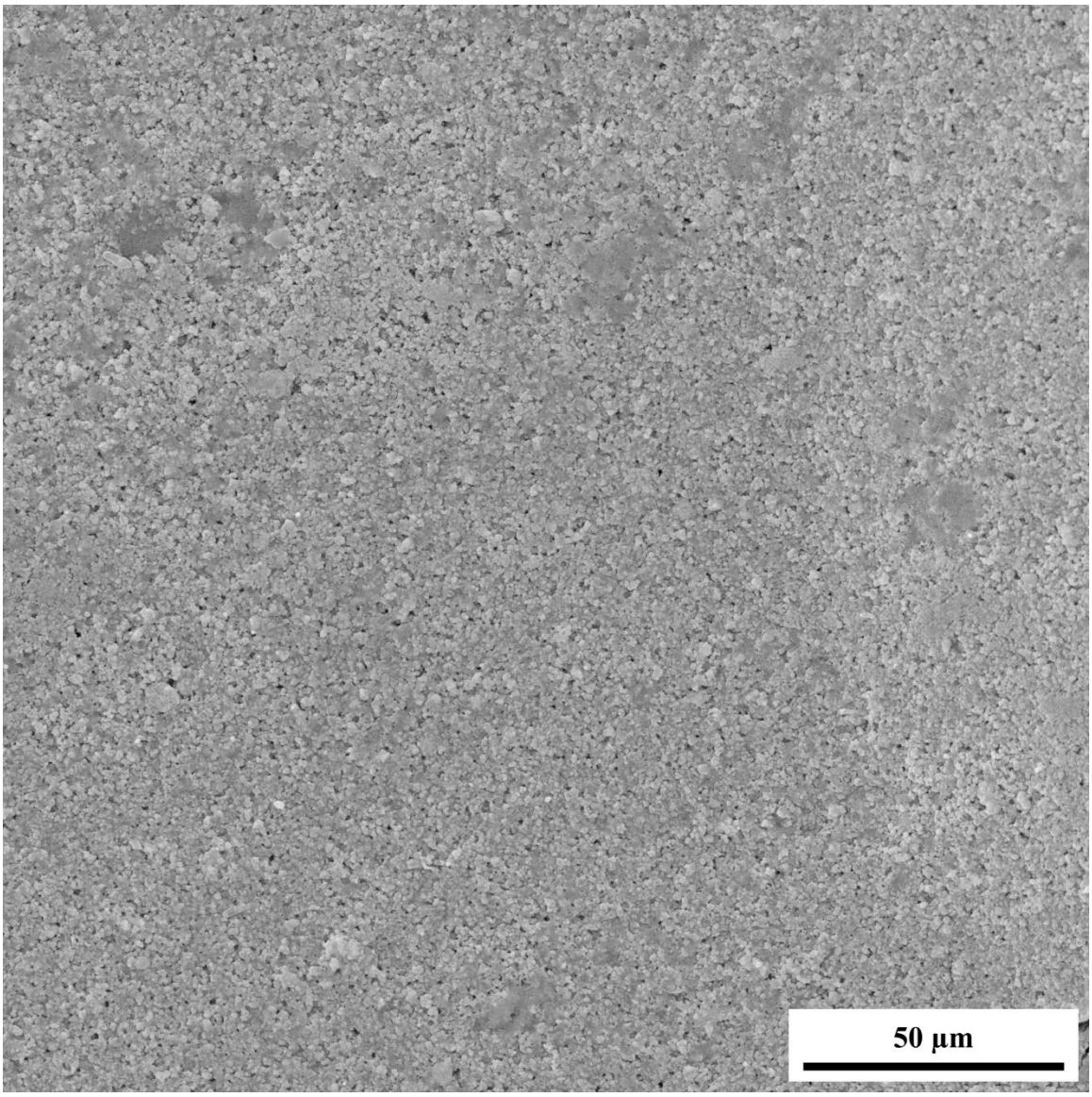

Figure 60. SEM micrograph of the surface of a composite with a volume fraction of zinc oxide of 0.08 at a magnification of 2.67 kx, a working distance of 7.50 mm, and voltage of 30.0 kV.

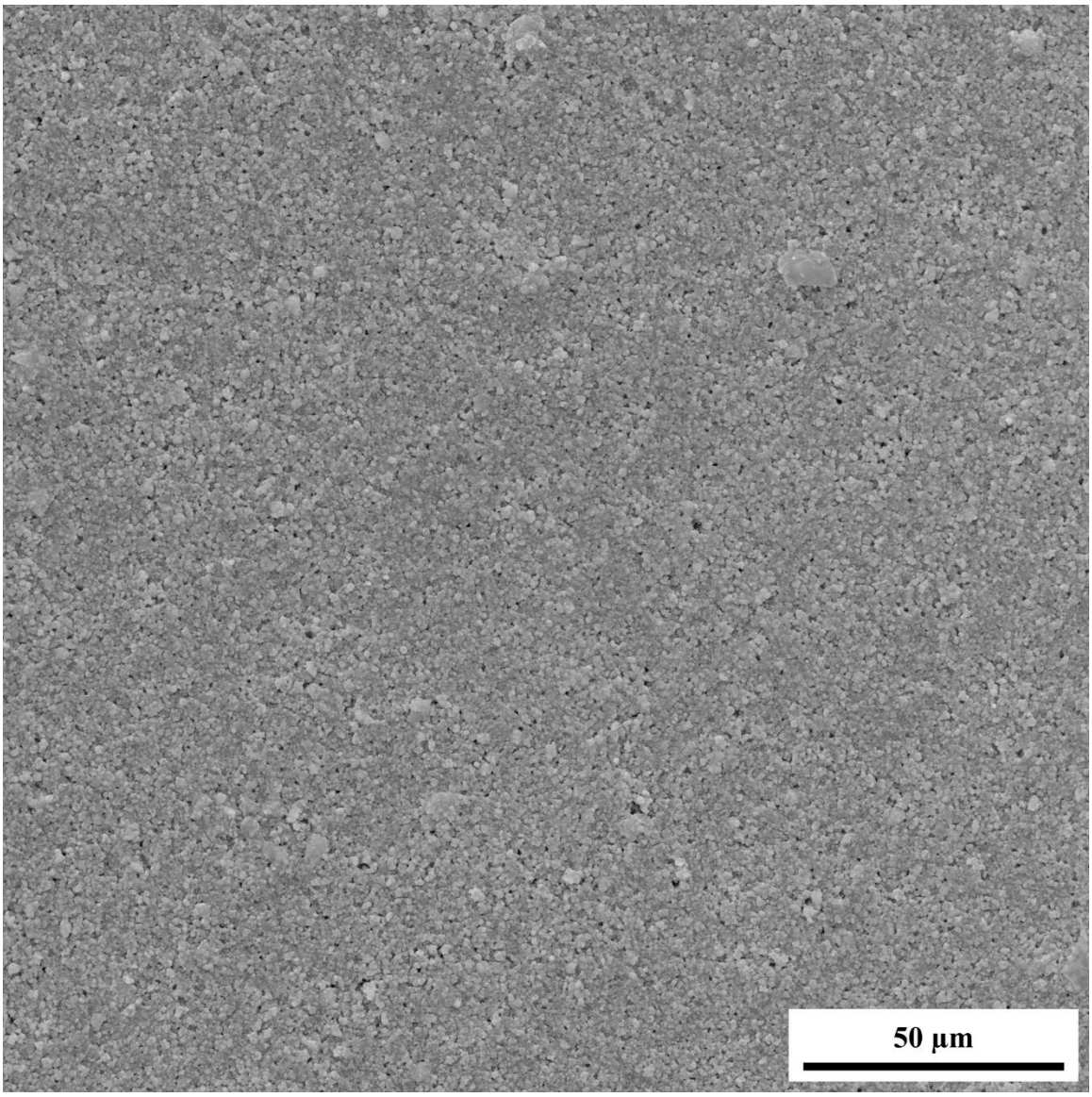

Figure 61. SEM micrograph of the surface of a composite with a volume fraction of zinc oxide of 0.09 at a magnification of 2.67 kx, a working distance of 7.50 mm, and voltage of 30.0 kV.

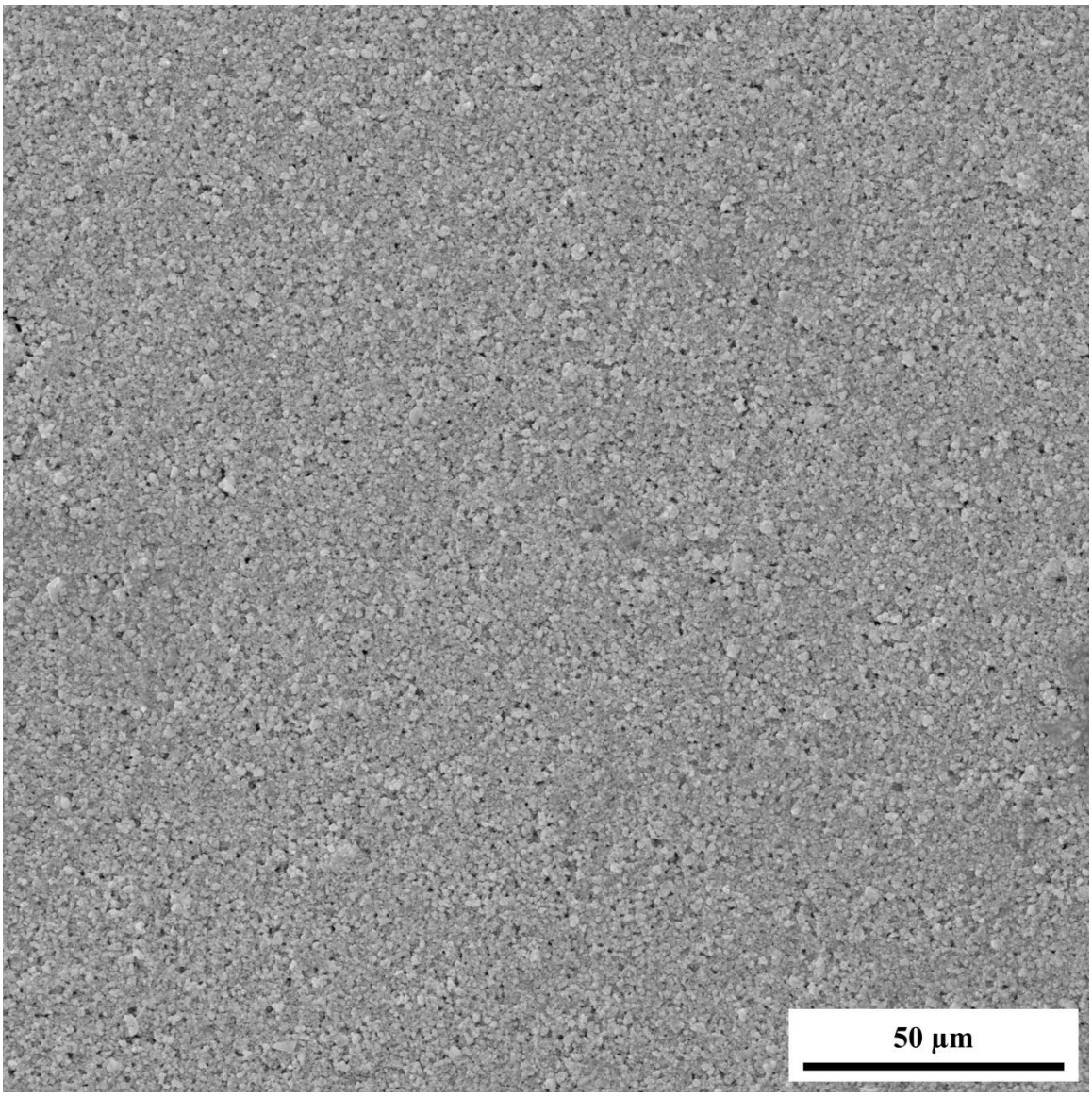

Figure 62. SEM micrograph of the surface of a composite with a volume fraction of zinc oxide of 0.10 at a magnification of 26.7 kx, a working distance of 7.50 mm, and voltage of 30.0 kV.

Figure 63-72 are SEM micrographs of the surface of the composites. The magnification is 26.7 kx, the working distance is 7.50 mm, and the voltage is 30.0 kV. The magnification is slightly less than the SEM micrographs used to determine the ZnO agglomerations. This makes it more difficult for post processing, since the ZnO agglomerations are smaller, but it is easier to see the severity of the number of agglomerations. For example, Figure 63 shows almost zero agglomerations for ZnO volume fractions of 0.01, whereas Figure 73 shows a large amount of agglomerations at a volume fraction of 0.10.

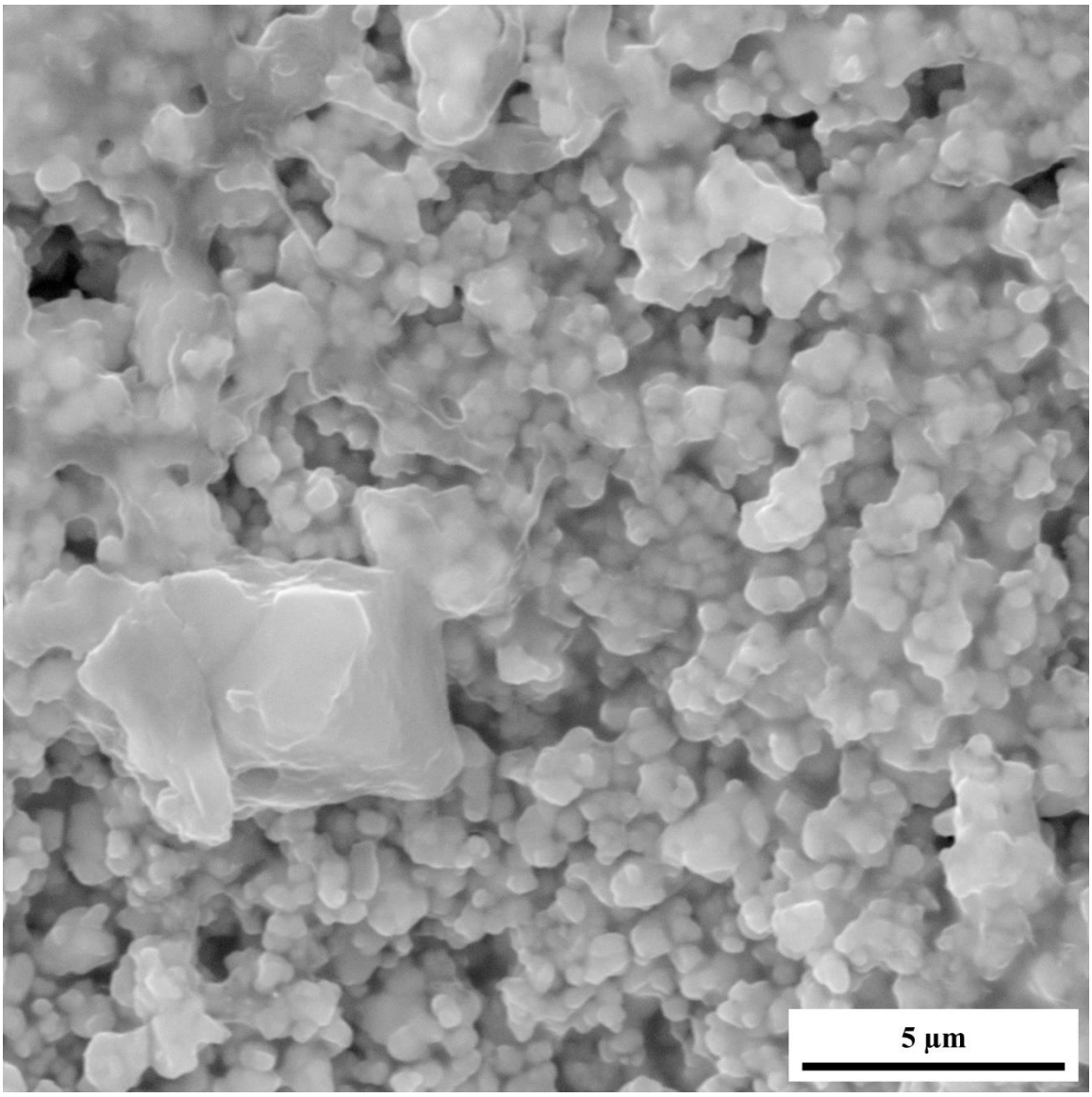

Figure 63. SEM micrograph of the surface of a composite with a volume fraction of zinc oxide of 0.01 at a magnification of 26.7 kx, a working distance of 7.50 mm, and voltage of 30.0 kV.

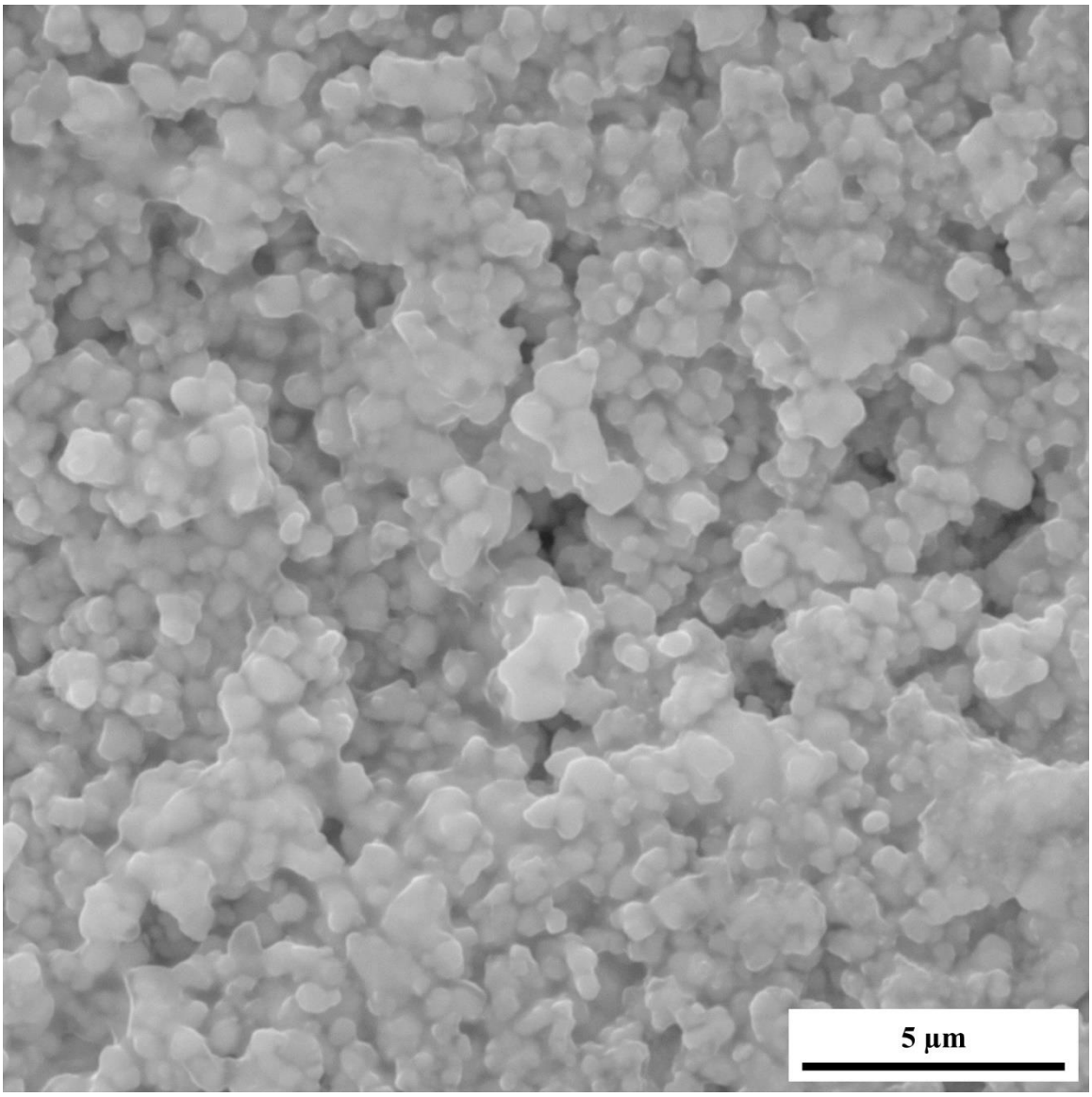

Figure 64. SEM micrograph of the surface of a composite with a volume fraction of zinc oxide of 0.10 at a magnification of 26.7 kx, a working distance of 7.50 mm, and voltage of 30.0 kV.

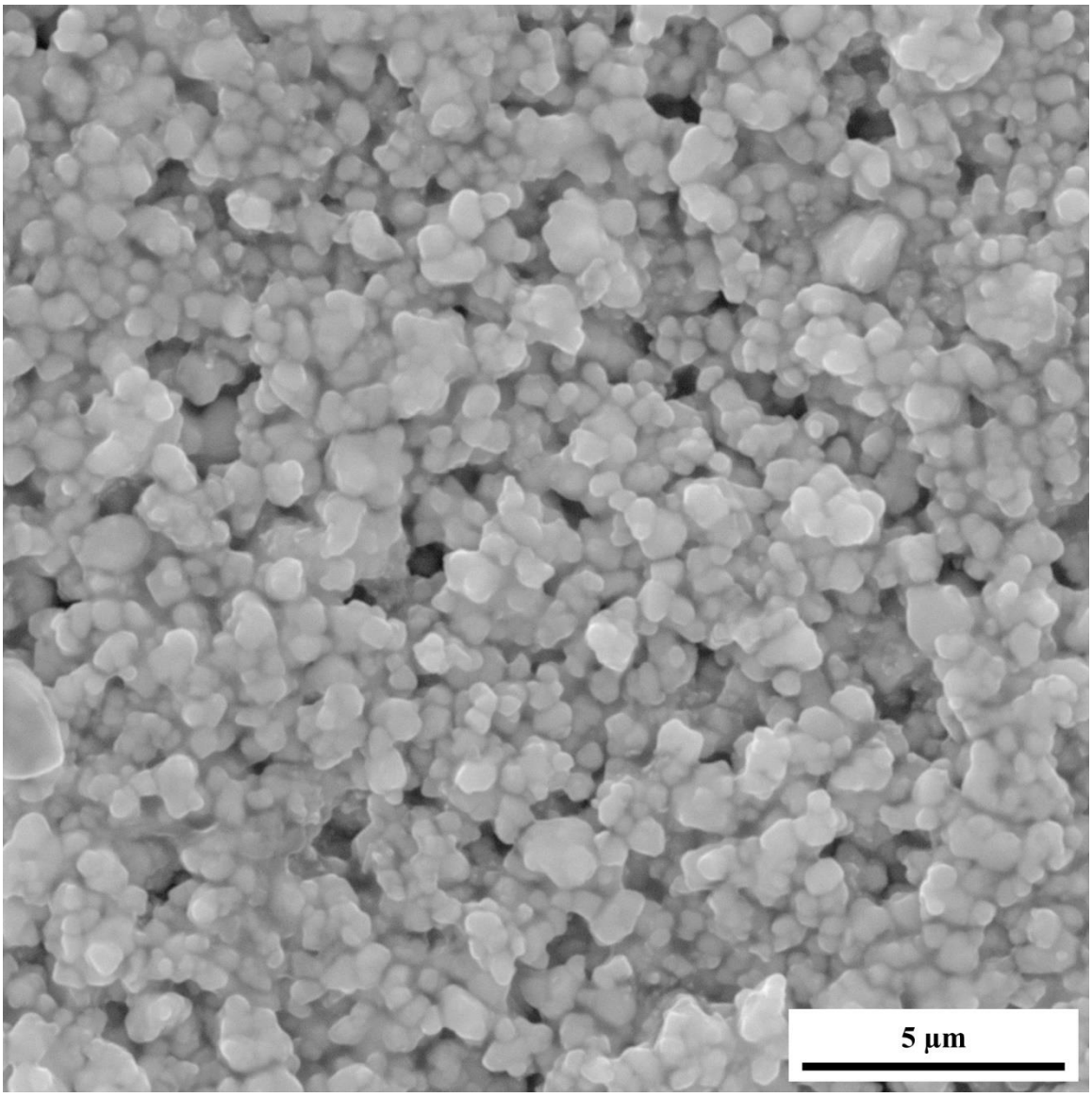

Figure 65. SEM micrograph of the surface of a composite with a volume fraction of zinc oxide of 0.02 at a magnification of 26.7 kx, a working distance of 7.50 mm, and voltage of 30.0 kV.

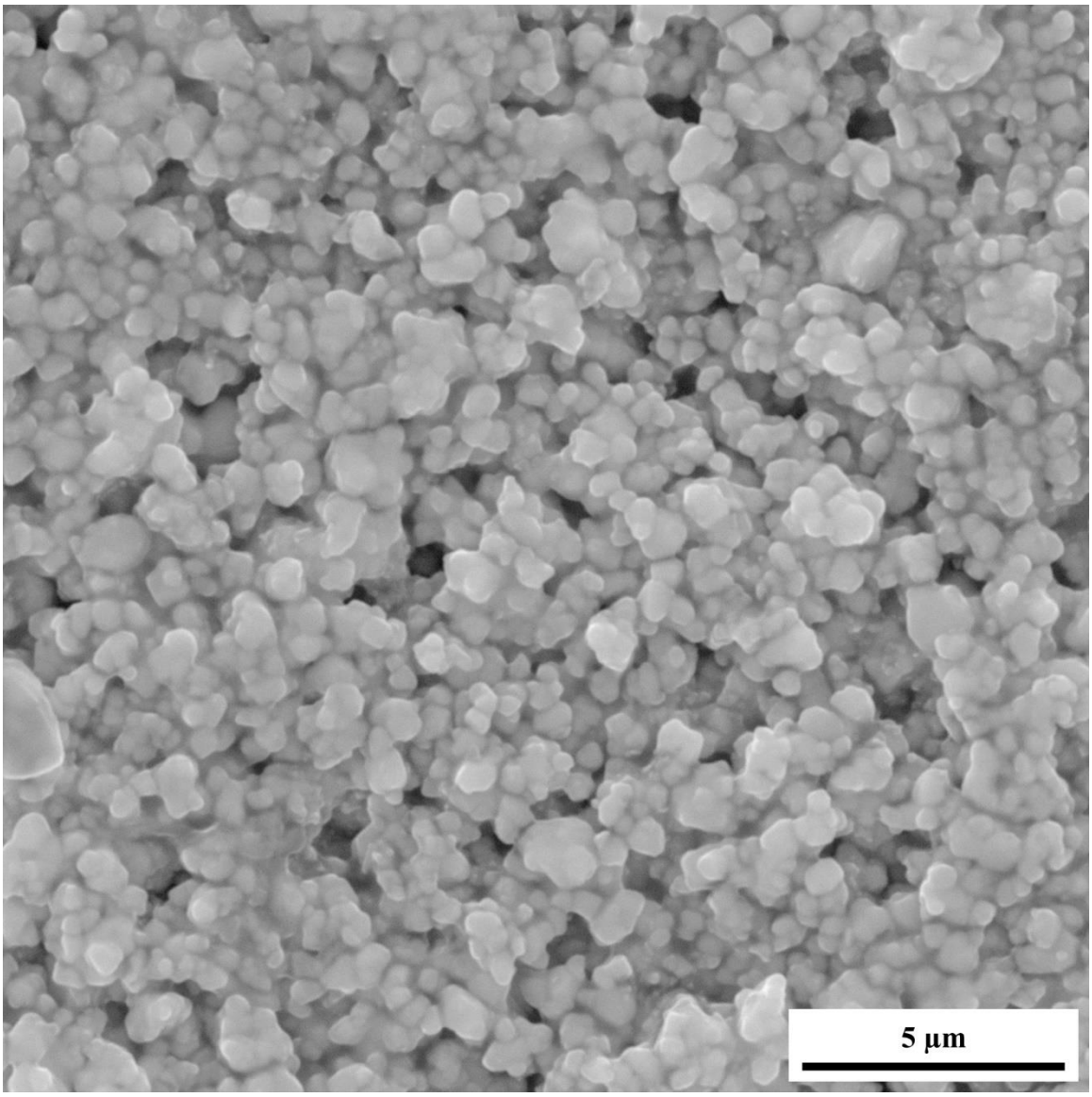

Figure 66. SEM micrograph of the surface of a composite with a volume fraction of zinc oxide of 0.03 at a magnification of 26.7 kx, a working distance of 7.50 mm, and voltage of 30.0 kV.

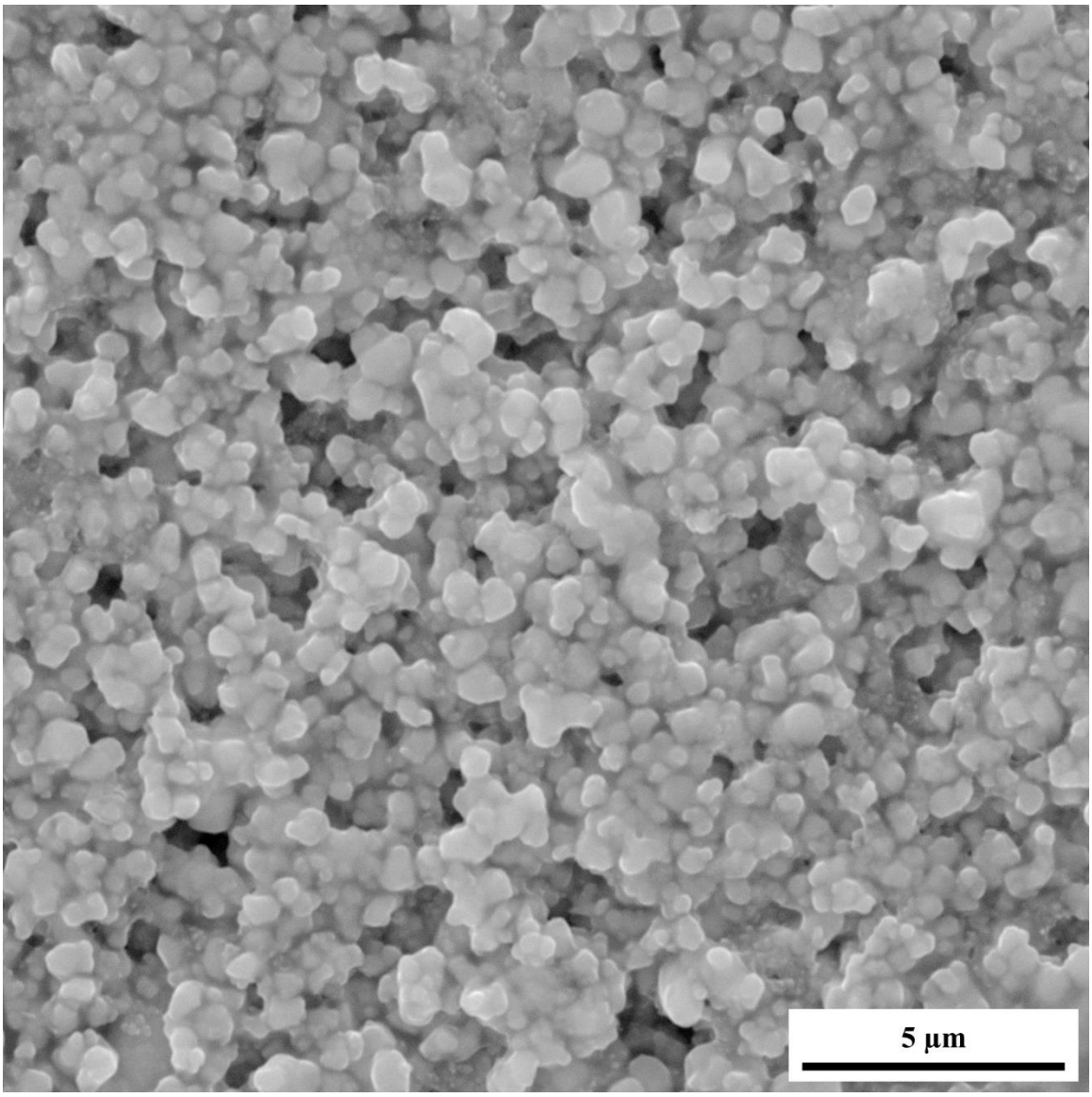

Figure 67. SEM micrograph of the surface of a composite with a volume fraction of zinc oxide of 0.04 at a magnification of 26.7 kx, a working distance of 7.50 mm, and voltage of 30.0 kV.

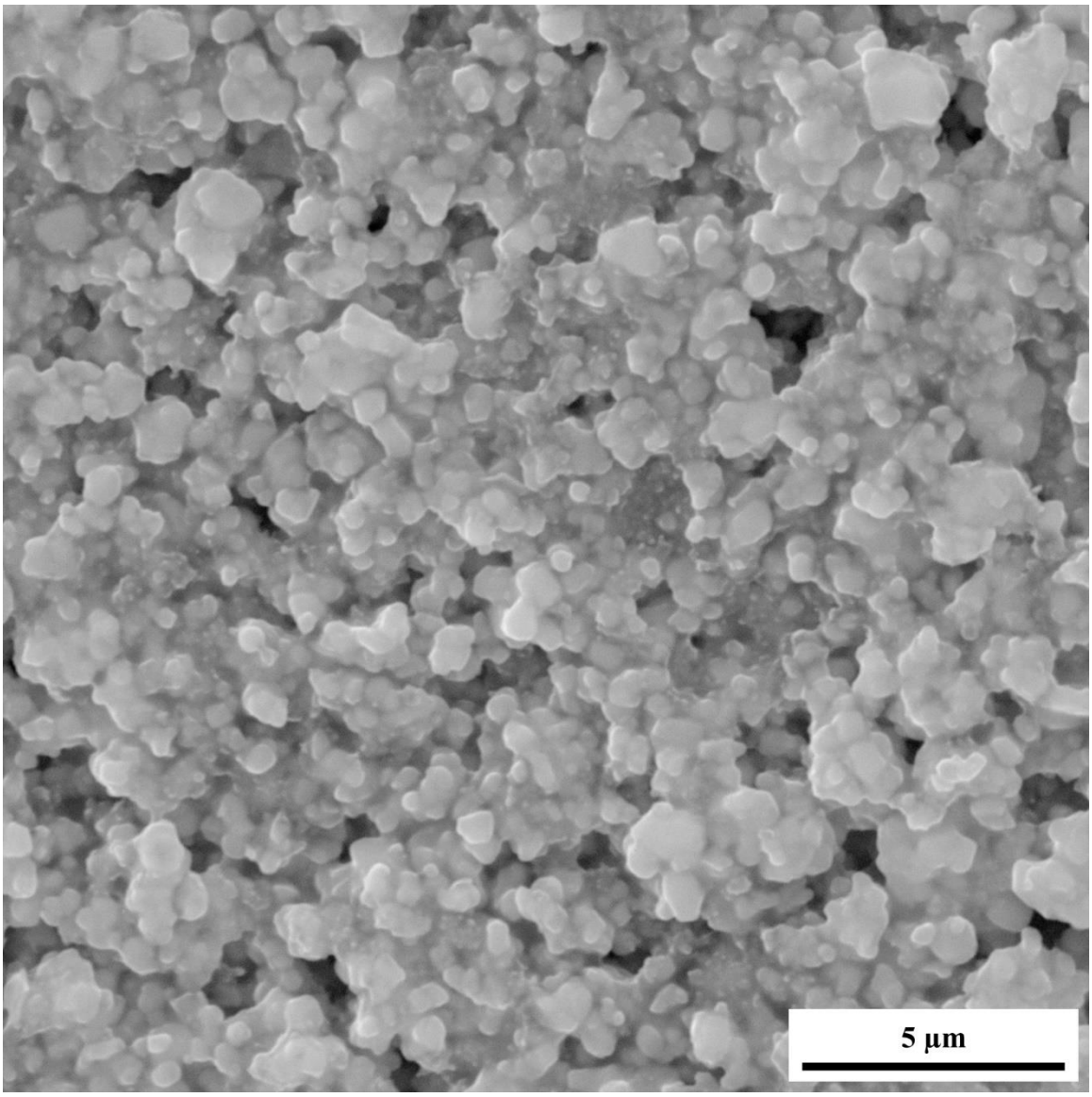

Figure 68. SEM micrograph of the surface of a composite with a volume fraction of zinc oxide of 0.05 at a magnification of 26.7 kx, a working distance of 7.50 mm, and voltage of 30.0 kV.

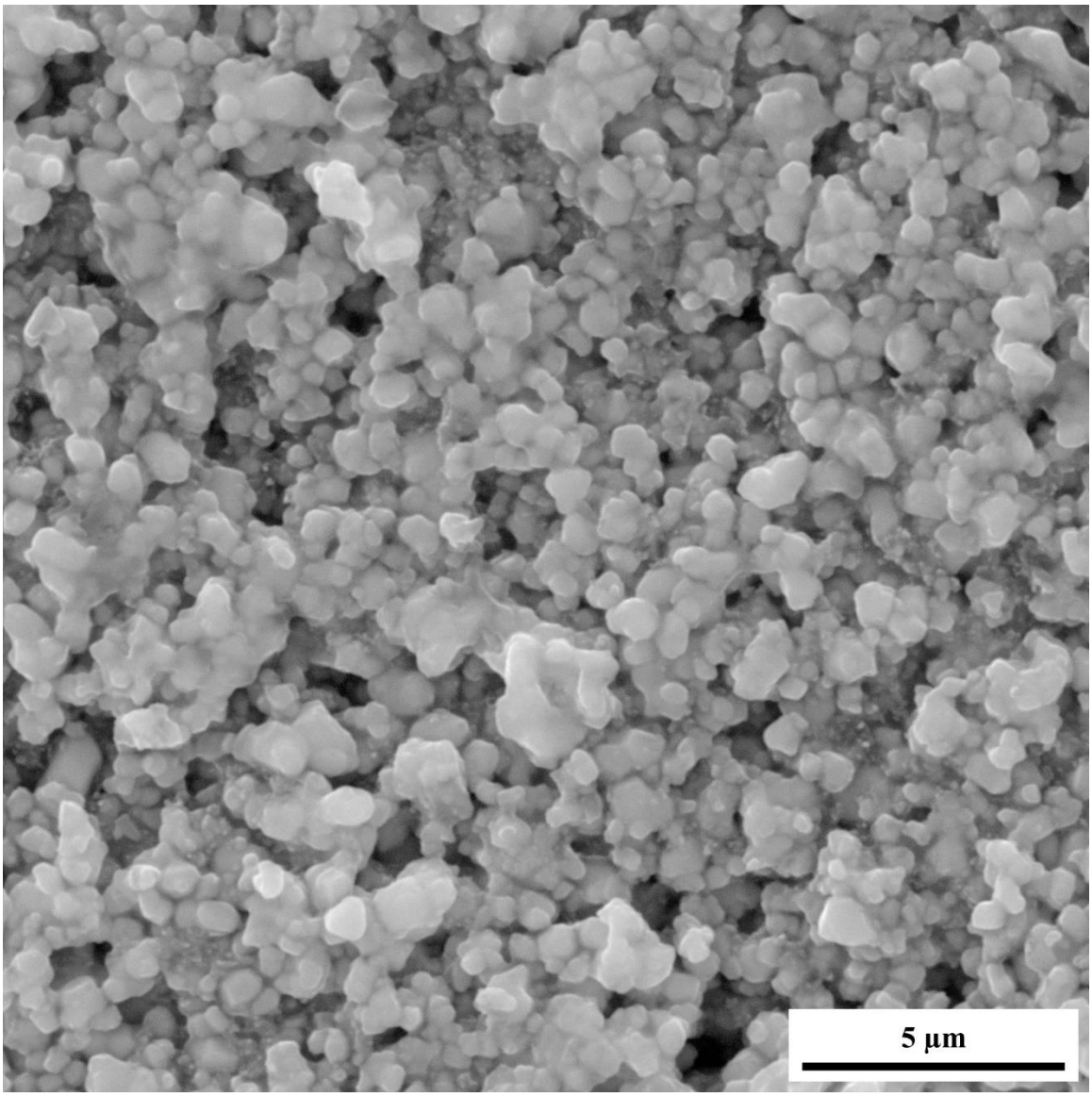

Figure 69. SEM micrograph of the surface of a composite with a volume fraction of zinc oxide of 0.06 at a magnification of 26.7 kx, a working distance of 7.50 mm, and voltage of 30.0 kV.

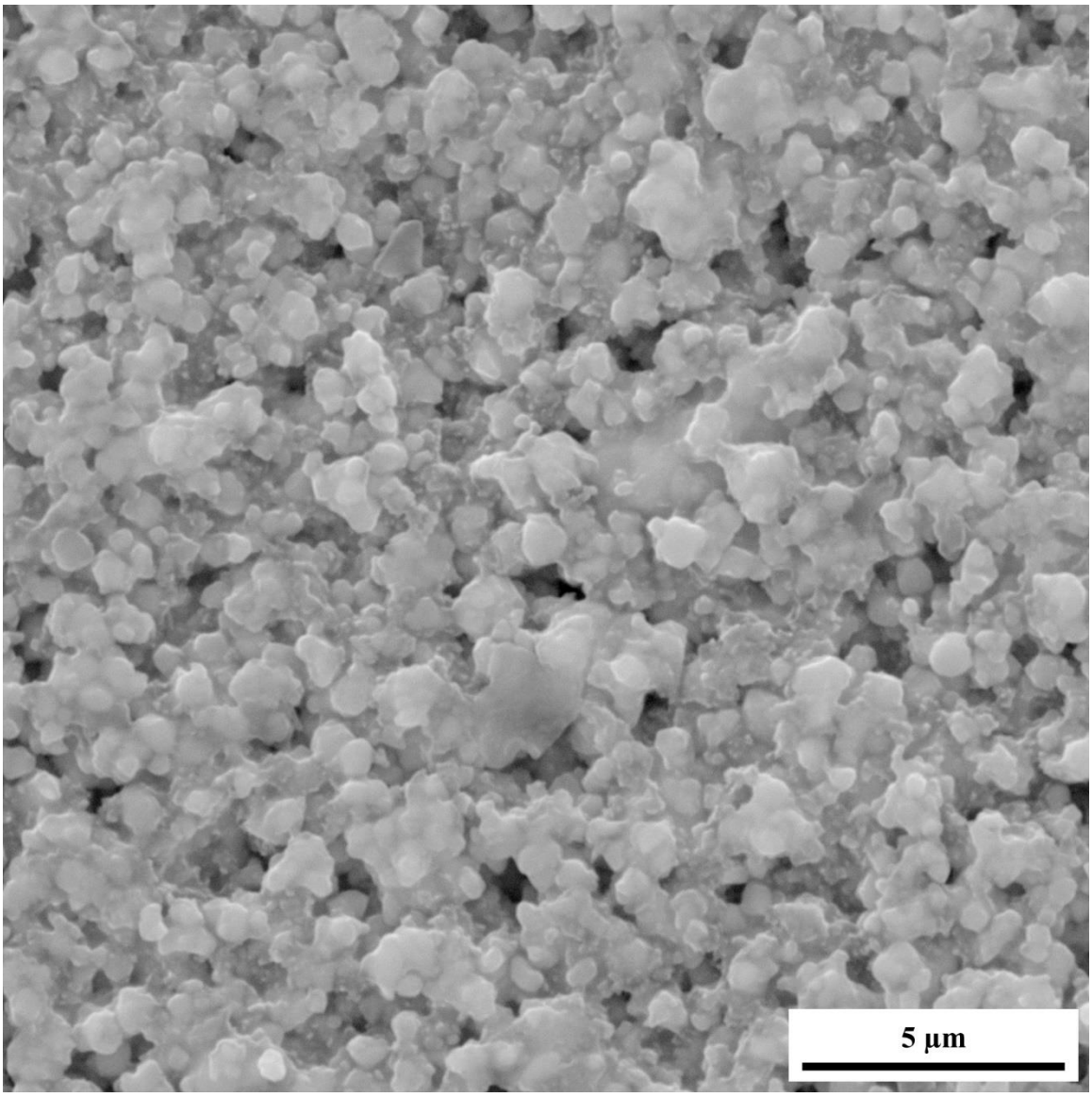

Figure 70. SEM micrograph of the surface of a composite with a volume fraction of zinc oxide of 0.07 at a magnification of 26.7 kx, a working distance of 7.50 mm, and voltage of 30.0 kV.

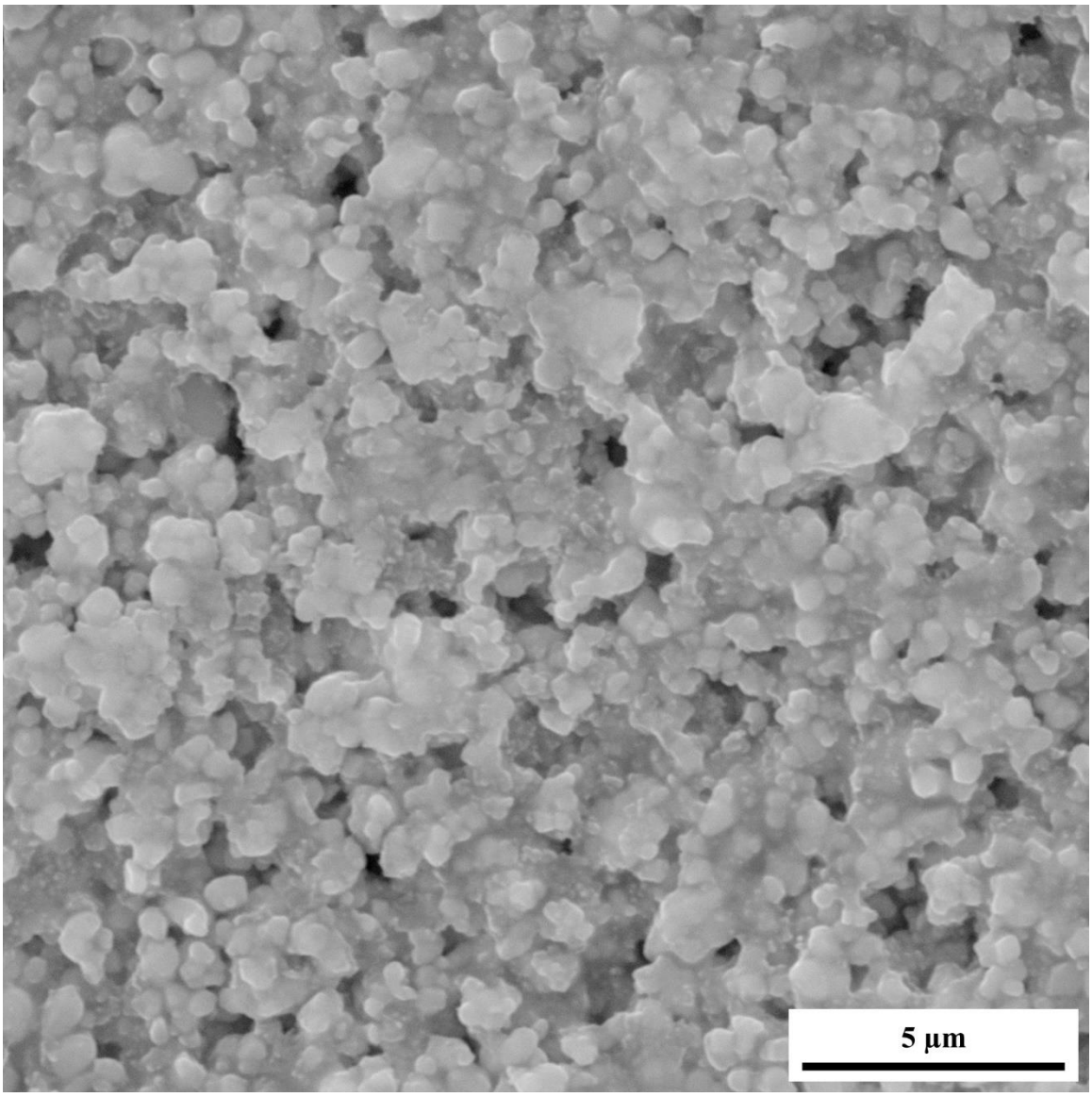

Figure 71. SEM micrograph of the surface of a composite with a volume fraction of zinc oxide of 0.08 at a magnification of 26.7 kx, a working distance of 7.50 mm, and voltage of 30.0 kV.

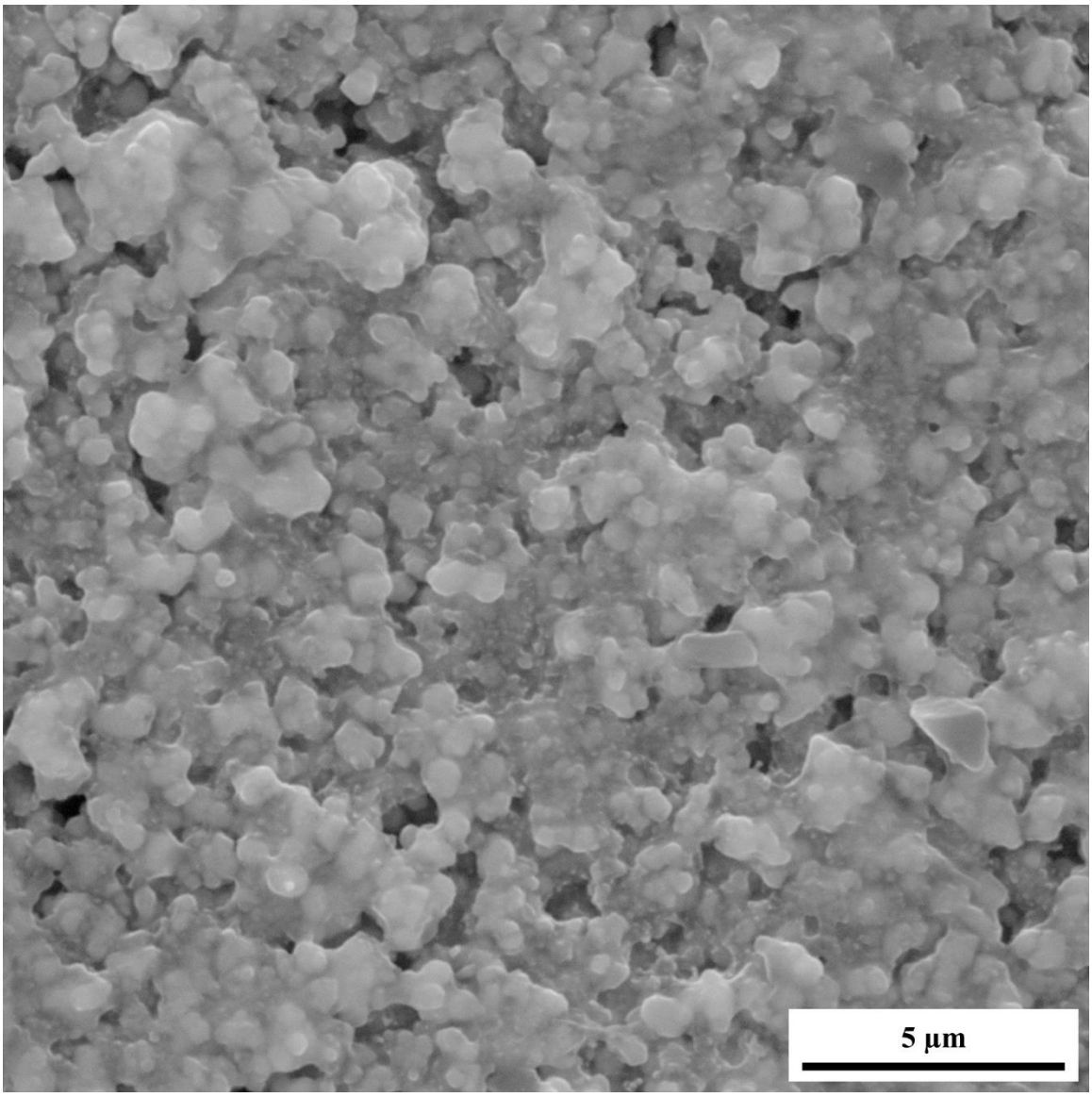

Figure 72. SEM micrograph of the surface of a composite with a volume fraction of zinc oxide of 0.09 at a magnification of 26.7 kx, a working distance of 7.50 mm, and voltage of 30.0 kV.

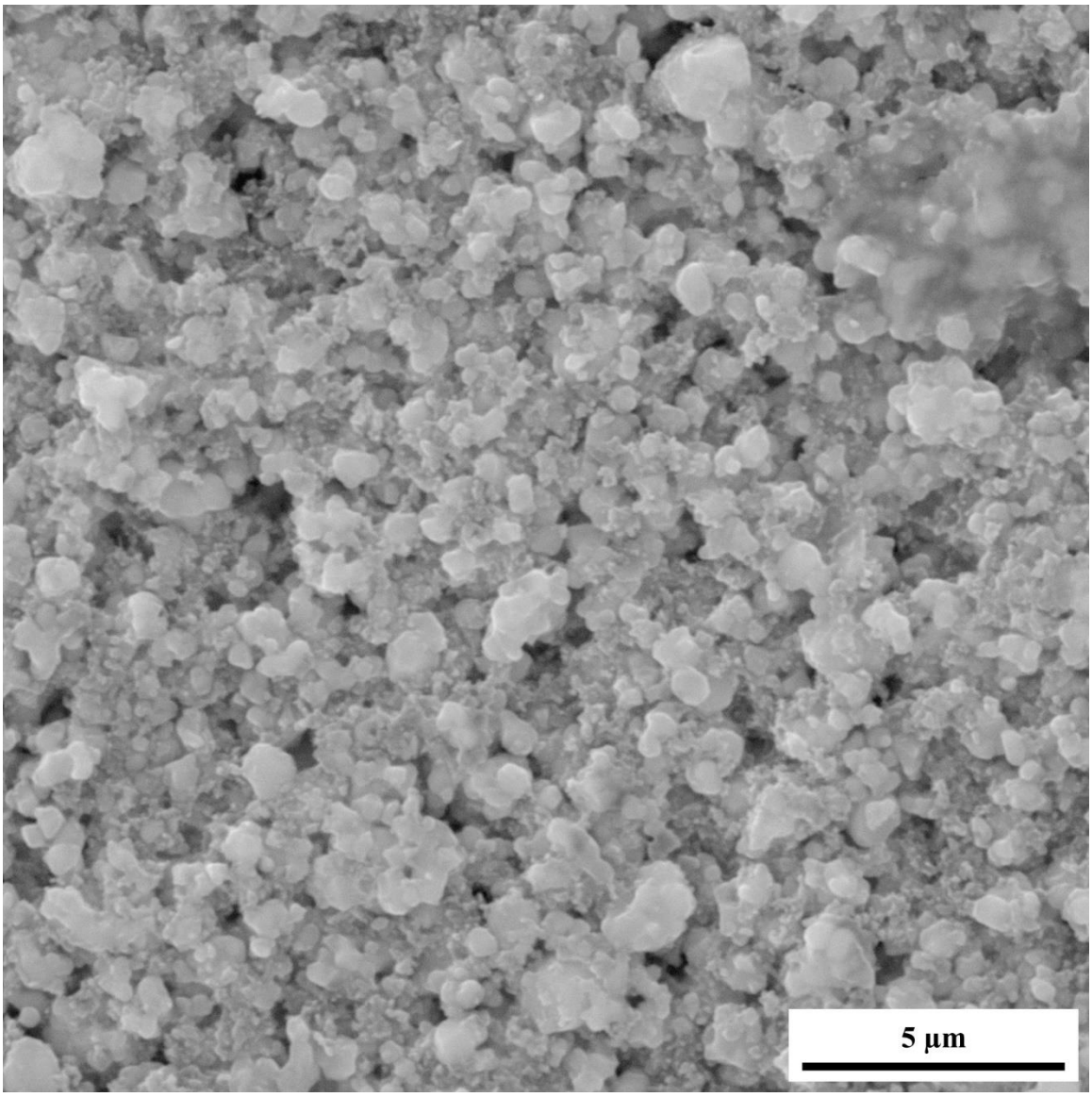

Figure 73. SEM micrograph of the surface of a composite with a volume fraction of zinc oxide of 0.10 at a magnification of 26.7 kx, a working distance of 7.50 mm, and voltage of 30.0 kV.

APPENDIX B: MATLAB PROGRAM

```
% RESEARCH DATA ANALYSIS PROGRAM %
% Values need to be filled in throughout the program.
The
% xlabel, ylabel, and title fucntions are left as they
% were used originally; therefore, if different
parameters
% and materials are being used, the xlabel, ylabel,
and
% title functions need to be changed.
clear
format compact
clc
% USER INPUTS %
% Enter the number of samples tested for each volume
% fraction:
Number_Of_Samples = ;
% Enter the number of testing parameters:
Number_Of_Parameters = ;
%Enter the number of data points collected for each
% parameter:
Number_Of_Data_Points = ;
% Enter the number of thickness measurements taken for
each
% sample:
Number_Of_Thicknesses = ;
% Enter each volume fraction:
%     For example:
%     Volume_Fractions = [0.01; 0.02; 0.03; 0.04;
0.05;
%         0.06; 0.07; 0.08; 0.09; 0.10];
Volume_Fractions = [];
% Enter the smallest volume fraction tested:
Volume_Fraction_Small = ;
% Enter the largest volume fraction tested:
```

```
Volume_Fraction_Large = ;
% Enter the volume fraction increment:
Volume_Fraction_Increment = ;
% Enter the thickness of the substrate (mm)
Substrate_Thickness = ;
% Enter the names of each parameter and their symbol:
%     For example:
%     Parameter_Names =
char({'Impedance';'Resistance';...
%         'Conductance';'Parallel Capacitance';...
%         'Series Capacitance';'Phase Angle';...
%         'Series Inductance';'Parallel Inductance'});
%     Parameter_Units =
char({'\Omega';'\Omega';'S';'F';...
%         'F';'\circ';'H';'H'});
Parameter_Names = char({});
Parameter_Units = char({});
% Enter how you want the graph to be plotted:
%     For example:
%     leg = ['k- ';'b- ';'g- ';'k--';'b--';'g--';'k-
.';...
%     'b-.';'g-.';'k: ';'b: ';'g: '];
leg = [];
% Enter location of excel files to import:
filename_Dim = '';
filename_Imp = '';
% IMPORT DATA FROM EXCEL %
Figure_Counter = 1;
% Math for importation:
Number_of_Volume_Fractions = size(Volume_Fractions,1);
Volume_Fractions_Char = num2str(Volume_Fractions);
Sample_Numbers = zeros(Number_Of_Samples,1);
for i = 1:Number_Of_Samples
    Sample_Numbers(i,1) = i;
end
```

```
Sample_Numbers = num2str(Sample_Numbers);
% Preallocating matrices
Dimensions = zeros(Number_Of_Samples,...
    Number_Of_Thicknesses+
2,Number_of_Volume_Fractions);
Impedances = zeros(Number_Of_Data_Points,...
    Number_Of_Samples.*Number_Of_Parameters + 1,...
    Number_of_Volume_Fractions);
% Importing from excel
for i = 1:Number_of_Volume_Fractions
    Dimensions(:,:,i) = xlsread(filename_Dim,i);
    Impedances(:,:,i) = xlsread(filename_Imp,i);
end
% CONVERT DIMENSIONS INTO USABLE DATA %
% Converts thickness measurements from inches to mm
and
% subtracts thickness of substrate
Dimensions(1:Number_Of_Samples,1:Number_Of_Thicknesses
,...
    1:Number_of_Volume_Fractions) =
25.4*Dimensions(1:...
    Number_Of_Samples,1:Number_Of_Thicknesses,1:...
    Number_of_Volume_Fractions) - Substrate_Thickness;
Dimensions = Dimensions/1000;
% CALCULATE THE AREA AND AVERAGE THICKNESS %
Average_Thicknesses = zeros(Number_Of_Samples,1,...
    Number_of_Volume_Fractions);
Areas = zeros(Number_Of_Samples,1,...
    Number_of_Volume_Fractions);
for j = 1:Number_of_Volume_Fractions
    for i = 1:Number_Of_Samples
        Average_Thicknesses(i,1,j) =
mean(Dimensions(i,...
            1:Number_Of_Thicknesses,j));
        Areas(i,1,j) = Dimensions(i,...
```

```
Number_Of_Thicknesses+1,j)*Dimensions(i,...
            Number_Of_Thicknesses+2,j);
    end
end
Thicknesses = zeros(Number_Of_Samples*...
    Number_Of_Thicknesses,1,
Number_of_Volume_Fractions);
Average_Average_Thicknesses = zeros(...
    Number_of_Volume_Fractions,1);
Std_Average_Thicknesses = zeros(...
    Number_of_Volume_Fractions,1);
for i = 1:Number_of_Volume_Fractions
    m = 1;
    for j = 1:Number_Of_Thicknesses
        for k = 1:Number_Of_Samples
            Thicknesses(m,1,i) = Dimensions(k,j,i);
            m = m + 1;
        end
    end
    Average_Average_Thicknesses(i,1) =
mean(Thicknesses(...
        :,1,i));
    Std_Average_Thicknesses(i,1) =
std(Thicknesses(:,1,i));
end
% PLOT AVERAGE THICKNESS %
hold on
for i = 1:Number_of_Volume_Fractions
    figure(Figure_Counter)

plot(1:Number_Of_Samples,Average_Thicknesses(:,1,i)*..
.
        10^6)
end
```

```
Figure_Counter = Figure_Counter + 1;
title('Average Thickness of the Samples of Each
Batch')
xlabel('Order That Samples Were Fabricated')
ylabel('Thickness (\mum)')
figure(Figure_Counter)
Figure_Counter = Figure_Counter + 1;
errorbar(Volume_Fractions,Average_Average_Thicknesses*
...

10^6,Std_Average_Thicknesses*10^6,'d','MarkerSize',...

5,'MarkerEdgeColor','black','MarkerFaceColor','black')
title('Average Thickness of Each Volume Fraction')
xlabel('Volume Fractions')
ylabel('Thickness (\mum)')
% CONSOLIDATE PARAMETERS %
Parameters = zeros(Number_Of_Data_Points,...
    Number_Of_Samples*Number_of_Volume_Fractions+1,...
    Number_Of_Parameters);
for i = 1:Number_Of_Parameters
    Parameters(:,1,i) = Impedances(:,1,1);
    for j = 1:Number_of_Volume_Fractions
        for k = 2 + Number_Of_Samples*(j - 1):1 + ...
                Number_Of_Samples*j
            Parameters(:,k,i) = Impedances(:,mod(...
                Number_Of_Parameters*(k-2),...

Number_Of_Samples*Number_Of_Parameters) ...
                + (i + 1),j);
        end
    end
end
% GRAPH PARAMETERS %
% Insert the number(s) into the 'i = []' corresponding
```

```
to
% the parameter(s) that are to be graphed
for i = []
    for j = 1:Number_of_Volume_Fractions
        figure(Figure_Counter)
        Figure_Counter = Figure_Counter + 1;
        hold on
        for k = Number_Of_Samples*(j - 1) + ...
                2:Number_Of_Samples*j + 1
            if Parameters(:,k,i) ~= 0

plot(Parameters(:,1,i),Parameters(:,k,...
                    i),leg(Legend_Counter,:))
                Legend_Counter = Legend_Counter + 1;
            end
        end
        Legend_Counter = 1;
        title(strcat(Volume_Fractions_Char(j,:),'-
',...
            Parameter_Names(i,:),' vs. Frequency'))
        xlabel('Frequency (Hz)')
        ylabel(strcat(Parameter_Names(i,:),' (',...
            Parameter_Units(i,:),')'))
        legend(Sample_Numbers)
        hold off
    end
end
% GRAPH LOG OF PARAMETERS %
m = 0;
% Insert the number(s) into the 'i = []' corresponding
to
% the parameter(s) that are to be graphed on a log
scale
for i = []
    for j = 1:Number_of_Volume_Fractions
```

```
        figure(Figure_Counter)
        Figure_Counter = Figure_Counter + 1;
        for l = Number_Of_Samples*(j - 1) + ...
                2:Number_Of_Samples*j + 1
            if Parameters(:,l,i) ~= 0
                m = m + 1;
            end
        end
        Legend_Counter = 1;
        semilogy(Parameters(:,1,i),Parameters(:,...
            Number_Of_Samples*(j - 1) + 2,i),leg(...
            Legend_Counter,:))
        Legend_Counter = Legend_Counter + 1;
        hold on
        for k = Number_Of_Samples*(j - 1) + ...
                3:Number_Of_Samples*(j - 1) + m + 1

semilogy(Parameters(:,1,i),Parameters(:,k,...
                i),leg(Legend_Counter,:))
            Legend_Counter = Legend_Counter + 1;
        end
        hold off
        title(strcat(Volume_Fractions_Char(j,:),'-
',...
            Parameter_Names(i,:),' vs. Frequency'))
        xlabel('Frequency (Hz)')
        ylabel(strcat(Parameter_Names(i,:),' (',...
            Parameter_Units(i,:),')'))
        legend(Sample_Numbers)
        m = 0;
    end
end
% AVERAGE PARAMETERS %
Average_Parameters = zeros(Number_Of_Data_Points,...
    Number_of_Volume_Fractions +
```

```
1,Number_Of_Parameters);
Std_Parameters = zeros(Number_Of_Data_Points,...
    Number_of_Volume_Fractions +
1,Number_Of_Parameters);
for i = 1:Number_Of_Parameters
    Average_Parameters(:,1,i) = Impedances(:,1,1);
    Std_Parameters(:,1,i) = Impedances(:,1,1);
    for j = 1:Number_of_Volume_Fractions
        for k = 1:Number_Of_Data_Points
            Average_Parameters(k,j+1,i) = mean(...
                Parameters(k,Number_Of_Samples*(j-
1)+...
                2:Number_Of_Samples*j+1,i));
            Std_Parameters(k,j+1,i) =
std(Parameters(k,...
                Number_Of_Samples*(j-1)+...
                2:Number_Of_Samples*j+1,i));
        end
    end
end
% GRAPH AVERAGE PARAMETERS %
% Insert the number(s) into the 'i = []' corresponding
to
% the parameter(s) that are to be graphed
for i = []
    figure(Figure_Counter)
    Figure_Counter = Figure_Counter + 1;
    Legend_Counter = 1;
    hold on
    for j = 2:Number_of_Volume_Fractions + 1
        plot(Average_Parameters(:,1,1),...
            Average_Parameters(:,j,i),leg(...
            Legend_Counter,:))
        Legend_Counter = Legend_Counter + 1;
    end
```

```
    hold off
    xlabel('Frequency (Hz)')
    ylabel(strcat(Parameter_Names(i,:),' (',...
        Parameter_Units(i,:),')'))
    title(strcat('Average ',Parameter_Names(i,:),...
        ' vs. Frequency'))
    legend(Volume_Fractions_Char)
end
% GRAPH LOG OF AVERAGE PARAMETERS %
% Insert the number(s) into the 'i = []' corresponding
to
% the parameter(s) that are to be graphed
for i = []
    figure(Figure_Counter)
    Figure_Counter = Figure_Counter + 1;
    Legend_Counter = 1;
    semilogy(Average_Parameters(:,1,1),...

Average_Parameters(:,2,i),leg(Legend_Counter,:))
    Legend_Counter = Legend_Counter + 1;
    hold on
    for j = 3:Number_of_Volume_Fractions + 1
        semilogy(Average_Parameters(:,1,1),...
            Average_Parameters(:,j,i),leg(...
            Legend_Counter,:))
        Legend_Counter = Legend_Counter + 1;
    end
    xlabel('Frequency (Hz)')
    ylabel(strcat(Parameter_Names(i,:),' (',...
        Parameter_Units(i,:),')'))
    title(strcat(Parameter_Names(i,:),' vs.
Frequency'))
    legend(Volume_Fractions_Char)
end
% CALCULATE DIELECTRIC CONSTANT %
```

```
j = 1;
Vacuum_Permittivity = 8.854*10^-12;
for i = 1:Number_Of_Parameters
    found =
strfind(Parameter_Names(i,:),'Capacitance');
    if found > 0
        Capacitance_Location(j,1) = i;
        j = j + 1;
    end
end
if j == 1
    j = j + 1;
end
[r,c,~] = size(Parameters);
Dielectric_Constant = zeros(r,c,j-1);
[rr,~] = size(Capacitance_Location);
Dielectric_Constant(:,1) = Parameters(:,1,1);
for i = 1:rr
    k = 1;
    for j = 2:c
        Dielectric_Constant(:,j,i) =
Parameters(:,j,...
            Capacitance_Location(i,1))*...
            Average_Thicknesses(mod(j-2,...
            Number_Of_Samples)+1,1,k)/(...
            Vacuum_Permittivity*Areas(mod(j-2,...
            Number_Of_Samples)+1,1,k));
        if  mod(j-2,Number_Of_Samples)+1 == ...
                Number_Of_Samples
            k = k + 1;
        end
    end
end
% GRAPH DIELECTRIC CONSTANT %
[~,~,h] = size(Dielectric_Constant);
```

```
for i = 1:h
    for j = 1:Number_of_Volume_Fractions
        figure(Figure_Counter)
        Figure_Counter = Figure_Counter + 1;
        plot(Dielectric_Constant(:,1,1),...

Dielectric_Constant(:,Number_Of_Samples*...
            (j-1)+2:Number_Of_Samples*j+1,i))
        xlabel('Frequency (Hz)')
        ylabel('Dielectric Constant')
        title(strcat(Volume_Fractions_Char(j,:),...
            '-Dielectric Constant vs. Frequency'))
        legend(Sample_Numbers)
        figure(Figure_Counter)
        Figure_Counter = Figure_Counter + 1;
        semilogy(Dielectric_Constant(:,1,1),...

Dielectric_Constant(:,Number_Of_Samples*...
            (j-1)+2:Number_Of_Samples*j+1,i))
        xlabel('Frequency (Hz)')
        ylabel('Dielectric Constant')
        title(strcat(Volume_Fractions_Char(j,:),...
            '-Dielectric Constant vs. Frequency'))
        legend(Sample_Numbers)
    end
end
% CALCULATE AVERAGE DIELECTRIC CONSTANT %
[r,~,h] = size(Dielectric_Constant);
Average_Dielectric_Constant = zeros(r,...
    Number_of_Volume_Fractions + 1,h);
Std_Dielectric_Constant = zeros(r,...
    Number_of_Volume_Fractions + 1,h);
for i = 1:h
    Average_Dielectric_Constant(:,1,i) = ...
        Dielectric_Constant(:,1,1);
```

```
    for j = 1:Number_of_Volume_Fractions
        for k = 1:r
            Average_Dielectric_Constant(k,j+1,i) =
mean(...

Dielectric_Constant(k,Number_Of_Samples*...
                (j-1)+2:Number_Of_Samples*j+1,i));
            Std_Dielectric_Constant(k,j+1,i) = std(...

Dielectric_Constant(k,Number_Of_Samples*...
                (j-1)+2:Number_Of_Samples*j+1,i));
        end
    end
end
% GRAPH AVERAGE DIELECTRIC CONSTANT %
figure(Figure_Counter)
Figure_Counter = Figure_Counter + 1;
Legend_Counter = 1;
hold on
for j = 2:Number_of_Volume_Fractions + 1
    plot(Average_Dielectric_Constant(:,1,1),...
        Average_Dielectric_Constant(:,j,1),leg(...
            Legend_Counter,:))
    Legend_Counter = Legend_Counter + 1;
end
hold off
xlabel('Frequency (Hz)')
ylabel('Dielectric Constant')
title('Dielectric Constant vs. Frequency')
legend(Volume_Fractions_Char)
% GRAPH AVERAGE DIELECTRIC CONSTANT WITH ERRORBARS %
[~,~,h] = size(Dielectric_Constant);
for i = 1:h
    for j = 1:Number_of_Volume_Fractions
        figure(Figure_Counter)
```

```
        Figure_Counter = Figure_Counter + 1;

errorbar(Average_Dielectric_Constant(:,1,1),...
            Average_Dielectric_Constant(:,j+1,i),...
            Std_Dielectric_Constant(:,j+1,i),'-d',...

'MarkerSize',1,'MarkerEdgeColor','black',...
            'MarkerFaceColor','black')
        xlim([min(Average_Dielectric_Constant(:,1,1))
...
            max(Average_Dielectric_Constant(:,1,1))])
        xlabel('Frequency (Hz)')
        ylabel('Dielectric Constant')
        title(strcat(Volume_Fractions_Char(j,:),...
            '-Dielectric Constant vs. Frequency'))
        figure(Figure_Counter)
        Figure_Counter = Figure_Counter + 1;

errorbar(Average_Dielectric_Constant(:,1,1),...
            Average_Dielectric_Constant(:,j+1,i),...
            Std_Dielectric_Constant(:,j+1,i),'-d',...
                'MarkerSize',1,'MarkerEdgeColor',...
                'black','MarkerFaceColor','black')
        set(gca,'YScale','log');
        xlim([min(Average_Dielectric_Constant(:,1,1))
...
            max(Average_Dielectric_Constant(:,1,1))])
        ymin =
min(Average_Dielectric_Constant(:,j+1,i));
        ymax =
max(Average_Dielectric_Constant(:,j+1,i));
        if ymin < 0, ymin = ymin*10; else, ymin =
ymin*...
                0.1; end
        if ymax < 0, ymax = ymax*0.1; else, ymax =
```

```
ymax...
                *10; end
        ylim([ymin ymax])
        xlabel('Frequency (Hz)')
        ylabel('Dielectric Constant')
        title(strcat(Volume_Fractions_Char(j,:),...
            '-Dielectric Constant vs. Frequency'))
    end
end
% CALCULATE RESISTIVITY %
j = 1;
for i = 1:Number_Of_Parameters
    found =
strfind(Parameter_Names(i,:),'Resistance');
    if found > 0
        Resistance_Location(j,1) = i;
        j = j + 1;
    end
end
if j == 1
    j = j + 1;
end
[r,c,~] = size(Parameters);
Resistivity = zeros(r,c,j-1);
[rr,~] = size(Resistance_Location);
Resistivity(:,1) = Parameters(:,1,1);
for i = 1:rr
    k = 1;
    for j = 2:c
        Resistivity(:,j,i) = Parameters(:,j,...
            Resistance_Location(i,1))*Areas(mod(j-
2,...
            Number_Of_Samples)+1,1,k)/...
            Average_Thicknesses(mod(j-2,...
            Number_Of_Samples)+1,1,k);
```

```
        if  mod(j-2,Number_Of_Samples)+1 == ...
                Number_Of_Samples
            k = k + 1;
        end
    end
end
% GRAPH RESISTIVITY %
[~,~,h] = size(Resistivity);
for i = 1:h
    for j = 1:Number_of_Volume_Fractions
        figure(Figure_Counter)
        Figure_Counter = Figure_Counter + 1;
        plot(Resistivity(:,1,1),Resistivity(:,...
            Number_Of_Samples*(j-
1)+2:Number_Of_Samples*...
            j+1,i))
        xlabel('Frequency (Hz)')
        ylabel('Resistivity (\Omega-m)')
        title(strcat(Volume_Fractions_Char(j,:),...
            '-Resistivity vs. Frequency'))
        legend(Sample_Numbers)
        figure(Figure_Counter)
        Figure_Counter = Figure_Counter + 1;
        semilogy(Resistivity(:,1,1),Resistivity(:,...
            Number_Of_Samples*(j-1)+...
            2:Number_Of_Samples*j+1,i))
        xlabel('Frequency (Hz)')
        ylabel('Resistivity (\Omega-m)')
        title(strcat(Volume_Fractions_Char(j,:),...
            '-Resistivity vs. Frequency'))
        legend(Sample_Numbers)
    end
end
% CALCULATE AVERAGE RESISTIVITY %
clc
```

```
%-----%
[r,~,h] = size(Resistivity);
Average_Resistivity =
zeros(r,Number_of_Volume_Fractions...
    + 1,h);
Std_Resistivity = zeros(r,Number_of_Volume_Fractions +
...
    1,h);
for i = 1:h
    Average_Resistivity(:,1,i) = Resistivity(:,1,1);
    for j = 1:Number_of_Volume_Fractions
        for k = 1:r
            Average_Resistivity(k,j+1,i) = mean(...
                Resistivity(k,Number_Of_Samples*(j-
1)+...
                2:Number_Of_Samples*j+1,i));
            Std_Resistivity(k,j+1,i) = std(...
                Resistivity(k,Number_Of_Samples*(j-
1)+...
                2:Number_Of_Samples*j+1,i));
        end
    end
end
% GRAPH AVERAGE RESISTIVITY WIHT ERRORBARS %
[~,~,h] = size(Resistivity);
for i = 1:h
    for j = 1:Number_of_Volume_Fractions
        figure(Figure_Counter)
        Figure_Counter = Figure_Counter + 1;
        errorbar(Average_Resistivity(:,1,1),...

Average_Resistivity(:,j+1,i),Std_Resistivity...
            (:,j+1,i),'-d','MarkerSize',1,...

'MarkerEdgeColor','black','MarkerFaceColor',...
```

```
            'black')
        xlim([min(Average_Resistivity(:,1,1)) max(...
            Average_Resistivity(:,1,1))])
        xlabel('Frequency (Hz)')
        ylabel('Resistivity (\Omega-m)')
        title(strcat(Volume_Fractions_Char(j,:),...
            '-Resistivity vs. Frequency'))
        figure(Figure_Counter)
        Figure_Counter = Figure_Counter + 1;
        errorbar(Average_Resistivity(:,1,1),...

Average_Resistivity(:,j+1,i),Std_Resistivity...
            (:,j+1,i),'-d','MarkerSize',1,...

'MarkerEdgeColor','black','MarkerFaceColor',...
            'black')
        set(gca,'YScale','log');
        xlim([min(Average_Resistivity(:,1,1)) max(...
            Average_Resistivity(:,1,1))])
        xlabel('Frequency (Hz)')
        ylabel('Resistivity (\Omega-m)')
        title(strcat(Volume_Fractions_Char(j,:),...
            '-Resistivity vs. Frequency'))
    end
end
% GRAPH AVERAGE RESISITIVITY %
figure(Figure_Counter)
Figure_Counter = Figure_Counter + 1;
Legend_Counter = 1;
semilogy(Average_Resistivity(:,1,1),...
    Average_Resistivity(:,2,1),leg(Legend_Counter,:))
Legend_Counter = Legend_Counter + 1;
hold on
for j = 3:Number_of_Volume_Fractions + 1
    semilogy(Average_Resistivity(:,1,1),...
```

```
Average_Resistivity(:,j,1),leg(Legend_Counter,:))
    Legend_Counter = Legend_Counter + 1;
end
hold off
xlabel('Frequency (Hz)')
ylabel('Resistivity (\Omega-m)')
title('Average Resistivity vs. Frequency')
legend(Volume_Fractions_Char)
% CALCULATE CONDUCTIVITY %
j = 1;
for i = 1:Number_Of_Parameters
    found =
strfind(Parameter_Names(i,:),'Conductance');
    if found > 0
        Conductance_Location(j,1) = i;
        j = j + 1;
    end
end
if j == 1
    j = j + 1;
end
[r,c,~] = size(Parameters);
Conductivity = zeros(r,c,j-1);
[rr,~] = size(Resistance_Location);
Conductivity(:,1) = Parameters(:,1,1);
for i = 1:rr
    k = 1;
    for j = 2:c
        Conductivity(:,j,i) = Parameters(:,j,...
            Conductance_Location(i,1))*...
            Average_Thicknesses(mod(j-2,...
            Number_Of_Samples)+1,1,k)/Areas(mod(j-
2,...
            Number_Of_Samples)+1,1,k);
```

```
        if  mod(j-2,Number_Of_Samples)+1 == ...
                Number_Of_Samples
            k = k + 1;
        end
    end
end
% GRAPH CONDUCTIVITY %
[~,~,h] = size(Conductivity);
for i = 1:h
    for j = 1:Number_of_Volume_Fractions
        figure(Figure_Counter)
        Figure_Counter = Figure_Counter + 1;
        plot(Conductivity(:,1,1),Conductivity(:,...
            Number_Of_Samples*(j-
1)+2:Number_Of_Samples*...
            j+1,i))
        xlabel('Frequency (Hz)')
        ylabel('Conductivity (S/m)')
        title(strcat(Volume_Fractions_Char(j,:),...
            '-Conductivity vs. Frequency'))
        legend(Sample_Numbers)
        figure(Figure_Counter)
        Figure_Counter = Figure_Counter + 1;

semilogy(Conductivity(:,1,1),Conductivity(:,...
            Number_Of_Samples*(j-
1)+2:Number_Of_Samples*...
            j+1,i))
        xlabel('Frequency (Hz)')
        ylabel('Conductivity (S/m)')
        title(strcat(Volume_Fractions_Char(j,:),...
            '-Conductivity vs. Frequency'))
        legend(Sample_Numbers)
    end
end
```

```
% CALCULATE AVERAGE CONDUCTIVITY %
[r,~,h] = size(Conductivity);
Average_Conductivity = zeros(r,...
    Number_of_Volume_Fractions + 1,h);
Std_Conductivity = zeros(r,Number_of_Volume_Fractions
+...
    1,h);
for i = 1:h
    Average_Conductivity(:,1,i) = Conductivity(:,1,1);
    for j = 1:Number_of_Volume_Fractions
        for k = 1:r
            Average_Conductivity(k,j+1,i) = mean(...
                Conductivity(k,Number_Of_Samples*(j-
1)+...
                2:Number_Of_Samples*j+1,i));
            Std_Resistivity(k,j+1,i) = std(...
                Conductivity(k,Number_Of_Samples*(j-
1)+...
                2:Number_Of_Samples*j+1,i));
        end
    end
end
% GRAPH AVERAGE CONDUCTIVITY %
figure(Figure_Counter)
Figure_Counter = Figure_Counter + 1;
Legend_Counter = 1;
hold on
for j = 2:Number_of_Volume_Fractions + 1
    plot(Average_Conductivity(:,1,1),...

Average_Conductivity(:,j,1),leg(Legend_Counter,:))
    Legend_Counter = Legend_Counter + 1;
end
hold off
xlabel('Frequency (Hz)')
```

```
ylabel('Conductivity (S/m)')
title('Average Conductivity vs. Frequency')
legend(Volume_Fractions_Char)
% GRAPH AVERAGE CONDUCTIVITY WITH ERRORBARS %
[~,~,h] = size(Conductivity);
for i = 1:h
    for j = 1:Number_of_Volume_Fractions
        figure(Figure_Counter)
        Figure_Counter = Figure_Counter + 1;
        errorbar(Average_Conductivity(:,1,1),...
            Average_Conductivity(:,j+1,i),...
            Std_Conductivity(:,j+1,i),'-
d','MarkerSize',...
            1,'MarkerEdgeColor','black',...
            'MarkerFaceColor','black')
        xlim([min(Average_Conductivity(:,1,1)) max(...
            Average_Conductivity(:,1,1))])
        xlabel('Frequency (Hz)')
        ylabel('Conductivity (S/m)')
        title(strcat(Volume_Fractions_Char(j,:),...
            '-Conductivity vs. Frequency'))
        figure(Figure_Counter)
        Figure_Counter = Figure_Counter + 1;
        errorbar(Average_Conductivity(:,1,1),...
            Average_Conductivity(:,j+1,i),...
            Std_Conductivity(:,j+1,i),'-
d','MarkerSize',...
            1,'MarkerEdgeColor','black',...
            'MarkerFaceColor','black')
        set(gca,'YScale','log');
        xlim([min(Average_Conductivity(:,1,1)) max(...
            Average_Conductivity(:,1,1))])
        xlabel('Frequency (Hz)')
        ylabel('Conductivity (S/m)')
        title(strcat(Volume_Fractions_Char(j,:),...
```

```
            '-Conductivity vs. Frequency'))
    end
end
% GRAPH AVERAGE PARAMETERS WITH ERRORBARS %
for i = 1:Number_Of_Parameters
    for j = 1:Number_of_Volume_Fractions
        figure(Figure_Counter)
        Figure_Counter = Figure_Counter + 1;
        errorbar(Average_Parameters(:,1,1),...
            Average_Parameters(:,j+1,i),...
            Std_Parameters(:,j+1,i),'-
d','MarkerSize',1,...

'MarkerEdgeColor','black','MarkerFaceColor'...
            ,'black')
        xlim([min(Average_Parameters(:,1,1)) max(...
            Average_Parameters(:,1,1))])
        xlabel('Frequency (Hz)')
        ylabel(strcat(Parameter_Names(i,:),' (',...
            Parameter_Units(i,:),')'))
        title(strcat(Volume_Fractions_Char(j,:),'-
',...
            Parameter_Names(i,:),' vs. Frequency'))
        figure(Figure_Counter)
        Figure_Counter = Figure_Counter + 1;
        errorbar(Average_Parameters(:,1,1),...

Average_Parameters(:,j+1,i),Std_Parameters(...
            :,j+1,i),'-d','MarkerSize',1,...

'MarkerEdgeColor','black','MarkerFaceColor',...
            'black')
        set(gca,'YScale','log')
        xlim([min(Average_Parameters(:,1,1)) max(...
            Average_Parameters(:,1,1))])
```

```
        ymin = min(Average_Parameters(:,j+1,i));
        ymax = max(Average_Parameters(:,j+1,i));
        if ymin < 0, ymin = ymin*10; else, ymin =
ymin*...
                0.1; end
        if ymax < 0, ymax = ymax*0.1; else, ymax =
ymax*...
                10; end
        ylim([ymin ymax])
        xlabel('Frequency (Hz)')
        ylabel(strcat(Parameter_Names(i,:),' (',...
            Parameter_Units(i,:),')'))
        title(strcat(Volume_Fractions_Char(j,:),'-
',...
            Parameter_Names(i,:),' vs. Frequency'))
    end
end
% SPECIFIC FREQUENCY VALUES %
Frequency_Values = [];
Columns = zeros(1,Number_Of_Samples);
for i = 1:Number_Of_Smaples
    Columns(i) = Number_of_Parameters*i - ...
        Number_Of_Samples;
end
Specific_Impe =
Average_Parameters(Frequency_Values,...
    2:Number_of_Volume_Fractions+1,1);
Impe_Min(1:3,:) = min(Impedances(Frequency_Values,...
    Columns,:),[],2);
Impe_Max(1:3,:) = max(Impedances(Frequency_Values,...
    Columns,:),[],2);
Specific_Resi =
Average_Resistivity(Frequency_Values,...
    2:Number_of_Volume_Fractions+1);
Specific_Cond =
```

```
Average_Conductivity(Frequency_Values,...
    2:Number_of_Volume_Fractions+1);
Specific_Diel = Average_Dielectric_Constant(...

Frequency_Values,2:Number_of_Volume_Fractions+1,1);
for i = 1:Number_of_Volume_Fractions
    Resi_Min(:,i) =
min(Resistivity(Frequency_Values,...
        Number_Of_Samples*(i-
1)+2:Number_Of_Samples*i+1)...
        ,[],2);
    Resi_Max(:,i) =
max(Resistivity(Frequency_Values,...
        Number_Of_Samples*(i-
1)+2:Number_Of_Samples*i+1)...
        ,[],2);
    Cond_Min(:,i) =
min(Conductivity(Frequency_Values,...
        Number_Of_Samples*(i-
1)+2:Number_Of_Samples*i+1)...
        ,[],2);
    Cond_Max(:,i) =
max(Conductivity(Frequency_Values,...
        Number_Of_Samples*(i-
1)+2:Number_Of_Samples*i+1)...
        ,[],2);
    Diel_Min(:,i) = min(Dielectric_Constant(...
        Frequency_Values,Number_Of_Samples*(i-1)+...
        2:Number_Of_Samples*i+1,1),[],2);
    Diel_Max(:,i) = max(Dielectric_Constant(...
        Frequency_Values,Number_Of_Samples*(i-1)+...
        2:Number_Of_Samples*i+1,1),[],2);
end
% GRAPH VALUES AT SPECIFIC FREQUENCIES %
r = size(Frequency_Values);
```

```
for i = 1:r
    figure(Figure_Counter)
    Figure_Counter = Figure_Counter + 1;
    errorbar(Volume_Fractions,Specific_Impe(i,:),...
        Specific_Impe(i,:) -
Impe_Min(i,:),Impe_Max(i,:)...
        - Specific_Impe(i,:),'d','MarkerSize',6,...

'MarkerEdgeColor','black','MarkerFaceColor',...
        'black')
    xlabel('Volume Faction of ZnO')
    ylabel('Impedance (\Omega)')
    if i == 1
        title('Impedance at 1.0 MHz')
    elseif i == 2
        title('Impedance at 2.0 MHz')
    else
        title('Impedance at 3.0 MHz')
    end
end
for i = 1:r
    figure(Figure_Counter)
    Figure_Counter = Figure_Counter + 1;
    errorbar(Volume_Fractions,Specific_Resi(i,:),...
        Specific_Resi(i,:) -
Resi_Min(i,:),Resi_Max(i,:)...
        - Specific_Resi(i,:),'d','MarkerSize',6,...

'MarkerEdgeColor','black','MarkerFaceColor',...
        'black')
    xlabel('Volume Faction of ZnO')
    ylabel('Resistivity (\Omega-m)')
    if i == 1
        title('Resistivity at 1.0 MHz')
    elseif i == 2
```

```
        title('Resistivity at 2.0 MHz')
    else
        title('Resistivity at 3.0 MHz')
    end
end
for i = 1:r
    figure(Figure_Counter)
    Figure_Counter = Figure_Counter + 1;
    errorbar(Volume_Fractions,Specific_Cond(i,:),...
        Specific_Cond(i,:) -
Cond_Min(i,:),Cond_Max(i,:)...
        - Specific_Cond(i,:),'d','MarkerSize',6,...

'MarkerEdgeColor','black','MarkerFaceColor',...
        'black')
    xlabel('Volume Faction of ZnO')
    ylabel('Conductivity (S/m)')
    if i == 1
        title('Conductivity at 1.0 MHz')
    elseif i == 2
        title('Conductivity at 2.0 MHz')
    else
        title('Conductivity at 3.0 MHz')
    end
end
for i = 1:r
    figure(Figure_Counter)
    Figure_Counter = Figure_Counter + 1;
    errorbar(Volume_Fractions,Specific_Diel(i,:),...
        Specific_Diel(i,:) -
Diel_Min(i,:),Diel_Max(i,:)...
        - Specific_Diel(i,:),'d','MarkerSize',6,...

'MarkerEdgeColor','black','MarkerFaceColor',...
        'black')
```

```
    xlabel('Volume Faction of ZnO')
    ylabel('Dielectric Constant')
    if i == 1
        title('Dielectric Constant at 1.0 MHz')
    elseif i == 2
        title('Dielectric Constant at 2.0 MHz')
    else
        title('Dielectric Constant at 3.0 MHz')
    end
end
% VOLUME FRACTIONS, d33, AND d31 %
Figure_Counter = 1;
% Insert the values of d33 and d31 with each row being
% the values for each volume fraction
d33 = [];
d31 = [];
% Insert the volume fractions tested
Volume_Fractions = [];
% AVERAGE d33 AND d31 %
d33_average = mean(d33);
d31_average = mean(d31);
% GRAPH d33 AND d31 %
figure(Figure_Counter)
Figure_Counter = Figure_Counter + 1;
errorbar(Volume_Fractions,d33_average,'d',...
    'MarkerSize',6,'MarkerEdgeColor','black',...
    'MarkerFaceColor','black')
title('d33 of BT-Epoxy-ZnO Composites')
xlabel('Volume Fraction of ZnO')
ylabel('d33 (pC/N)')
figure(Figure_Counter)
Figure_Counter = Figure_Counter + 1;
errorbar(Volume_Fractions,d31_average,'d',...
    'MarkerSize',6,'MarkerEdgeColor','black',...
```

```
    'MarkerFaceColor','black')
title('d31 of BT-Epoxy-ZnO Composites')
```

APPENDIX C: AGGLOMERATION MATLAB PROGRAM

```
% AGGLOMERATIONS %
clear
format compact
clc
% IMPORT DATA
%Insert the location of the agglomeration data to be
% imported
filename = '';
data = xlsread(filename);
fig_count = 1;
% Insert the cross-sectional area of the agglomerations
CC_Area = ;
% Inster the number of volume fractions tested
Number_Of_Volume_Fractions
% HISTOGRAMS %
edges = linspace(0,3,51);
for i = 1:10
    fig_count = fig_count + 1;
    figure(fig_count)
    histogram(data(:,i),edges)
    ylim([0 700])
end
edges = linspace(0,1,51);
for i = 1:10
    fig_count = fig_count + 1;
    figure(fig_count)
    histogram(data(:,i),edges)
    ylim([0 350])
end
edges = linspace(0,0.5,31);
for i = 1:10
    fig_count = fig_count + 1;
    figure(fig_count)
    histogram(data(:,i),edges)
    ylim([0 300])
```

```
end
edges = linspace(0,0.1,31);
for i = 1:10
    fig_count = fig_count + 1;
    figure(fig_count)
    histogram(data(:,i),edges)
    ylim([0 100])
end
% GRAPH AGGLOMERATION PERCETNAGES
in = ones(1,Number_Of_Volume_Fractions);
for i = 1:Number_Of_Volume_Fractions
    while data(in(i),i) <= CC_Area
        in(i) = in(i) + 1;
    end
    in(i) = in(i) - 1;
end
nans = isnan(data);
in_total = ones(1,10);
in_total(10) = 1363;
for i = 1:9
    while nans(in_total(i),i) < 1
        in_total(i) = in_total(i) + 1;
    end
    in_total(i) = in_total(i) - 1;
end
percentages = in./in_total*100;
figure(fig_count)
fig_count = fig_count + 1;
% Insert the volume fractions in the brackets '[]'
plot([],percentages,'-d','MarkerSize',6,...
            'MarkerEdgeColor','black',...
            'MarkerFaceColor','black')
% Insert the min and max volume fractions tested
% in the brackets '[]'
xlim([])
xlabel('Volume Fraction of ZnO')
```

```
ylabel('Percent of ZnO Agglomerations (%)')
title('The Increase of ZnO Agglomerations')
```